ROYAUME DU MAROC
Université Mohammed V - RABAT -
جامعة محمد الخامس – الرباط –
Faculté des sciences
كلية العلوم
CENTRE D'ÉTUDES DOCTORALES - SCIENCES ET TECHNOLOGIES

N° d'ordre : 3907

THÈSE

en vue de l'obtention du : **DOCTORAT**

Structure de Recherche : Physique des Hautes Energies- Modélisation et Simulation.
Discipline : Physique
Spécialité : Physique Médicale

Présentée et Soutenue le : *14 / 03 / 2024*

par :

Morad ERRAOUDI

Effectiveness of treatment associated with external beam and assessment of dose delivered to the tumor volume by advanced radiotherapy techniques

Devant le JURY :

Allal GHALMI	PES	Faculté des sciences Université Mohammed V	Président
Rachid AHL LAAMARA	PES	Faculté des sciences Université Mohammed V	Examinateur/Rapporteur
Lahoucine BAHMAD	PES	Faculté des sciences Université Mohammed V	Examinateur/Rapporteur
Wissal IRAQI HOUSSANI	PH	CRMEF, Fés Meknés	Examinateur/Rapporteur
Rahma ADHIRI	PES	Faculté des sciences Université Hassan II	Examinateur/Rapporteur
Farida BENTAYEB	PES	Faculté des sciences Université Mohammed V	Invité
Lalla Btissam DRISSI	PES	Faculté des sciences Université Mohammed V	Directrice de thèse

Année Universitaire : 2023 - 24

DEDICATION

I am dedicating this thesis work to my father, mother, brother, sister, nephew, and the entire family. Thank you so much for everything! You have been my source of inspiration, motivation, and support. You always gave me the strength, help, encouragement, and courage to complete this thesis. I am truly thankful and honored to have you as my family. I also dedicate this dissertation to my friends who always supported me and for having the pleasure of interacting for many valuable discussions and shared moments.

Acknowledgments

No creation in this world is the result of a solitary effort; this is thus the same for this work. It would not have been possible without the kind support and help of many individuals. I take this opportunity to express my gratitude to all of them.

I Thank ALLAH for providing me with everything I needed to successfully complete this task.

I would like to extend my warmest thanks to Professor **El Hassan SAIDI**, head of the Laboratory of High Energy Physics, Modeling and Simulation (LHEP-MS), for granting me the opportunity to join the ranks of PhD researchers in this distinguished laboratory.

Furthermore,I would like to express my heartfelt appreciation to professor **Lalla Btissam DRISSI**, Professor at the physics department of the Faculty of Sciences, University Mohammed V in Rabat, for her acceptance to be the director of this thesis and here kindness and gentleness in the entire period under her supervision.

I'd also like to extend my sincere thanks to Professor **Rachid AHLLAMARA** for the help, support and for his monitoring since the start of this work.

I had been immeasurably enriched by working under the supervision of **Pr. Farida Bentayeb** from the beginning of my career in medical physics, who has great level of knowledge and who has an art of encouraging, correcting and directing me in every possible situation. I owe her a great debt of thanks for all her support.

I wish to express my gratitude to the esteemed jury members who have kindly agreed to

assess my work. Thanks to Professor **Allal GHANMI** for presiding the jury, to Pr. **Rachid AHLLAMARA** Professor at the physics department of the Faculty of Sciences, University Mohammed V in Raba, **Pr. Lahoucine BAHMAD** Professor at the physics department of the Faculty of Sciences, University Mohammed V in Raba, Pr. Wissal **IRAQI HOUSSAINI** Regional Center for Education and Training Professions of Meknes, and Pr. **Rahma ADHIRI**, Professor at the physics department of the Faculty of Sciences Ben M'sik, University Hassan II in Casablanca. I appreciate your valuable time in reviewing this manuscript. I extend my heartfelt gratitude to each of them for bestowing upon me the privilege of participating as examiners on the jury, and for generously sharing their invaluable comments and suggestions with me.

I extend my sincere gratitude to **Dr. Houda BENJELLON** director of radiotherapy department at HPC, for her willingness to review my thesis. Working with her, allowed me to enhance my skills and gain a deeper understanding of the field of medical physics through our discussion during the work, and this because of her spirit of research. Her exceptional quality and competence significantly contributed to elevating the skill level within our department, fostering a strong sense of teamwork, and enhancing the overall quality of our work.

A special thanks to **Dr. HERRASI Yassine** Area Sales Manager (MEA) at IBA Dosimetry in Schwarzenbruck, Germany. Through him I am presented into the realm of medical physics, where I subsequently pursued a professional career as a medical physicist. Additionally, collaborating with him in the research domain was a valuable opportunity, as he possesses exceptional skills in transforming concepts into high-quality scientific articles. Working with him, I not only learned how to practice medical physics, but also discovered how to enjoy it.

I would like also to thank sincerely **Mr. Mohammed El GHALMI** Head Medical Physicist ofAkdital group. I appreciate the time I worked with him in the same radiotherapy department under his leadership, where I learned from his valuable experience accumulated for years. He consistently keeps the door open for addressing any questions. Moreover, our discussions on enhancing work quality in practical applications and his meticulous observations in research have consistently enriched my understanding. At last, I would like to express my gratitude for your rational kindness, gentleness, and understanding in every situation.

I would like to thank **Dr. BENMANSSOUR** Mustafa for his support and his positive energy he infused into our team. Working with him provided me with the opportunity to enhance my

work by engaging in discussions about intriguing cases, which in turn served as a source of inspiration to further develop my research.

I want to convey my heartfelt thanks to Akdital group, a prominent figure in Morocco's healthcare domain. I'd like to specifically acknowledge **Dr. TALIB Rochdi**, the CEO, for his invaluable support. His visionary perspective and exceptional leadership have consistently inspired me throughout my academic journey. I would also like to express my sincere gratitude to **Dr. Jaouad ZAKARIA**, Vice President and Medical Director of HPC AKDITA Group, for his steadfast dedication and support. Your combined influence has played a substantial role in shaping my growth and advancement within the field.

Many thanks are extended to my friends **Dr. Mohammed TALBI** and **Dr. Oussama Nhila** for their support and valuable contributions, as they generously shared their expertise and actively participated in writing articles.

I thank my radiotherapy team at Private hospital Clinic Ain Sebaa Casablanca (HPC), AKDITAL group for the help and support they have provided me during the preparation of this work at HPC AIN SEBAA.

It has been a pleasure working with such highly qualified and competent radiotherapy team. I extend my gratitude to all the members of this exceptional team (**Asmae ABROUM** , **Houda FOUZI** , **Hicham SEMMONI** , **ABDESLAM ADAL**, **Youssra SAALAOUI** , **Ouafae CHFIK** , **El GHALMI Mohammed** , **Dr. BENMANSSOUR Mustafa**, **Dr. Houda BENJELLOUN** and me).

I would like to express my profound gratitude to the trainees for their immense effort and dedication during the preparation of this work. Their invaluable contributions greatly assisted me and made the task significantly more manageable.

A special thanks to the radiotherapy team of Fes for the opportunity of my first experience in radiotherapy, many thanks to **El BARAK Mohammed**, **OUBEL Marouane**, El **OUARDIKhalid**, **RAOUI Yasser** and many thanks to **Dr. Moulay Ali Youssoufi** for his unwavering sup- port, valuable advice, and for sharing his extensive expertise and competence with me.

A special expression of gratitude goes to my friend **Dr. Mohamed Amin LOUALIDI** for generously sharing his experience and research techniques with me.

At last, I would like to address my special thanks to the The Abdus Salam International

Ackowlegment

Centre for Theoretical Physics (ICTP) joint Universita Degli Studi di Trieste and International Agency Energy Atomic (IAEA), I am profoundly grateful for the opportunity they provided me to be part of the inaugural cohort of the International Medical Physics program. This program has been instrumental in enabling me to attain a high level of quality and competence in both practical applications and research within this field.

I heartily thank My family for giving me their wonderful support and motivation to complete the work successfully. I am extremely grateful to my parents for providing such a great encouragement and guidance throughout all these years.

Abstract

Cancer is a major disease burden worldwide, during the past years, the world has witnessed many landmark discoveries in cancer treatment, and one of the key milestones in the historyof cancer research is the discovery of x-rays in 1895 and of radioactivity in 1896, which hasled to the birth of radiotherapy by using ionizing radiation to kill cancer cells in the treatedarea by damaging the DNA of these cells. It is always a balance between destroying the cancer cells and minimizing damage to the healthy tissue. Advanced radiotherapy techniques enable a significant improvement in dose distribution precision and better dose conformation to the tumor, compared with ancient and conventional techniques. Consequently, these new techniques enable higher doses to be delivered to the PTV, while more optimally sparing healthy tissue close to the tumor.The advances in technology associated with these techniques include inten- sity modulation of treatment beams, i.e. modulation of photon fluence within the beam andthe use of virtual inverse planning. The TPS then calculates the processing beams needed to satisfy these criteria in the optimum way, or modify the ballistics, i.e. the number and orienta- tion of the beams. This optimization is performed iteratively.Modulation of the beams to meet the constraints is carried out automatically by the software. Finally, processing is monitored byon-board imaging for precise repositioning of the patient in relation to planning before and during treatment.

Keywords: Radiotherapy, Dose, Treatment,Cancer, Computed tomography, TPS

Résumé

Le cancer est une charge de morbidité majeure dans le monde, au cours des derniéres années, le monde a été témoin de nombreuses découvertes marquantes dans le traitement du cancer, et l'une des étapes clés de l'histoire de la recherche sur le cancer est la découverte des rayons X en 1895 et de la radioactivité en 1896, qui a conduit à la naissance de la radiothérapie en utilisant des rayonnements ionisants pour tuer les cellules cancéreuses dans la zone traitée en endommageant l'ADN de ces cellules. C'est toujours un équilibre entre la destruction des cellules cancéreuses et minimiser les dommages aux tissus sains. Les techniques avancées de radiothérapie permettent une amélioration significative de la précision de la distribution de dose et une meilleure conformation de la dose à la tumeur, par rapport aux techniques anciennes et conventionnelles. Par conséquent, ces nouvelles techniques permettent de délivrer des doses plus élevées au PTV, tout en épargnant de maniére plus optimale les tissus sains proches de la tumeur. Les avancées technologiques associées à ces techniques comprennent la modulation d'intensité des faisceaux de traitement, c'est-à-dire la modulation de la fluence des photons dans le faisceau et l'utilisation de la planification inverse virtuelle. Le TPS calcule alors les faisceaux de traitement nécessaires pour répondre de maniére optimale à ces critéres, ou modifie la balistique, c'est-à-dire le nombre et l'orientation des faisceaux. Cette optimisation est effectuée de maniére itérative. La modulation des faisceaux pour répondre aux contraintes est réalisée automatiquement par le logiciel. Enfin, le traitement est suivi par imagerie embarquée pour un repositionnement précis du patient par rapport à la planification avant et pendant le traitement.

Résumé Détaillé

Le cancer constitue un lourd fardeau pour la santé mondiale. Au cours des dernières années, des avancées marquantes ont été réalisées dans le traitement du cancer. L'une des découvertes fondamentales dans l'histoire de la recherche sur le cancer est celle des rayons X en 1895 et de la radioactivité en 1896, menant à la naissance de la radiothérapie qui utilise les rayonnements ionisants pour tuer les cellules cancéreuses en endommageant leur ADN. L'équilibre entre la destruction des cellules cancéreuses et la minimisation des dommages aux tissus sains est crucial.

Au Maroc, le cancer est un problème majeur de santé publique. Le taux d'incidence annuel national est estimé à 30 500 nouveaux cas par an, dont 16 775 chez les femmes et 13 725 chez les hommes, selon le registre des cancers du Grand Casablanca. La prise en charge de cette maladie est multidisciplinaire, impliquant différentes spécialités telles que la chirurgie, la chimiothérapie et la radiothérapie. La radiothérapie, fondée sur l'utilisation de rayonnements ionisants, existe depuis un peu plus d'un siècle et a évolué grâce aux avancées en physique théorique, médecine, sciences de l'ingénierie, informatique et intelligence artificielle. Cette évolution a rendu le traitement du cancer plus efficace et précis. Les machines de radiothérapie actuelles sont le résultat de cette longue évolution, intégrant des avancées en physique médicale, ingénierie mécanique et informatique.

La transition de la radiothérapie 2D à la radiothérapie conformationnelle 3D (3D CRT) a marqué un grand progrès. Introduite au début des années 1960 par le radiologue S. Takahashi, cette technique utilise plusieurs faisceaux de rayonnement façonnés pour conformer au volume cible. L'étape la plus importante en 3D CRT fut l'introduction de champs d'irradiation de forme irrégulière. Toutefois, cette méthode est coûteuse et chronophage. Les collimateurs multilames (MLC) ont permis d'ajuster rapidement et de manière flexible les champs d'irradiation à la forme de la tumeur et des organes à risque.

Les traitements radiothérapeutiques se classent principalement en deux catégories : la radiothérapie interne et la radiothérapie externe. La radiothérapie interne implique l'utilisation d'un élément radioactif placé près ou dans la tumeur, tandis que la radiothérapie externe utilise une source de radiation externe produisant un faisceau de photons énergétiques. Les machines d'accélération de particules sont généralement utilisées, et dans les années 1950, les machines de télécobalt 60 ont été introduites comme méthode de radiothérapie externe.

Les collimateurs multilames, introduits commercialement dans les années 1980, ont simplifié la livraison de champs conformés et permis la thérapie par modulation d'intensité (IMRT) et la radiothérapie par arc modulé en volume (VMAT). Ces avancées ont permis de créer des volumes de haute dose conformes à la forme des cibles complexes. L'intégration de récepteurs d'images aux linacs a permis l'imagerie du patient avant chaque session et le suivi du mouvement tumoral pendant le traitement, améliorant ainsi la précision du positionnement et limitant le mouvement tumoral pendant la livraison du traitement.

Récemment, il y a un intérêt croissant pour l'amélioration des linacs en termes de vitesse de rotation, vitesse des lames et taux de dose pour renforcer l'efficacité temporelle de la livraison VMAT. L'objectif principal est désormais d'optimiser le dépôt de la dose physique, proportionnelle à l'énergie déposée par les particules ionisantes dans les tissus. En augmentant la dose à la tumeur tout en épargnant les tissus sains, le risque de récidive est réduit, les effets secondaires sont contrôlés et la probabilité de développer un cancer induit par les radiations est minimisée.

Avec la mise en œuvre des collimateurs multilames, une conception innovante des machines de radiothérapie a été formulée. Les machines de tomothérapie, introduites en 2002, et les linacs Halcyon, développés en 2017, représentent des avancées significatives. Ces machines permettent un haut degré d'automatisation, réduisant ainsi le besoin de réglages manuels et potentiellement le risque d'erreur humaine, tout en fournissant un traitement plus rapide et efficace.

Cependant, il est crucial de noter que ces machines doivent répondre aux besoins spécifiques du patient traité, ce qui peut présenter des défis pour traiter des volumes plus grands que la taille du champ de la machine. Des solutions potentielles à cette limitation seront discutées dans ce travail, qui évalue l'efficacité du traitement radiothérapeutique externe et la dose délivrée à la région d'intérêt.

La thèse est structurée en trois chapitres. Le premier chapitre traite des objectifs principaux et des principes de la radiothérapie par faisceau externe et du flux de travail des patients. Il fournit un aperçu des concepts et quantités dosimétriques utilisés en radiothérapie pour calculer et évaluer la distribution de dose résultant de l'interaction entre les rayonnements et la matière. Il aborde également les principes et implications de diverses méthodes de radiothérapie et étudie les effets des incertitudes des marges de sécurité pendant le traitement.

Le deuxième chapitre explore le mécanisme opérationnel de l'algorithme AAA et le principe de fonctionnement de l'algorithme de convolution/superposition.

Le troisième chapitre se divise en quatre sections principales : l'évaluation de la marge supplémentaire du volume cible clinique (CTV) pour le traitement du cancer de la prostate, l'évaluation de la délivrabilité de la dose pour le traitement du cancer du larynx en comparant trois approches d'optimisation utilisant la technique IMRT, l'impact de la séquence des lames dans le traitement des cancers de la tête et du cou, de la prostate et du sein traités par la technique VMAT, et enfin, une proposition pour surmonter les limitations de la machine Halcyon dans la gestion des volumes importants par la technique VMAT.

List of Publications

Erraoudi, M., et al. " *A planning study to optimise a simultaneously integrated boost treatment of larynx cancer with seven intensity-modulated radiation therapy (IMRT) beams.* " Journal of Radiotherapy in Practice 17.4 (2018): 447-454.

Erraoudi, Morad, et al. "*CTV to PTV margins based on CBCT method for prostate cancer of Patients treated with VMAT technique.*" Iranian Journal of Medical Physics (2022).

Morad Erraoudi, et al. "*Performance of different Strength Aperture Shape Controller in Optimization with VMAT technique for Head and Neck, Pelvic and Breast Cancer using Halcyon Machine.*" Iranian Journal of Medical Physics (2023).

Morad Erraoudi, et al. "*Solution for processing pelvic bone metastases with HalcyonTM 2.0 on lateral and longitudinal isocenters treatment plans using the VMAT technique: A comparative study.*" Iranian Journal of Medical Physics (2023).

M Es-Semyhy, M Ouahman, O El Bounagui, F Bentayeb, N Tahiri, **M Erraoudi**. "*Ab Initio Study of Electronic and Magnetic Properties in ZnO-Doped and Co-doped by Vanadium and Silver.*" Journal of Superconductivity and Novel Magnetism 31 (2018): 2201-2206.

Nhila, O., Talbi, M., El Mansouri, M., Youssoufi, M., **Erraoudi, M.**, Chakir, E., Azougagh, M. (2023). "*The effect of CT reconstruction filter selection on Hounsfield units in radiotherapy treatment planning.*" Journal of Radiotherapy in Practice, 22, E102.

Talbi, Mohammed, Mounir Ben Messaoud, Rajaa Sebihi, **Morad Erraoudi**, Yassine Aza-

List of Publications

Erraoudi, M., et al. " *A planning study to optimise a simultaneously integrated boost treatment of larynx cancer with seven intensity-modulated radiation therapy (IMRT) beams.* " Journal of Radiotherapy in Practice 17.4 (2018): 447-454.

Erraoudi, Morad, et al. "*CTV to PTV margins based on CBCT method for prostate cancer of Patients treated with VMAT technique.*" Iranian Journal of Medical Physics (2022).

Morad Erraoudi, et al. "*Performance of different Strength Aperture Shape Controller in Optimization with VMAT technique for Head and Neck, Pelvic and Breast Cancer using Halcyon Machine.*" Iranian Journal of Medical Physics (2023).

Morad Erraoudi, et al. "*Solution for processing pelvic bone metastases with HalcyonTM 2.0 on lateral and longitudinal isocenters treatment plans using the VMAT technique: A comparative study.*" Iranian Journal of Medical Physics (2023).

M Es-Semyhy, M Ouahman, O El Bounagui, F Bentayeb, N Tahiri, **M Erraoudi**. "*Ab Initio Study of Electronic and Magnetic Properties in ZnO-Doped and Co-doped by Vanadium and Silver.*" Journal of Superconductivity and Novel Magnetism 31 (2018): 2201-2206.

Nhila, O., Talbi, M., El Mansouri, M., Youssoufi, M., **Erraoudi, M.**, Chakir, E., Azougagh, M. (2023). "*The effect of CT reconstruction filter selection on Hounsfield units in radiotherapy treatment planning.*" Journal of Radiotherapy in Practice, 22, E102.

Talbi, Mohammed, Mounir Ben Messaoud, Rajaa Sebihi, **Morad Erraoudi**, Yassine Aza-

khmam, and Mohammed Khalis. "*Local radiation dosimetry method using optically stimulated pulsed luminescence and Monte Carlo simulation.*" Advancements in Life Sciences 8, no. 2 (2021): 160-166.

Raoui Yasser1, El Ouardy Khalid, Elghemary Nihad, Chehab Fatim Zahra, Chouib Fatima Ezzahra, Elghalmi Mohammed, Herrassi Yassine, VP Pandey, Teerthraj Verma, Sebihi Rajaa and **Erraoudi Mourad1**,. "*Pre-treatment verification of carcinoma breast VMAT plan based on mono-isocentric technique: Assessment of the combined fields feature of new 2D MatriXX arrays resolution*" Oncology and Radiotherapy 16 (8) 2022: 14-20

List of Figures

List of Tables

List of Abbreviations

MLCs	Multi-Leaf Collimators
IMRT	Intensity Modulates Radition Therapy
VMAT	VolumerticModulated Arc Therapy
MPC	Machine Performance Check
AAA	Anisotropic Analytical Algorithm
GTV	Gross Target Volume
CTV	Clinical Target Volume
PTV	Planning Target Volume
TPS	Treatment Planning System
DRRs	Digital Reconstracted Radiographs
MRI	Magnetic Resonance Imaging
NTCP	Normal Tissue Complication Probability
TCP	Tumour Control Probability
DVH	Dose Volume Histogram
OARs	Organ At Risk
BED	Biolgic Effective Dose
TERMA	Kinetic Energy Released per unit Mass
CPE	Charged Particle Equilibrium
TCPE	Transient Charged Particle Equilibrium
SBRT	Steriotactic Body Radition Therapy
ROI	Region of Interest
DTA	Distance to agreement
DD	Dose Difference
RTOG	Radition Therapy Ocology Group

HI: Homgegeneity Index
CI: Coformity Index
LUF: Lesion Under dose volume Factor
HTOF: Healthy Tissue over dose volume Factor
ICRU: International Center of Radiation and Unit
IGRT: Image Guided Radiation Therapy
CBCT: Cone Beam Computed Tomography
CN: Conformation Number

Contents

Introduction

Cancer is a major disease burden worldwide, during the past years, the world has witnessed many landmark discoveries in cancer treatment, and one of the key milestones in the history of cancer research is the discovery of x-rays in 1895 and of radioactivity in 1896, which has led to the birth of radiotherapy by using ionizing radiation to kill cancer cells in the treated area by damaging the DNA of these cells. It is always a balance between destroying the cancer cells and minimizing damage to the healthy tissue.

In Morocco, it is one of the major healthcare problems. The annual national incidence rate is estimated at 30,500 new cases of cancer per year, including 16,775 new cases in women and 13,725 new cases in men, according to the cancer registry of Greater Casablanca [1]. The management of this disease is multidisciplinary involving different specialties namely surgery, chemotherapy and radiotherapy that is based on ionizing radiation to treat cancer for a bit more than a century old. In its history, radiotherapy has undergone numerous evolutions because it has always been enriched by scientific advances in theoretical physics, medicine, engineering sciences and now computer science and artificial intelligence. This development in radiotherapy over the years has made cancer treatment more effective and more accurate. Radiotherapy machines currently used in clinical practice are the result of evolution over a long period of time of various scientific fields, such as medical physics, mechanical engineering, and computer engineering.

Great progress in radiotherapy was achieved by transition from 2D radiotherapy to 3D conformal radiotherapy. This was introduced in the early 1960s by radiation oncologist S. Takahashi, who came up with many ideas of how to concentrate the dose to the target volume. 3D CRT plans generally use an increased number of radiation beams that are shaped using

beam's-eye-view (BEV) planning to conform to the target volume. The most important step in 3D CRT was the introduction of irregularly shaped irradiation fields, ("cerrobend" blocks). This method is expensive and time consuming since a block has to be made for each individual beam. During the treatment, the block should be changed between different beams. Therefore, major improvement in conformal distributions achieved with MLCs turned out to be equivalent to conformal blocks.

The types of treatment are classified mainly in two main categories. The Internal radiotherapy concerns techniques in which a radioactive element is placed on or near the tumor,either by implanting radioactive seeds (as in brachytherapy) or by injecting radiopharmaceutical molecules capable of targeting cancer cells to which a radioactive agglomerate has been chemically fixed. These techniques are however used in very specific cases, and are often shownn to be invasive and uncomfortable for the patient. External radiationtherapy, on which the present work is focused, involves the use of an external radiation source that produces a beam of energetic photons. The sources generally considered are particle acceleration machines, also in the early 1950s, the use of cobalt-60 teleterapy machine as a method for external radiotherapy in cancer treatment, relying on gamma radiation as the energy source.

Multi-leaf collimators permit the quick and flexible adjustment of the irradiation fields to the tumor shape and the shape of the organs at risk. In spite of this strategy was proposed by Takahashi in 1960, it took nearly 25 years before the first commercial computer controlled MLCs appeared on the market because of the fact that MLCs are mechanical devices with high mechanical complexity, and they have to fulfill very rigid technical, dosimetric, and safety constraints.For more than three decades, MLCs have been used and considered as a cornerstone of radiotherapy [2–10]. Initially, beam-formers were used to get rid of heavy shielding blocks, and soon after for intensity modulated radiation therapy (IMRT) and volumetric modulated arc therapy (VMAT) [11]. In addition, various MLC designs throughout the years have been described, each version aimed to further enhance the outcomes and the quality of radiation therapy [12–16].

After the invention of medical linac, major advancements in RT have been made in the area of treatment planning, and in the related field of computer controlled hardware. The multi-leaf collimator (MLC) which appeared in the market in 1980s, made it easier to deliver fields conforming to the projection of the target [17]. In more advanced applications, the individual leaves of the MLC are moved separately in a computer control at desired speeds during beam-on. This enables the generation of spatially modulated radiation fields, since each leaf attenuates the beam for a different time period. The resulting intensity modulated radiotherapy (IMRT) has enabled the creation of high dose volumes that conform more closely

to the shape of complicated targets. The integration of x-ray image receptors to the linac has enabled the imaging of the patient before each treatment session and the tracking of tumor motion during treatment delivery. These so-called image-guided RT methods have improved patient positioning accuracy, and have lead to techniques for restricting tumor motion during treatment.

Recently, there is a growing interest in LINAC improvement of gantry speed, leaf speed and dose rate that may strengthen the time efficiency of VMAT delivery. With the constant progress of treatment techniques, the main objective is now to optimize the deposition of the physical dose, and this quantity is proportional to the energy deposited by the ionizing particles in the tissues. By increasing the dose to the tumor while sparing the surrounding healthy tissue as much as possible, the risk of recurrence after treatment is reduced, the side effects are controlled and the probability of developing radiation-induced cancer, i.e. caused by the dose to healthy tissue, which often occurs several years after treatment, is minimized.

With the implementation of MLC, an innovative radiotherapy machine design, rooted in the existing C-arm LINAC framework, was formulated and made available. Tomotherapy machines, which put into practice with new principal technology in 2002 [18] are a specialized form of intensity-modulated radiotherapy, designed with a rotating gantry that moves around the patient as the treatment table moves through the gantry. In 2017, Varian medical system developed a new type o linear accelerator called Halcyon machine, which almost had a similar function of tomotherapy. The first installation of this machine was at Pittsburg University Hospital and, in Morocco, just a few months later it was installed and used in clinical practice. Six Halcyon devices have been installed and used in 2022. The use of this machine enables a high degree of automation, which however reduces the need for manual adjustments. This can lead to more consistent and efficient processing, which potentially reducing the risk of human error. Providing a faster and more effective treatment while maintaining high treatment quality. Moreover, the combination of automation and advanced treatment techniques can lead to shorter treatment sessions, which can be especially beneficial for patients and can increase the machine's throughput. The machine's design and features contribute to efficient treatment delivery, potentially allowing clinics to treat more patients in a given time frame. In terms of quality assurance, the machine performance check (MPC) is designed to ensure that the machine is operating within established tolerances and is capable of delivering radiation with the desired precision. This routine check helps identify any deviations or anomalies in the machine's performance. In the other hand, the only available field size for Halcyon 1.0 is 28cm x 28cm, in version 2.0, the use of two isocenters is permitted with an additional longitudinal distance of 8cm. In the third version, two isocenters are also allowed, with the potential for an

additional longitudinal distance of 10cm.

It's important to note that while the Halcyon machine offers numerous advantages,the type and the volume of cancer being treated, should meet the specific needs of the treated patient. Otherwise, this could present some difficulties in treating volumes bigger than the machine field size.Possible solutions to this limitation, will be discussed through the present work. This work involves assessing the effectiveness of external radiotherapy treatment and evaluating the dose delivered to the region of interest.

This thesis is structured around three chapters, organized as follows:

In the first chapter, discusses the main objectives and principal of external beam radiation therapy and workflow of the patients.we will provide a concise overview of the dosimetric parameters concepts and quantities employed in radiotherapy to calculate and evaluate the dose distribution resulting from the interaction between radiation and matter. Subsequently, we will delve into the principles and implications of diverse radiotherapy methods. the last part of this chapter devoted to the study of the effects of the uncertainties of safety margins during the treatment.

The second chapter,I discussed the operational mechanism of the AAA algorithm and explored the operational principle of the Convolutions/Superposition Kernel algorithm.

The third chapter is structured into four primary sections. The first part appraises the additional margin from the clinical target volume 'CTV), taking into account for both, translational and rotational axes applicable to prostate cancer treatment. In the subsequent section, an evaluation of dose deliverability for larynx cancer treatment is conducted, comparing three optimization approaches employing IMRT technique. The third part examines the impact of leaf sequencing in the treatment of Head and Neck, Prostate, and Breast cancer treated by VMAT technique. Lastly, a proposition is presented to address the limitations of the Halcyon machine in managing substantial volumes through the utilization of VMAT technique.

Chapter I

Background

1 External radiation therapy

1.1 Principle of external radiotherapy

External radiotherapy remains the most important non-surgical treatment in the management of cancer and it owes its success mainly to the important discoveries in the field of physics, which allowed us to understand the essence of the interaction of ionizing radiation with matter, in particular living matter.
During the treatment, high energy radiation is delivered to tumors by means of a linear accelerator. A beam of electrons is generated and accelerated through a waveguide that increases their energy. These electrons strike a tungsten target and produce x-rays.
Radiation therapy damages cells by destroying the genetic material that controls how cells grow and divide. While both healthy and cancerous cells are damaged by radiation therapy. The goal of radiation therapy is to destroy as few normal, healthy cells as possible. Normal cells can often repair much of the damage caused by radiation, and this is the reason why in treatment planning we used fractional radiation.
Safe use of radiotherapy as one of the methods of oncological treatment requires proficient knowledge of the basics of radiobiology and the physics of nuclear interactions.

1.2 The course of radiotherapy treatment

In clinical practice, the implementation of a radiotherapy treatment is the result of teamwork within several specialties at the interface between medicine and physics. The first step in the process is patient assessment and deciding how the patient should be treated. During assessment various diagnostic and investigative procedures are undertaken to define the state of the disease. This involves imaging, biochemical testing and review of pathologic information to identify the type, stage and grade of the cancer.

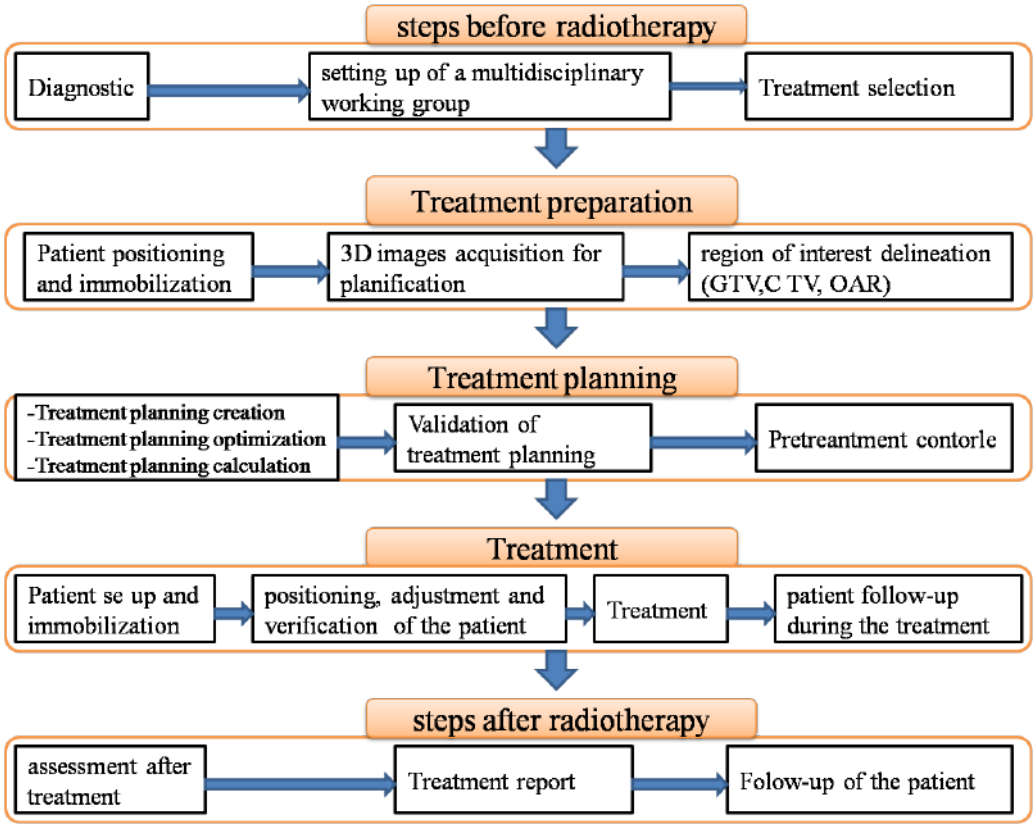

Figure I.1 – shematic representation of patients care workflow in external radiotherapy.

Then, the target volume (tumor cells) and organs at risk are segmented on these images. Doses are finally calculated and optimized with the TPS to meet the clinical objectives. Once the treatment plan is verified, simulated images of the patient, referred to as Digitally Reconstructed Radiographs (DRRs), are generated using CT images. These images simulate the imaging process within the treatment room. They enable the patient to be repositioned on the treatment table in the same position as when the CT images were acquired. Finally, the data

are transferred to the console of the linear accelerator used for the treatment. Before the start of treatment, pre-processing checks are performed to validate the performance of the accelerator in delivering the doses according to the defined plan. After validation, the treatment can begin: The patient is treated with the sessions scheduled in advance and his or her progress is monitored as it occurs.

Different steps of the external radiotherapy treatment are summarized in **Figure I.1**.
1) Clinical diagnosis and therapeutic decision by a multidisciplinary team
2) Acquisition of 3D images for patient planning: MRI, CT scanner, PET scan, etc.
3) Treatment planning using a treatment planning system (TPS)
4) Pre-treatment checks to ensure that the dose can be delivered in accordance with the treatment plan
5) Treatment of the patient in accordance with the verified plan
6) Assessment of tumor progression during treatment
7) Final evaluation after treatment
8) Patient follow-up

1.3 Objectives and limits of external radiotherapy

Different treatment strategies for cancer are used, mainly combining surgery, chemotherapy and radiotherapy. The choice of treatment modalities varies according to the patient's condition, the type and location of the tumor and the stage of the disease. Advances in treatment techniques and protocols used, as well as early diagnosis, have led to a decrease in cancer mortality [19]. External beam radiation therapy is a cancer treatment technique that uses the ionizing properties of photon or electron radiation to kill cancer cells. A related technique known as hadron therapy uses beams of heavy particles such as protons or carbon ions. However, this thesis focuses on radiotherapy using photons,and the main objective of this technique in cancer treatment is always to deliver a curative and homogenous dose; and then control the disease locally. The challenge is to protect as much as possible the organs at risk and the healthy tissues surrounding the irradiated tumor area. The choice of a treatment plan will therefore be guided by a balance between local control and limitation of undesirable side effects.

The limitations of radiotherapy are related to the fact that there is no dose that ensures tumor sterilization without any risk of complication which can be consequent [20]. **Fig I.2** shows Clinical requirements for external radiation therapy based on dose-response curves (dose effect) of tumor control probability (TCP) and Normal tissue Complication Probability (NTCP), whose shape is a sigmoid. So a compromise on the delivered dose will have to be accepted.

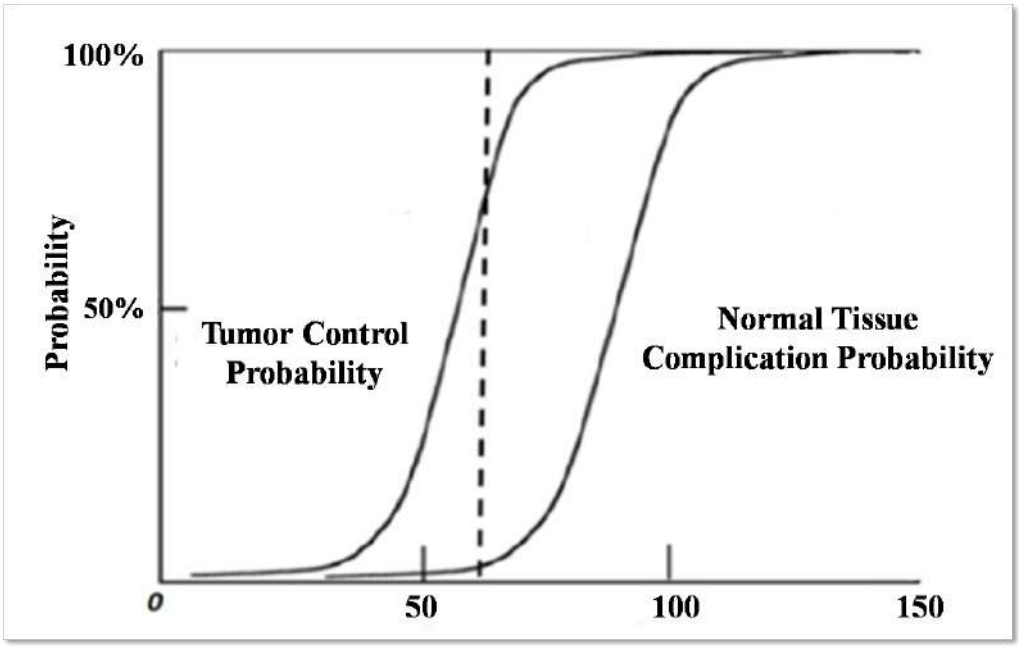

Figure I.2 – tumor control probability Curve (TCP) and the probability of complication of the healthy tissue (NTCP) as a function of dose. The optimal dose should be around 60 Gy (dotted line). dotted line)[21].

Where:

-TCP is a formalism derived for comparing treatment schemes of radiation therapy, which is defined as the probability that, for a prescribed dose, a tumor has been eradicated or controlled. The mathematical expression of the TCP is defined by a Poisson statistic [22]

$$TCP(D) = [1 - S(D)]^n \simeq exp[-nD(D)] = exp[-\overline{n}(D)] \tag{I.1}$$

-$\overline{n}$(D) is the number of cancer cells surviving a radiation dose.

-D and S(D) the probability of cell survival under ionizing radiation.

-NTCP is based on clinical and dosimetric indicators to reduce the toxicity of ionizing radiation on healthy tissue and increase the dose to the tumor for better tumor control. The dosimetric indicators are often extracted from Dose Volume Histograms (HDVs) calculated during treatment planning by "stair step" DVH reduction.

These two indices are based on the biological response of the tissues. In order to calculate them, it is necessary to contour organs at risk (and the target volume as well) and obtain a dose volume histogram.

In general, these two curves cross along the dose axis, so that the dose to the tumor is limited

by the maximum that can be tolerated by the healthy tissue at greatest risk. Optimization in radiotherapy and the numerous technological and technical advances aim to optimize these quantities, i.e. to maximize tumor control while maintaining tissue complications at an acceptable level. The clinically obtained TCP and NTCP slope data are presented in a number of publications [23–26] showing large variations in the slopes of the curves. This large variability depends on a number of factors such as the characteristics of the tissue, the effect obtained, dosimetric uncertainties, the radiobiological variability of each tissue (tumor and healthy tissue), the treatment technique used, or the dose per fraction.
An illustration of the TCP and NTCP curves is shown in **Figure I.3**. we observe that decreasing the dose to healthy tissues shifts the NTCP curve to the right (B to C), sparing as much healthy tissue as possible for the same dose (dose 1). On the other hand, maintaining the same level of NTCP, results in a higher dose (dose 2). In general, dose changes of 5% can produce changes of 10 to 20% on TCP and 20 to 30% for NTCP.

Based on clinical evaluations, various recommendations have been made on the accuracy required in radiotherapy:

-In its report No. 24, the ICRU reviewed the TCP data and concluded that a maximum uncertainty of 5% is required for the delivered dose on the target volume. This has been widely cited as a standard; however, it has not been shown to what confidence interval this corresponds. It is generally interpreted as being equal to 1.5 standard deviations or 2 standard deviations, and this assumption has been largely supported by more recent evaluations; for example, Mijnheer et al [26], consider the NTCP, and Brahme et al. in 1988, consider the effect of dose variations on the TCP, recommend an uncertainty of 3-3.5% (1 standard deviation) uncertainty on the delivered dose (i.e. 6% or 7% for a 95% confidence interval).

-Geometric uncertainty, e.g. systematic errors in the position of the treatment field, the position of accessories, etc..., in relation to target volumes or organs at risk, also lead to dose defects, either underdosing of the target volume (decrease in TCP) or overdosing of nearby structures (Organs At Risk (OARs,)) (increase in NTCP). Taking these effects into account has led to recommendations on the geometric (or spatial) uncertainty between 5 and 10 mm (with a 95% confidence interval). The 5 mm uncertainty is generally defined on the whole equipment related to mechanical/geometrical problems, while 8 or 10 mm is used to indicate the overall spatial accuracy, including uncertainties related to the patient and his positioning [26]. The latter parameters depend on the location, the method of immobilization, and the treatment techniques employed.
In conclusion, it is common to define for clinical routine in external radiotherapy, a precision of 5-7% on the delivered dose compared to the prescribed dose. An accuracy of 5-10 mm

is generally given for the geometric uncertainty, but this value is much lower, especially in radiotherapy under stereotactic conditions.

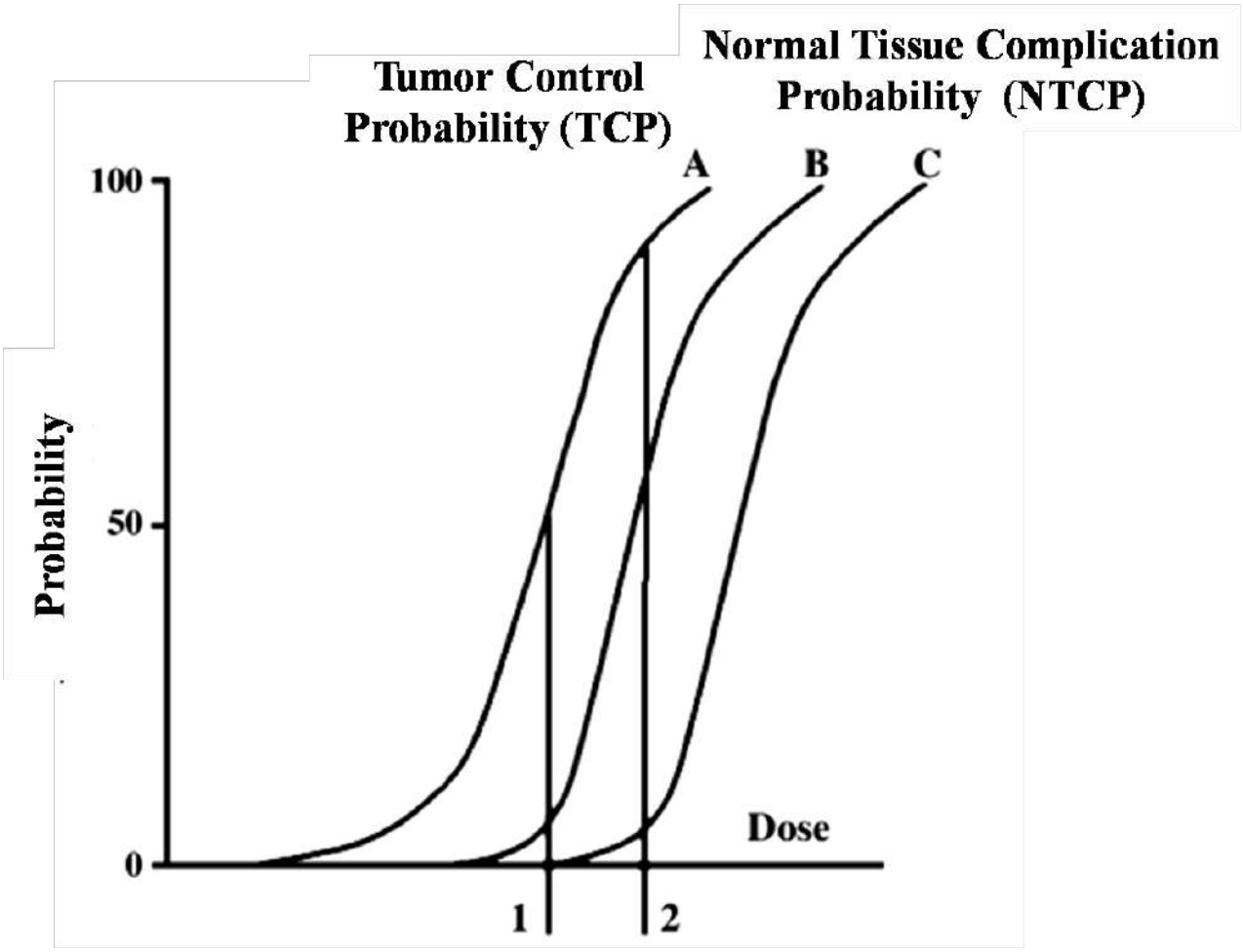

Figure I.3 – Schematic diagram of Tumor Control Probability (TCP) or Normal Tissue Complication Probability (NTCP) versus radiation therapy dose [28].

Nevertheless, in the sixth section of this chapter, we will examine the meanings of various parameters concerning geometric discrepancies and errors. Additionally, within the first section of the third chapter, we will utilize the van Herk formula to compute the extra margin from the Clinical Target Volume (CTV) in the context of prostate cancer treatment.

2 The quantities and concepts used in radiotherapy:.

2.1 Principles

The physical principles of interest in external radiotherapy using photon beams are the interactions of the photons coming from the medical accelerator in the patient's tissues and in the elements making up the head of the accelerator. These interactions cause "direct" damage to DNA and the radiolysis of water responsible for the effects on biological tissues. The probability of occurrence of these interactions depends both on the energy of the incident photon and on the nature of the target material which is characterized by its atomic number Z.

The penetration of matter by a particle beam results in the deposition of energy in that matter. In radiotherapy, which involves a beam of photons or electrons, the aim of dosimetry is to quantitatively assess this absorbed energy in order to determine the effects of treatments on both healthy and tumor tissue. In this thesis, we focused on high-energy photon beams.

2.2 Photon energy transport and ionization

In radiotherapy, photon beams are indirectly ionizing radiation that sets charged particles (electrons and positrons) in motion within the medium; these charged particles, then, interact with the medium, resulting in biological effects.

The photoelectric effect concerns photons of low energy (energy lower than 100 keV). This interaction corresponds to a complete absorption of the incident photon which transmits all it senergy to an electron of the procession which is then ejected.

For photons with energies below about 10 eV, there is generally no ionization: the photon does not possess sufficient energy to extract an electron from the atoms or molecules of matter. Above 10 eV, the photon's energy is sufficient for ionization to be possible.
The three principal ionizing processes illustrated in **Figure I.4** are :
Photoelectrc effect **(Figure I.4 (a))** : The energy of the incident photon is totally transferred to a peripheral electron of the atom, which is expelled from its electronic shell.
Compton effect **(Figure I.4 (b))**: The incident photon's energy is partially transferred to a peripheral electron of the atom, which is ejected from its electronic shell. The remaining energy is carried away by a scattered photon.
Pair production effect **(Figure I.4 (c))**: The energy of the incident photon is completely materialized in the form of an electron positron pair under the effect of the electric field of the atomic nucleus.

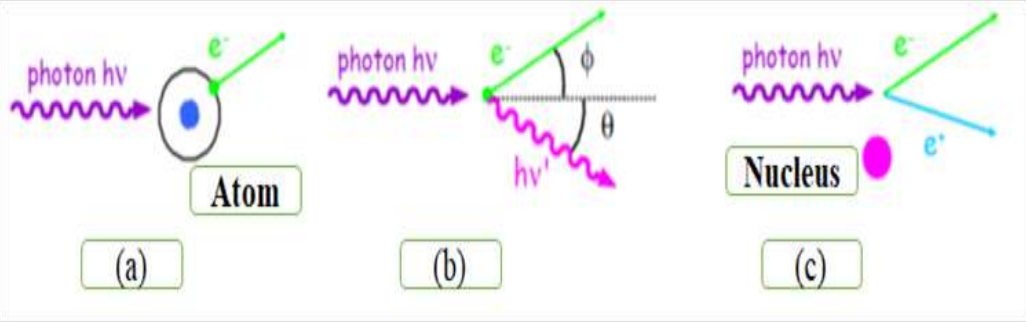

Figure I.4 – Ouabri, 2012) The three main ionizing processes of photons (a) photoelectric (b) Compton (c) pair production

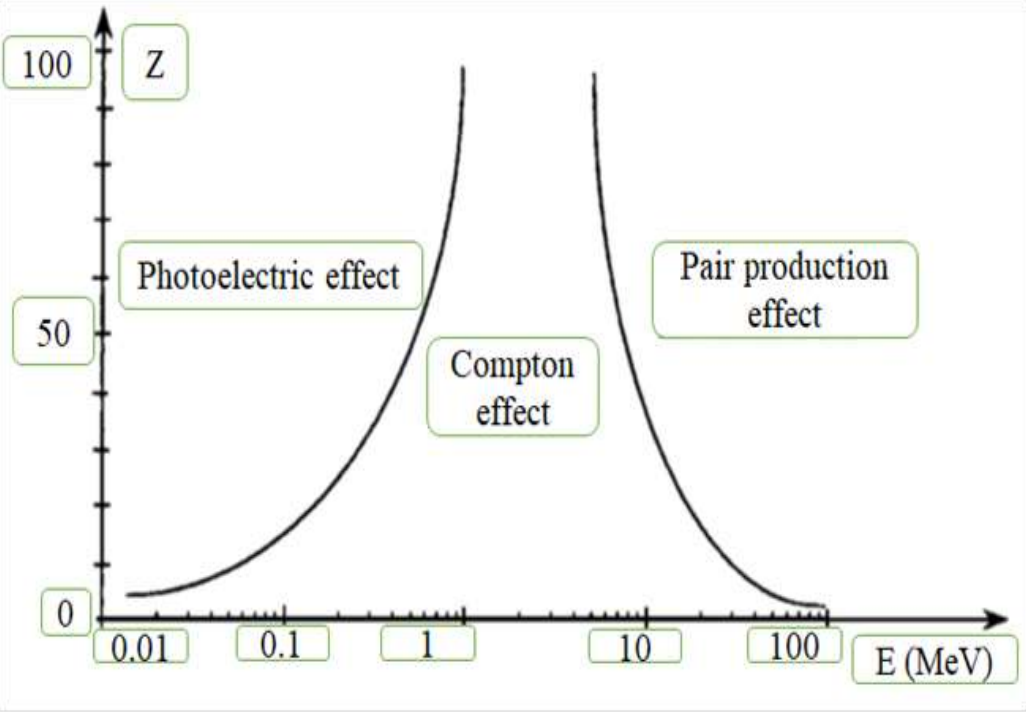

Figure I.5 – Photon interaction modes as a function of energy (Johns, et al., 1983)

In radiotherapy, the predominant interactions of high-energy photons used are : Compton effect between 0.3-20 MeV and pair production above 1.02 MeV **(Figure I.4)**. All these interactions lead to the production of high energy electrons.
When a photon penetrates matter, it's impossible to predict whether it will interact, and if so, where. The concept of probability is used to take this property into account: μ is the interaction

probability of a photon per unit length of material passed through (also known as the linear attenuation coefficient). The coefficient μ is expressed in m^{-2}. It depends only on the energy of the photon and the nature of the material. A photon always has the same probability of interacting with matter, whatever the thickness of the material it passes through. It therefore has a non-zero probability of passing through matter without interacting.

From the attenuation coefficient μ we deduce the mean free path of photons, which represents the average distance covered without interaction by photons of a given energy in a given material. This mean free path, expressed in meters, is given by :

$$l = 1/\mu \tag{I.2}$$

For example, the average free path in water for 3 MeV photons is 26 cm. This confirms the high penetration power of a high-energy photon beam. The probability of interaction μ is involved in the law that governs the attenuation of a beam N_0 of incident photons on a material of thickness x:

The number N(x) of photons that pass through a material of thickness x without interacting (the number of transmitted photons known as the primary fluence) is:

$$N(x) = e^{-\mu x} \tag{I.3}$$

Photons are attenuated exponentially with distance. Thus, the linear attenuation coefficient μ is sufficient to characterize the primary fluence at a given position.

Although it can easily be used to calculate the interaction density of primary photons, primary fluence is not sufficient to characterize the dose. The energy transferred by photons is not deposited locally, as electrons transport it over non-negligible lengths.

The Compton effect is the predominant photon-matter interaction for the energies of thephotons used for radiation therapy beams. In this case, the incident photon interacts with anelectron of the medium giving up part of its energy. The electron is then ejected and the photon is scattered with less energy,i.e.its trajectory is deviated.

Finally, pair production is an interaction generating the creation of an electron positron pairfrom a single energetic photon.This reaction occurs for photons with a minimum energy of energy of 1.022MeV, which is twice the rest mass energy of an electron(511keV).

The electrons generated by the interactions of the photons in the matter will then transfer their energy by collisions with the electrons of the medium generating the excitation and ionization of the matter.their energy by collisions with the electrons of the medium generating the excitation and the ionization of the matter.

2.3 Energy deposition by electrons

In the energy deposition mechanism, the secondary electrons set in motion interact with the peripheral electrons of the atoms in the medium, and consequently the electron can ionize several atoms in its path.The main interactions of electrons with atoms are :

elastic scattering: Elastic scattering (or elastic collision) is an interaction between two or more objects in which the total kinetic energy is conserved, but the directions of propagation are changed.

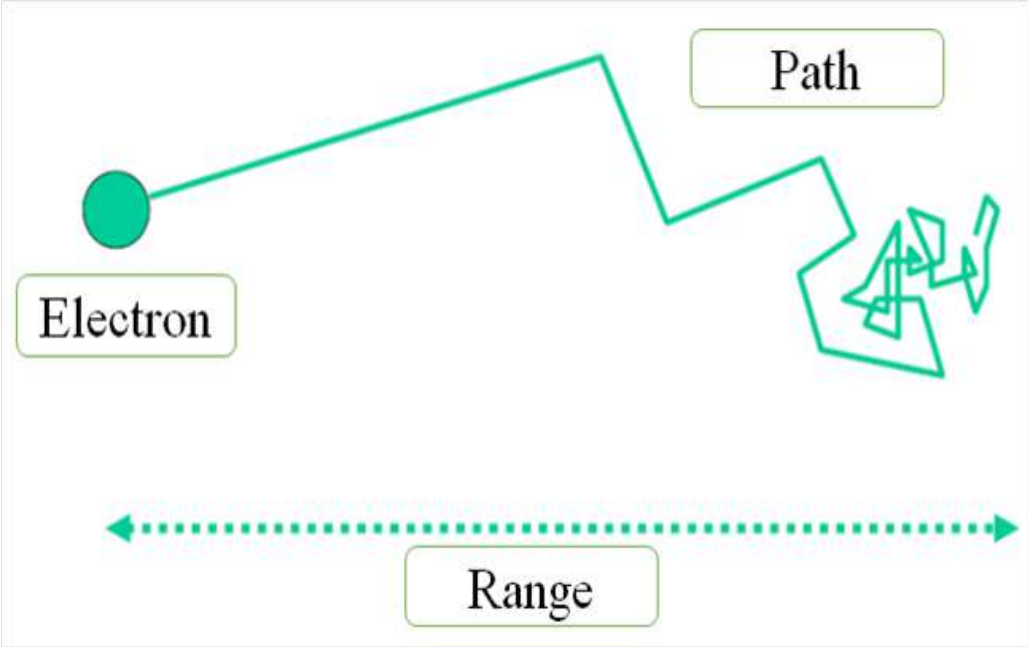

Figure I.6 – Photon interaction modes as a function of energy (Johns, et al., 1983)

inelastic scattering: which causes an electron to be ejected from the atom, at the cost of losing the energy of the incident electron.

braking radiation (bremsstrahlung): the electron is slowed down and deflected when it passes near an atomic nucleus. The energy lost by the electron is carried away by a photon, known as the secondary photon, which can interact with matter further away. This process, although small, is not negligible in the calculations and explains why a non-zero dose deposit is observed outside the beam, at a distance well beyond the range of the electrons (see below).

The trajectory of an electron is highly random, and its path through matter is of limited length, as shown in **Figure I.6**. The average distance of an electron's path is proportional to

its initial energy, and inversely proportional to the material's electron density:
-the higher the electron's energy, i.e. the faster it moves, the longer its path will be
-the greater the electron density of the medium, the more the electron interacts, and the shorter its path.

Electrons have a much shorter range than photons. As an example, the range of an electron of 1 MeV is approximately 0.4 cm in water, while the mean free path of a photon of the same energy is 14 cm. In other words, electrons are rapidly absorbed and deposit all their energy in the tissue in the form of ionizations, enabling the high doses needed to sterilize tumors.

2.4 Photon fluence and energy fluence:.

The quantities used for ionizing radiation dosimetry have been defined in ICRU Report 85 [ICRU, 2011].
The fluence ϕ of a particle beam is the number of incident particles dN passing through an assumed small surface dA perpendicular to it, and defined as the quotient of dN by dA, where dN is the number of particles incident on a sphere of cross-sectional area dA:

$$\phi = \frac{dN}{dA} \tag{I.4}$$

the unit of fluence is m^{-2}

The energy fluence ψ is the quotient of dE by dA, where dE is the radiant energy incident on a sphere of cross-sectional area dA:

$$\psi = \frac{dE}{dA} \tag{I.5}$$

the unit of energy fluence is $J.m^{2}$

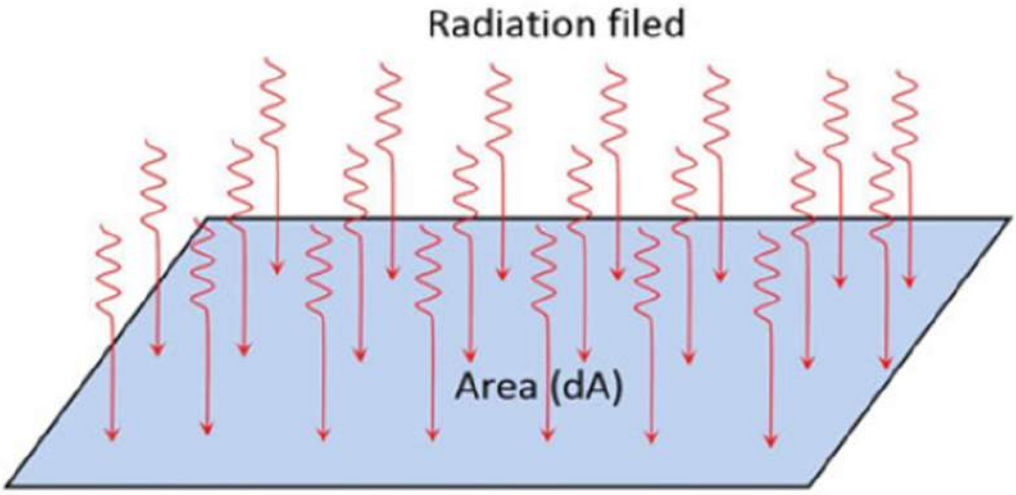

Figure I.7 – Particle/energy incident on a unit area [29].

Energy fluence can be calculated from particle fluence by using the following relation:

$$\psi = \frac{dN}{dA}E = E\phi \tag{I.6}$$

Where E is the energy of the particle and dN represents the number of particles with energy E. Almost all realistic photon or particle beams are polyenergetic, and the above defined concepts need to be applied to such beams. The concepts of particle fluence spectrum and energy fluence spectrum replace the particle fluence and energy fluence, respectively. The particle fluence spectrum differential in energy:

$$\phi_E(E) = \frac{d\phi}{dE}(E) \tag{I.7}$$

The energy fluence spectrum differential in energy:

$$\psi_E(E) = \frac{d\psi}{dE}(E) = \frac{d\phi}{dE}(E) \tag{I.8}$$

The particle fluence rate ϕ is the quotient of dϕ by dt, where d$\hat{\text{I}}$¦ is the increment of the particle fluence in time interval dt:

$$\phi = \frac{d\phi}{dt} \tag{I.9}$$

Unit of particle fluence rate is $m^{-2}.\ s^{-1}$ [30]

2.5 Terma, Kerma and absorbed dose

In Figure I.8, we consider an elementary sphere of mass dm, centered on P, within the irradiated material. For the duration of the irradiation, a certain number of photons penetrate the sphere, carrying an energy dwe. During the same period, photons that have passed through the sphere without interaction leave it. Assume that dws is the total energy of the photons leaving the sphere.

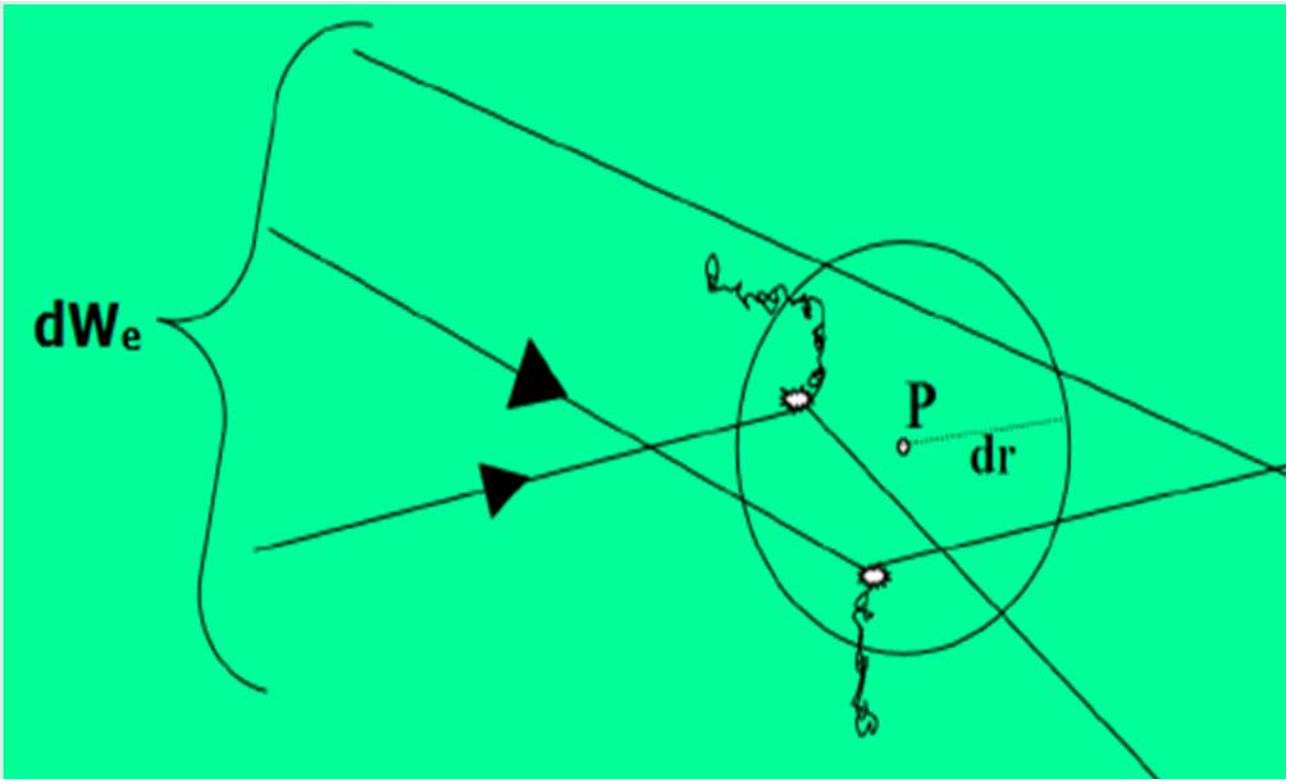

Figure I.8 – The kerma within the sphere (Vuillez, 2009)

$$dW_t = dw_e - dw_s \tag{I.10}$$

dW_t represents the total energy released per unit mass. The ratio of dwt to the mass of matter is called Terma (Total Energy Released per Mass):

$$T = \frac{dw_t}{dw_m} \tag{I.11}$$

Among this total energy released, part is transferred in the form of kinetic energy to charged particles, noted dwtr . The quotient per mass of matter is called kerma (kinetic energy released per mass unit), denoted K :

$$K = \frac{dw_{tr}}{dm} \tag{I.12}$$

The unit of kerma is the gray, abbreviated Gy, with 1 Gy equal to 1 J/kg.

Electrons set in motion in the sphere lose energy either by collision or by emitting braking radiation. The part of the kerma due to these two phenomena is identified as collision kerma and radiative kerma respectively. Note that the energy transferred in collision kerma is not necessarily absorbed in the sphere, since electrons may leave it.
The kinetic energy dwtr released to the electrons inside the sphere will be partially absorbed inside and partially outside the sphere. assume that dw_a is the absorbed energy inside the sphere, from electrons set in movement inside (dw_2 and dw_3) as well as outside (dw_1),illustrated in **Figure I.9**. The absorbed dose, denoted D, is the ratio of dwa to the mass of matter.

$$D = \frac{dw_a}{dm} \tag{I.13}$$

$$dw_a = dw_1 + dw_2 + dw_3 \tag{I.14}$$

In water, an absorbed dose of 1 Gy corresponds to a temperature rise of around $2 - 10^{-4} dgreeC$(Vuillez, 2009).

In most cases, only part of the energy carried away by electrons when ionizing radiation interacts with a material medium at a point P is actually absorbed in the volume element dv surrounding the point P (dw_2 and dw_3), while the rest of the transferred energy is absorbed outside the volume element.On the other hand, it absorbs all or part of the energy of electrons created externally but entering the volume element dv (dw_1). This implies that, automatically, collision kerma and absorbed dose are different. Under certain conditions, however, these two sources of difference compensate each other perfectly, resulting in equality between absorbed dose and collision kerma. To establish this relationship, the energy carried away by secondary electrons leaving the volume element in question must be compensated by the energy deposited in it by other secondary electrons produced in neighbouring elements. This situation is known as electronic equilibrium. To achieve electronic equilibrium, the following conditions must be met:

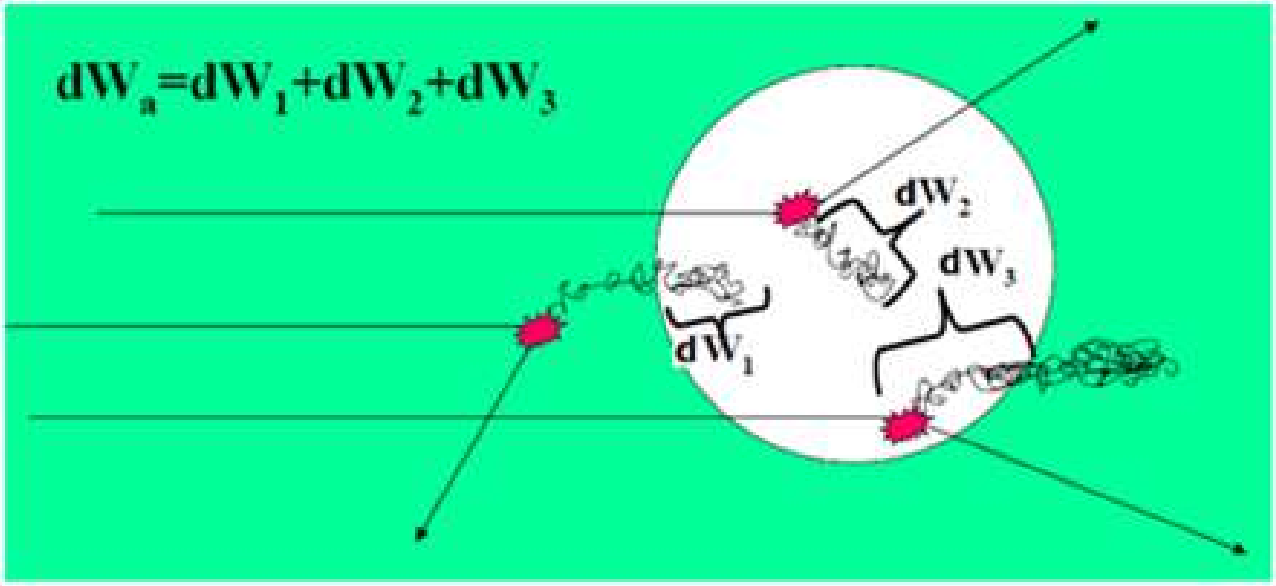

Figure I.9 – The absorbed dose in the sphere (Vuillez, 2009)

- The volume dv of mass dm is immersed in a much larger volume V of homogeneous matter, whose dimensions are commensurate with the range of the electrons.
- The radiation field is uniform (or can be considered as such) over V.

$$b = Dose/K_c \tag{I.15}$$

When high energy photons penetrate the medium, K_c is at its maximum at the surface of the irradiated material, because photon fluence is high at the surface, then decreases with depth. This process leads to an increase in the fluence of the secondary electrons, and therefore to an increase in the absorbed dose D, until the depth Ze or the dose reaches its maximum. At this level, entrance and exit fluences are balanced: photon fluence (approximate, as fluence decay is not perceptible over a small volume) and secondary electron fluence; they then decay at the same time. Three regions of b are defined:

b<1: D increase and Kc decrease
b=1: D=K_c (electronic equilibrium)
b>1: D and Kc decrese parallelly (electronic equilibrium) The curve shows how collision kerma and absorbed dose vary with depth.

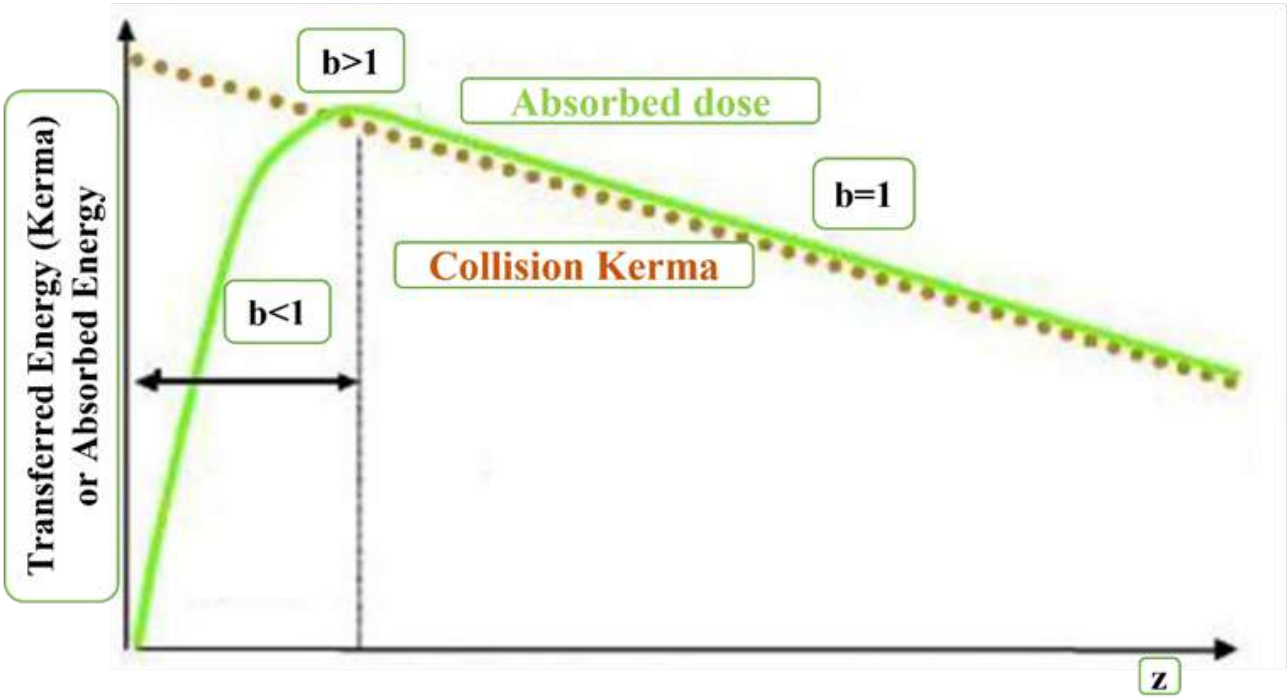

Figure I.10 – collision and absorbed dose as a function of depth in a medium (Gambini, et al., 2007)

The collision kerma is proportional to the fluence w (unit m^{-2}), the mass energy absorption coefficient μ_{en}/ρ (unit $m^{-2}\ kg^{-1}$), and the energy E of the incident photon. In a medium X :

$$K_c^X = E(\frac{\mu_{en}^X}{\rho^X})\omega \tag{I.16}$$

Consequently, for the same photon beam projected into two different media, the collision kerma ratio between medium A and medium B is :

$$\frac{K_c^A}{K_c^B} = \frac{\mu_{en}^A}{\rho^A} / \frac{\mu_{en}^B}{\rho^B} \tag{I.17}$$

If electronic equilibrium is achieved ("collision kerma" and "dose" are equal) :

$$\frac{Dose^A}{Dose^B} = \frac{\mu_{en}^A}{\rho^A} / \frac{\mu_{en}^B}{\rho^B} \tag{I.18}$$

Since electron disequilibrium phenomena are similar and occur in the same sense in all materials, we can extend the formula to first order and calculate the dose in a given medium by knowing the dose in a reference medium for the same photon beam.

2.6 Biologically Effective Dose

The biological effective dose or BED [Jones et al., 2000] is a quantity based on absorbed dose, which takes into account the fractionation regime used during radiotherapy treatment and the radiosensitivity of biological tissues. This concept is based on the quadratic linear model [Rossi and Kellerer, 1972]. This model describes cell survival according to the following equation (1.4):

$$S = e^{-(\alpha d + \beta d^2)} \tag{I.19}$$

Where S is the probability of cell survival, α is the probability of a cell-lethal event, β is the probability of a sublethal event, and d is the absorbed dose to the cells.The α/β ratio corresponds to the dose for which cell death is due in equal proportion to lethal damage and the accumulation of sublethal damage. This ratio is specific to each tissue and depends on its biological repair properties.
The BED, expressed in gray (Gy), is calculated as follows:

$$BED = nd(1 + \frac{d}{\alpha/\beta}) \tag{I.20}$$

Where n is the number of treatment fractions and d the dose delivered for a treatment fraction. This quantity is used clinically to optimize the dose per fraction and the number of fractions in relation to the effects on biological tissues.

2.7 Equivalent dose and effective dose

In the field of radiation protection, absorbed doses expressed in gray (Gy) are converted into equivalent dose conventionally noted H and effective dose E. These two quantities are expressed in sieverts (Sv. The equivalent dose allows the radiological effect of particles to be taken into account by a factor characteristic of the radiation involved, noted W_R. The effective dose is based on the equivalent dose but also takes into account the specific radiosensitivity of each organ by applying a tissue weighting factor called W_T [CIPR 60, 1991 ; CIPR 92, 2003 ; CIPR 103, 2007].

2.8 Electronic equilibrium :

In an absorbing medium, KERMA decreases continuously with increasing depth. This is due to the continuous decrease in the flux of indirectly ionizing radiation. On the other hand, the absorbed dose is initially lower than KERMA level at the surface and below the surface (to

some extent) in the medium. The increasing trend of absorbed dose continues until a maximum is reached. After reaching a maximum value, the dose starts decreasing with increasing depth. The ratio of dose and collision kerma is often denoted as:

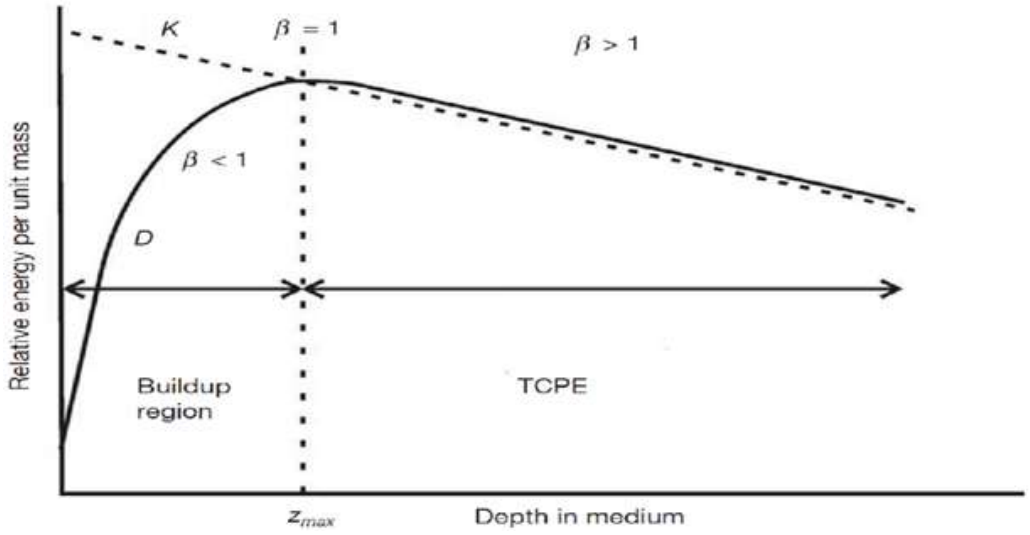

Figure I.11 – Illustration of the relationship between absorbed dose D and collisional kerma K_{col}. [31]

$$\beta = \frac{D}{K_{col}} \tag{I.21}$$

The buildup region $\beta < 1$
The region between the surface (z=0) and depth $z = z_{max}, \beta = 1$

In the hypothetical situation where charged particle equilibrium (CPE) is established and no photon attenuation occurs β equals unity. CPE exists in a volume, if each charged particle of given energy leaving the volume is replaced by an identical particle.

$$D = K_{col} \tag{I.22}$$

The region of transient charged particle equilibrium $\beta > 1$.
Due to the attenuation of photons in reality, a complete CPE is never achieved, but a transient CPE (TCPE) can be defined.
In TCPE region, kerma and dose are attenuated exponentially (solid curves) with

$$D > K_{col} \tag{I.23}$$

3 Volumes of interest in radiotherapy

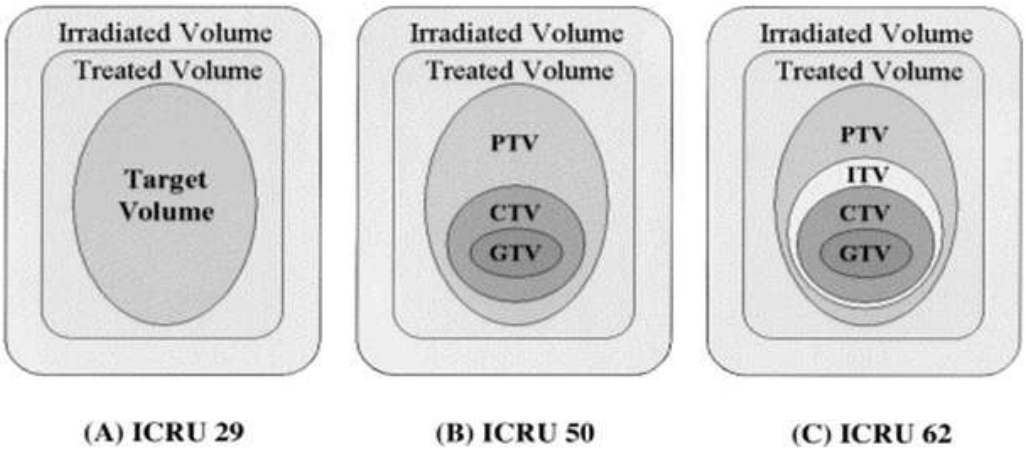

Figure I.12 – Schematic illustration of the boundaries of the volumes defined by ICRU reports (A) Report 29, (B) Report 50, (c) Report 62.

3.1 Gross Tumor Volume: GTV

The gross tumor volume (GTV) is the gross palpable or visible/demonstrable extent and location of the malignant growth. The GTV may consist of primary tumor (GTV-T), metastatic lymphadenopathy (GTV-N), or other metastases (GTV-M). The GTV corresponds almost always to those parts of the malignant growth where the tumor cell density is the highest. If the tumor has been removed prior to radiotherapy then no GTV can be defined. [32]

3.2 Clinical Target Volume: CTV

The clinical target volume (CTV) is a tissue volume that contains a demonstrable GTV and/or is considered to contain microscopic, subclinical extensions at a certain probability level. [32]

3.3 Internal Target Volume: ITV

The internal target volume (ITV) is referred to the patient coordinate system and is defined by the internal margin (IM). An internal margin (IM) must be added to the CTV to compensate for physiologic movements and the variations in size, shape, and position of the tissues which contain or are adjacent to the CTV, resulting from e.g.: respiration, variable filling of the bladder, variable filling of the rectum, swallowing, heartbeat, movements of the bowel.[32]

3.4 Planning Target Volume: PTV

It is a geometrical concept, and is defined to select appropriate beam sizes and arrangements, taking into consideration the net effect of all possible geometrical variations, in order to ensure that the prescribed dose is actually absorbed in the CTV. [32]

3.5 Organs at Risk: OAR

Organs at Risk ("critical normal structures") are normal tissues whose radiation sensitivity may significantly influence treatment planning and/or prescribed dose. [32] Any movements of the OARs, as well as uncertainties in the set-up must be considered, thus an integrated margin has to be added to the OAR which leads, by analogy with the PTV, to the concept of Planning Organ at Risk Volume (PRV).

3.6 Treated volume:

Due to the limitations of irradiation techniques and in some specific clinical situations, the volume receiving the prescribed dose may not accurately match the PTV; it may be larger (sometimes much larger) and in general of a simpler shape. This leads to the concept of treated volume.
The treated volume is the tissue volume which is planned to receive at least a dose selected and specified by the radiation oncologist as being appropriate to achieve the purpose of the treatment (tumor eradication, or palliation) [32].Usually taken as the volume enclosed by the 95 per cent isodose curve.

3.7 Irradiated volume:

The irradiated volume is the tissue volume which receives a dose that is considered significant in relation to normal tissue tolerance. [32] Usually taken as the volume enclosed by the 50 pe cent isodose curve

4 Conventional and modern radiotherapy techniques:

4.1 3D conformal radiotherapy

In conformal radiation therapy treatment fields are shaped to conform to the target volume in order to reduce the dose to normal tissues. Relatively uniform radiation intensities are

delivered over the beam's aperture and organs at risk are protected by adequate selection of beam orientations. Thus, a high dose is delivered to the target volume, where all treatment fields overlap, while lower doses are given to regions avoided by some of the fields [30, 33].
In the past, fields were shaped by means of customized blocks that were fixed to trays and placed in the accessory holder, at the end of the treatment head. However, the construction of these individualized blocks was tough and time consuming. Moreover, their use reduced the clearance between the treatment head and the patient's skin and introduced interruptions between treatment fields, since blocks had to be placed manually. Nowadays, MLCs have replaced these customized blocks, avoiding the need for mould room time, for carrying heavy trays and for interrupting treatment sessions.

4.2 Advanced radiotherapy techniques

Advanced radiotherapy techniques offer a significant improvement in dose distribution precision and better dose conformation to the tumor **Fig I.13** compared to conventional techniques. This customization of the isodose shape to the target volume enables the treatment of complex tumor volumes with irregular or concave shapes. consequence, these new techniques enable higher doses to be delivered to the PTV while sparing healthy tissue close to the tumor.

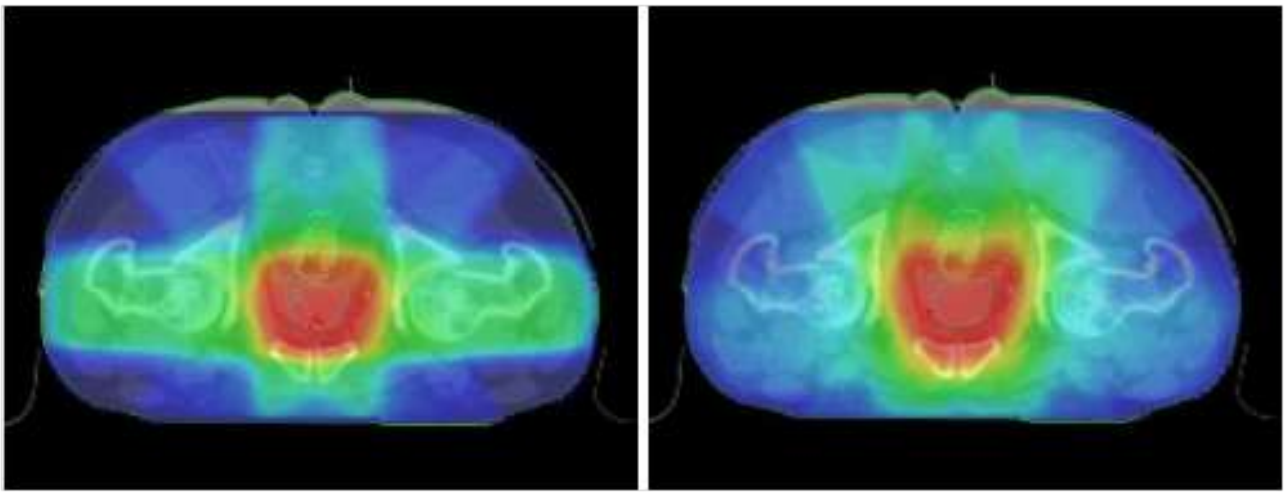

Figure I.13 – Dose distributions obtained with 3D conformal radiotherapy (middle), and intensity-modulated radiotherapy (right) for prostate treatment

The technological advances associated with these techniques are intensity modulation of the treatment beams, i.e. modulation of photon fluence within the beam **Fig I.14**, and the

use of inverse virtual planning. This consists in selecting the parameters of the desired dose distribution in terms of prescribed dose and target coverage, and also in terms of dose constraints on the organs at risk. The TPS then calculates the processing beams required to satisfy these criteria. If the user deems the plan unacceptable, he can modify the constraints set or modify the beams number and orientation. This optimization is carried out iteratively. Modulation of the beams to satisfy the constraints is carried out automatically by the software. Finally, treatments are monitored by on-board imaging, enabling precise repositioning of the patient in relation to the planning before and during treatment.

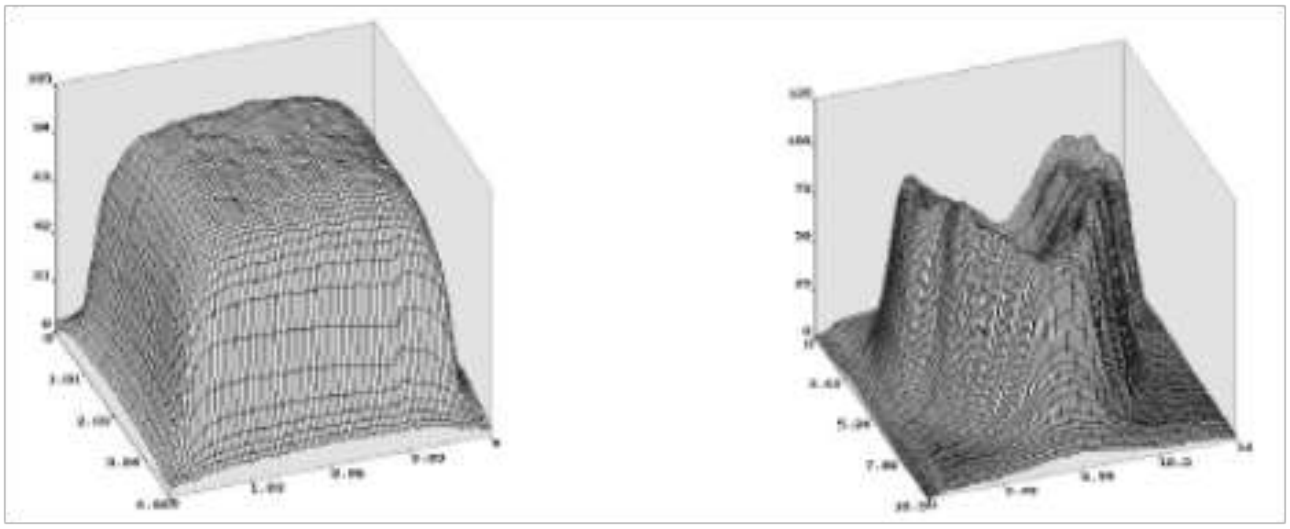

Figure I.14 – Fluence profile of a conventional beam (left) and an intensity-modulated beam (right)

Intensity Modulated Radiation Therapy (IMRT) is an evolution of conformal radiotherapy. Developed in the late 1990s, IMRT not only allows radiation to be shaped to the contour of the target area, but also uses multiple angular radiation beams and non-uniform intensities.
The primary objective of IMRT is to reduce dose to selected normal tissue structures in an effort to preserve function, while maintaining full dose delivery to tumor targets.
The delivery of IMRT with a multileaf collimator (MLC) requires the delivery of radiation from several beam orientations. The intensity profile for each beam direction is described as a MLC leaf sequence, which is developed using a leaf sequencing algorithm **Fig I.15**.

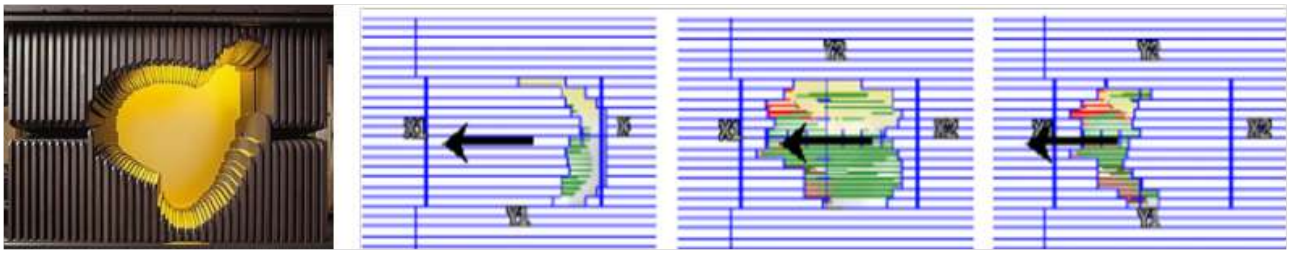

Figure I.15 – Multi-leaf collimator (left) and MLC movement during treatment(right)

The purpose of the leaf sequencing algorithm is to generate a sequence of leaf positions and/or movements that faithfully reproduce the desired intensity map once the beam is delivered, taking into consideration any hardware and dosimetric characteristics of the delivery system. The two most common methods of IMRT delivery with computer-controlled MLCs are the segmental multileaf collimator (SMLC) and dynamic multileaf collimator (DMLC).
In SMLC the beam is switched off while the leaves are in motion. In other words, the delivery is performed via multiple static segments or leaf settings. This method is also frequently referred to as the "step and shoot" method. In DMLC the beam is on while the leaves are in motion. The beam is switched on at the start of treatment and is switched off only at the end of treatment.
The fundamental difference between these two delivery methods is that the leaf-sequencing algorithm defines the sub-field shapes for SMLC-IMRT and trajectories of opposing pairs of leaves for DMLC-IMRT.

Volumetric modulated arc therapy (VMAT) makes it possible to deliver complex treatments on one or more arcs (or half-arcs) during which the gantry performs a continuous rotation around the patient **Fig I.16**. This technique is used with conventional acceleration. Dose rate, gantry rotation speed, collimator rotation and leaf movement speed are computer-adjusted to optimize dose deposition.

Helical tomotherapy delivers slice-by-slice treatment with simultaneous rotation of the gantry and translation of the table on which the patient is positioned. These movements are continuous throughout the irradiation. Treatment is delivered using a fine, fan-shaped, intensity-modulated beam, which is followed by imaging using the dedicated megavolt scanner (MV CT)**Fig I.16**.
For all these intensity-modulated techniques, treatments are conventionally performed with photon beams at 6 MV accelerating voltage [Cosset et al., 2019].

Finally, stereotactic radiotherapy was introduced in the 1950s to treat intracranial targets. In this case, the treatment is delivered in a hypofractionated manner (generally 5 fractions or less) with high doses per fraction, unlike normo-fractionated treatments. In recent years, the technique has benefited from the development of simultaneous imaging-guided treatment techniques and improved ballistics down to sub-millimetre precision, and has been extended to the treatment of small inoperable extra-cranial targets, notably the lungs, under the acronym SBRT: *"stereotactic body radiation therapy"* [Xu et al., 2008].

Figure I.16 – Principle of VMAT radiotherapy (left) and helical tomotherapy (right)

Treatments are delivered by a multitude of mini beams, often non-coplanar. This provides excellent control of the irradiated volume, with significant dose gradients dose to target volume, and real-time monitoring of mobile tumors. Initially developed for the treatment of early-stage tumors, it is today increasingly used for re-irradiation following tumor relapse or the appearance of a metastasis (lung, kidney, liver). metastasis (notably of the lung), due to the reduced overlapping of irradiated volumes compared with conventional radiotherapy [Peulen et al., 2011]. The machines used today to perform these treatments are the Cyberknife (Accuray), the Gamma-knife (Elekta) or a conventional linear accelerator with specific collimators (conical or mini-MLC collimators)**Fig I.16**.

4.3 The inverse optimization

Inverse optimization is a mathematical approach commonly used in fields such as engineering, physics, and computer science. In the context of radiation therapy and medical imaging, it

refers to a technique that aims to determine the best parameters or settings for a system in order to achieve a desired outcome.

In radiation therapy, for example, the goal is to deliver a specific dose of radiation to a tumor while minimizing the dose to healthy surrounding tissues. Instead of manually setting the parameters of the treatment plan, inverse optimization involves specifying the desired radiation dose distribution within the patient's body. The optimization algorithm then calculates the optimal settings for the treatment machine, such as the angles and shapes of radiation beams, to achieve the desired dose distribution.

This approach is called "inverse" optimization because it works in the opposite direction of traditional optimization methods. Instead of starting with parameters and calculating outcomes, it starts with desired outcomes and calculates the necessary parameters. In essence, it's about working backwards to find the inputs that will lead to the desired results.

Inverse optimization can lead to more effective treatment plans, as it considers the clinical goals and constraints upfront, allowing for a more tailored and patient-specific approach. This technique is particularly valuable in complex systems where finding a suitable solution through traditional methods might be challenging or time-consuming.

4.4 dose deposition

The modulation-different intensities for bixels-is possible due to the MLC. The collimator consists of several pairs of leaves that can move and block parts of the radiation beam. Each beam subdivides into beamlets (fractions of a beam). Each sub-unit of a treatment field is referred to as a bixel(**Fig.I.11**. This approach leads to a discretization of the radiation beam to a matrix of intensities, generally called intensity profile or fluence map **(Fig.I.12**, that maps coordinates within the beam to its respective intensity. The MLC modulates the intensity of a bixel by opening and closing the leaves for a fixed period, or by definitely blocking some areas that receive no radiation. The measure for the period the leaves remain open is monitor units. [On the three-objective static unconstrained leaf sequencing in IMRT Hudson Medeiros,Elizabeth Ferreira, Gouvea Goldbarg ,Marco Cesar Goldbarg]

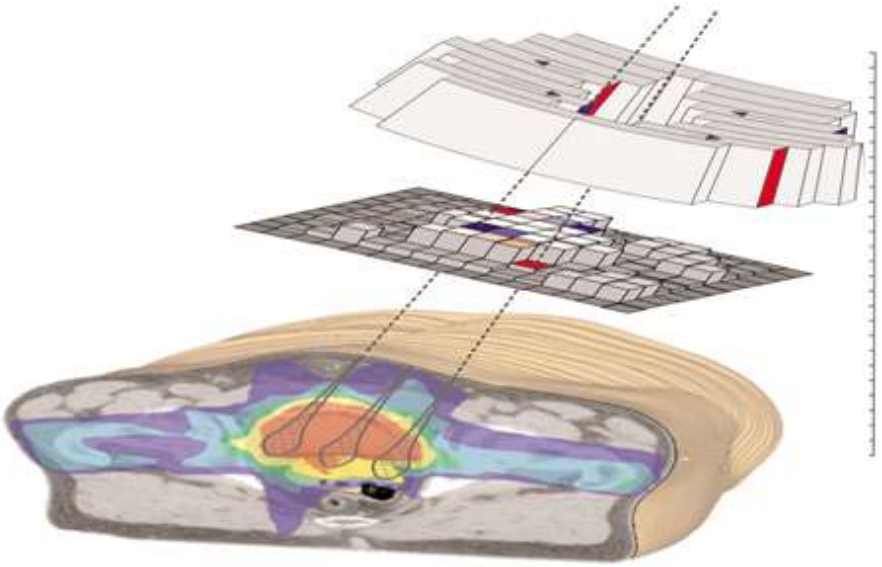

Figure I.17 – The shape of the MLC gives rise to a particular distribution of bixel fluences, which in turn contributes to the dose distribution in the patient volume.
On the three-objective static unconstrained leaf sequencing in IMRT Hudson Medeiros,Elizabeth Ferreira, Gouvea Goldbarg ,Marco Cesar Goldbarg

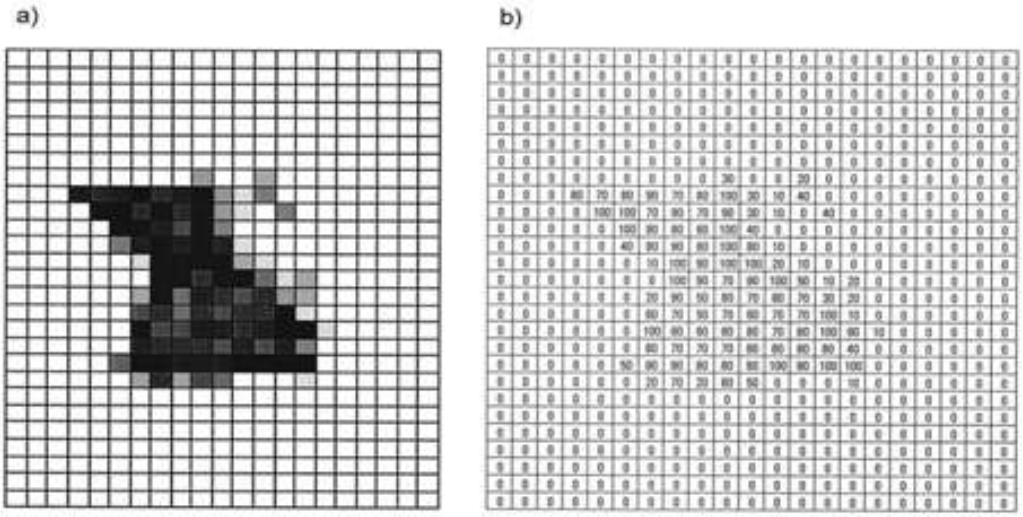

Figure I.18 – A typical a) intensity map and b) its matrix representation.[leaf sequencing techniques for mlc-based imrt cheng b. saw, ph.d., r. alfredo c. siochi, ph.d., komanduri m. ayyangar, ph.d., weining zhen, m.d., and charles a. enke, m.d. Department of Radiation Oncology, University of Nebraska Medical Center, Omaha, NE; Physics and Microwave Engineering, Siemens Medical Systems, Oncology Care Systems, Concord, CA 94520]

If we considered the patient is discretized into n voxels indexed by $i \in 1..., n$ and around him, l beams, indexed by $k \in 1..., n$ are set up, each composed of r bixels, indexed by $j \in 1..., n$. Then, the resulting dose distribution from several beam fluences can be presented as the sum of the dose distributions of each individual beam fluence.

$$d_i = \sum_{k=1}^{l} \sum_{j=1}^{r} p_{ijk} x_{jk} \tag{I.24}$$

Where p_{ijk} denotes the dose deposited into voxel i by bixel j of beam k at unit fluence and x_{jk} Is the fluence of jth bixel of beam k.

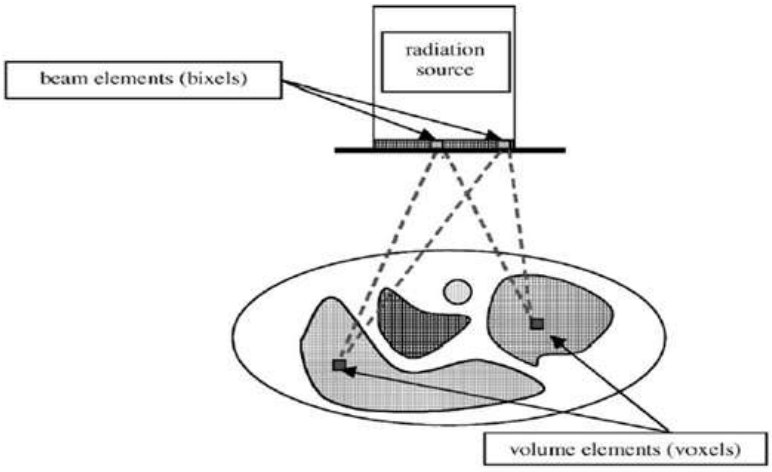

Figure I.19 – Volume elements and beam elements. Hamacher H. and Kufer K-H. Inverse radiation therapy planning|a multiple objective optimization approach. Discrete Applied Mathematics, 2002.

Equation (IV.1) can then be written as a linear system: d=Px
We assume that we have to consider s well-defined parts of the body (Fig. IV.3), where the target volume (i.e., the tumor) is indexed with s=1, and the risk organs are indexed with s=2....S . If written separately for each body part we get

$D_1 = P_1$ x s=1, target dose

$D_s = P_s$ x s=2,...,s, doses in organs at risk

Accordingly, the dose vectors in the s body parts should satisfy the following system of linear inequalities (dose constraints) in terms of the unknown intensity profilex:

$D_1 = P_1 \geqslant L_1 e$ x s=1

$D_s = P_s \leqslant U_s e$ x s=2,...S

L_s and U_s represent the desired minimum and maximum dose levels of the target and of the

organs at risk, respectively. The vector e contains entries equal to one in each component.

4.5 The objective function:

Once the ROIs are defined, it is possible to formulate objectives and constraints based on the desired clinical outcomes. In practice, there are several objectives $f_1, ..., f_N$ which should be minimized in order to achieve the optimal plan. These objectives are often in partial conflict with each other (Some objective might penalize target underdosage, while another penalizes the overdosage of some organ nearby). This gives a total objective function the form : Mathematical Optimization of Radiation Therapy Goal Fulfillment Biorn Andersson

$$f(x) = w_i f_i(x) \tag{I.25}$$

♣ The objective function: example of "beamlet" method The dose at a voxel i can be presented as the sum of dose contributions from all the beamlets 1,2,...,k from all beams, weighted by w_k:

$$D_i = \sum_{k=1}^{l} w_k D_{k,i} \tag{I.26}$$

Where $D_{(k,i)}$ denotes the dose released to voxel i by the k^th beamlet, and $w_{(k)}$ is the weight for the k^{th} beamlet, and can be vary to obtain the respect of the clinical objectives If D_p is the dose objective in the voxel i, the best D_i is equal to D_p:

$$D_i - D_{p_i} = ((\sum_{k=1}^{l} w_k D_{k,i}) - D_{pi}) = 0 \tag{I.27}$$

With this formalism a function can be written:

$$F_{obj}(w) = \sum_{i=1}^{n} (D_i - D_p)^2 = \sum_{i=1}^{n} ((\sum_{k=1}^{l} w_k D_{i,k}) - D_p)^2 \tag{I.28}$$

Ideally the best solution is the set of w_k that give a value equal to 0 for the objective function which is impossible hence, the absolute minimum of the objective function will be an optimal solution to this problem
The minimum of a function is equivalent to set its derivate to 0:

$$\bigtriangledown F_{obj}(w) = 0 \tag{I.29}$$

$$P\sum_{i=1}^{n}(D_i - D_p)^2 = 0 \tag{I.30}$$

$$P\sum_{i=1}^{n}((\sum_{k=1}^{l} w_k D_{ik}) - D_p)^2 = 0 \tag{I.31}$$

Where P is the priority for a ROI. [34]

5 Tools related to spatial dose distribution

5.1 The Dose Variation throughout the Planning Target Volume:

As a minimum requirement, the maximum dose and the minimum dose to the PTV shall be reported, together with the dose at the ICRU Reference Point. The three dose values then represent the dose to the Clinical Target Volume and the dose variation.

• **Minimum dose D_{min}:**

The minimum dose is the smallest dose in a defined volume. In contrast to the situation with the maximum absorbed dose, no volume limit is recommended when reporting minimum dose. The Minimum Planning Target Dose is the lowest dose in the Planning Target Volume.

• **Maximum dose D_{max}:**

The maximum dose to normal tissues is of importance for limiting and for evaluating side-effects of treatment. However, a significant tissue volume must be irradiated for the dose level to be reported as maximum.

The Maximum Dose to the PTV has to be taken into account for evaluating the homogeneity of the dose distribution (part of the optimization criteria). When the maximum dose outside the PTV exceeds the prescribed dose, then a "hot spot" can be identified [35].

5.2 Hot spots

A hot spot represents a volume outside the PTV which receives a dose larger than 100 per cent of the specified PTV Dose. It is considered significant only if the minimum diameter exceeds 15 mm (in a small organ like eye, optic nerve, larynx, a dimension smaller than 15 mm has to be considered) [36].

5.3 Gamma index

The gamma index γ is one of the most commonly used metrics for the verification of complex radiotherapy deliveries such as intensity modulated radiotherapy (IMRT) and volumetric modulated arc radiotherapy (VMAT).

The gamma value is a measure of a two-component user-selected criterion consisting of distance-to-agreement (DTA) and dose-difference [36]. The criterion for acceptable calculation performance is generally defined as a tolerance of the dose and DTA in regions of low and high dose gradients, respectively. The DTA is the distance between a measured data point and the nearest point in the calculated dose distribution that exhibits the same dose. A dose-difference distribution can be displayed that identifies the regions where the calculated dose distributions disagree with measurement. The dose difference and DTA distributions complement each other in their useful regions [37].

The γ is calculated based on finding the minimum Euclidean distance for each reference point. For each reference point in the dose distribution, calculate against each point in the evaluated distribution:

- the distance between reference to evaluated point
- the dose difference between the reference and evaluated point

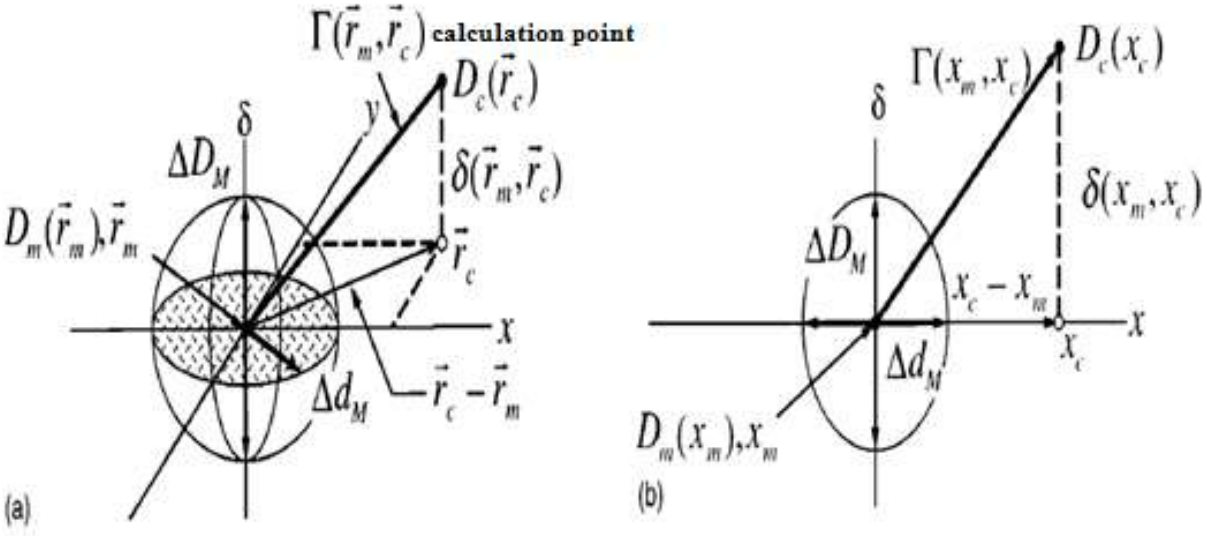

Figure I.20 – Geometric representation of dose distribution evaluation criteria using the combined ellipsoidal dose-difference and distance-to-agreement tests. (a) Two-dimensional representation. (b) One-dimensional representation.

$$\Gamma(r_m, r_c) = \sqrt{\frac{r^2(r_m, r_c)}{\Delta d_M^2} + \frac{\delta^2(r_m, r_c)}{\Delta D_M^2}} \tag{I.32}$$

$r(r_m, r_c) = |r_c, r_m|$

$\delta(r_m, r_c) = D_c(r_c) - D_m(r_m)$

ΔD_M: the dose difference criterion

Δd_m: the distance to agreement (DTA)criterion

$$\gamma(r_m) = min\Gamma(r_m, r_c) \forall r_c \tag{I.33}$$

$\gamma(r_m) \leq 1$; calculation passes

$\gamma(r_m) > 1$: calculation fails

6 Tools related to volumetric dose distribution

6.1 Dose volume histograms

Evaluation of treatment plans for the determination of best plan among the different plans is done by analysis of dose volume histogram (DVH) as well as two-dimensional and three-dimensional spatial dose distributions.

A dose-volume histogram is created by dividing a volume into a three-dimensional grid of volume elements, known as voxels. The size of the voxel element is small enough such that an assumption can be made that the dose delivered to one voxel is constant within the voxel. In order to evaluate the dose delivered to each voxel a DVH is calculated using bins of equal dose. The volume of interest is divided into dose bins and the voxels are sorted according to their dose bins with no regard for anatomical location [38].
A dose-volume histogram is a two-dimensional graph that comes in one of two standard forms: a differential DVH or a cumulative DVH

Cumulative dose volume histogram (cDVH) :
The cumulative DVH is the standard method of viewing dose volume histograms because it

offers easily interpreted data which a physician can quickly review **Fig I.21**.

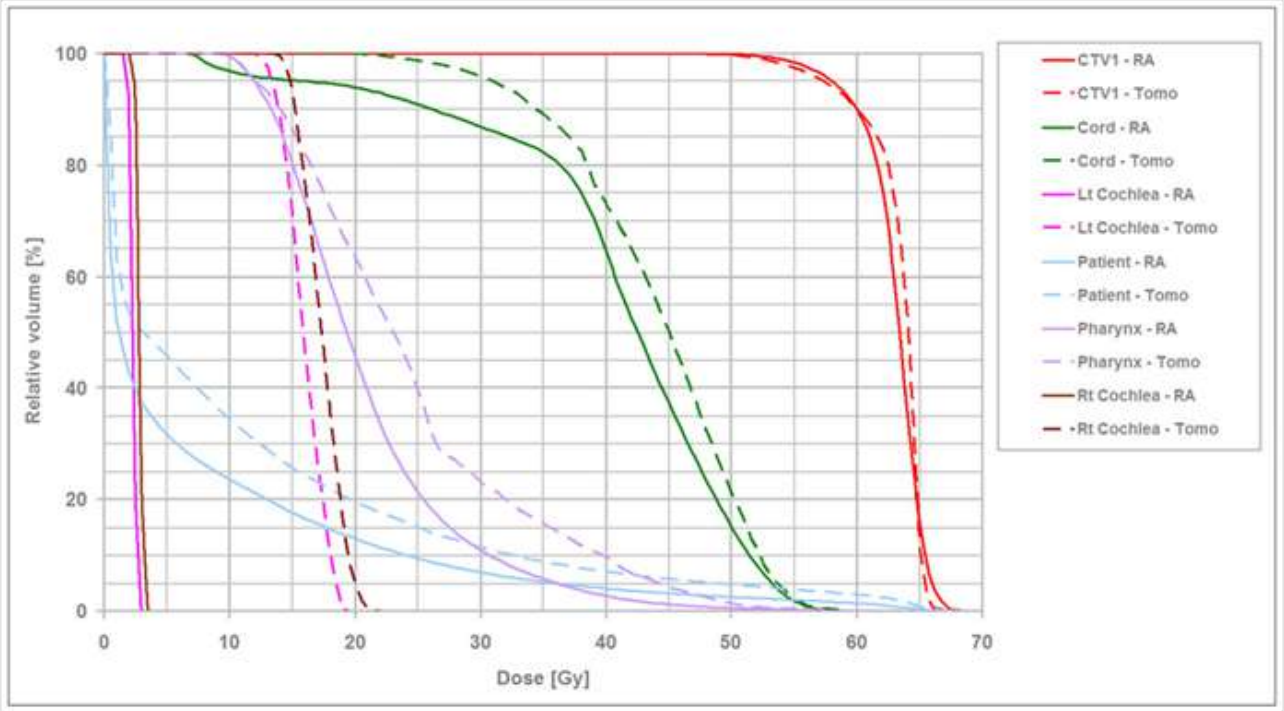

Figure I.21 – A clinically used dose volume (HDV) histogram

Cumulative dose volume frequency distributions are plots of the volume receiving a dose greater than, or equal to, a given dose, against dose. The volume accumulates starting at the highest dose bin continuing towards zero dose, eventually reaching 100% of the total volume). Normally volumes are expressed as a percentage of the total volume; however, in some situations the absolute volume may be more appropriate [39].

Differential dose volume histograms dDVH Differential dose volume histograms appear as a standard histogram comparing the number of bins receiving the same amount of dose on the x-axis to the volume of the bins on the y-axis **Fig I.22**
Relationships between both functions can be obtained easily:

$$DVH_c(x) = \int_x^{\infty} DVH_d(Y)dy \tag{I.34}$$

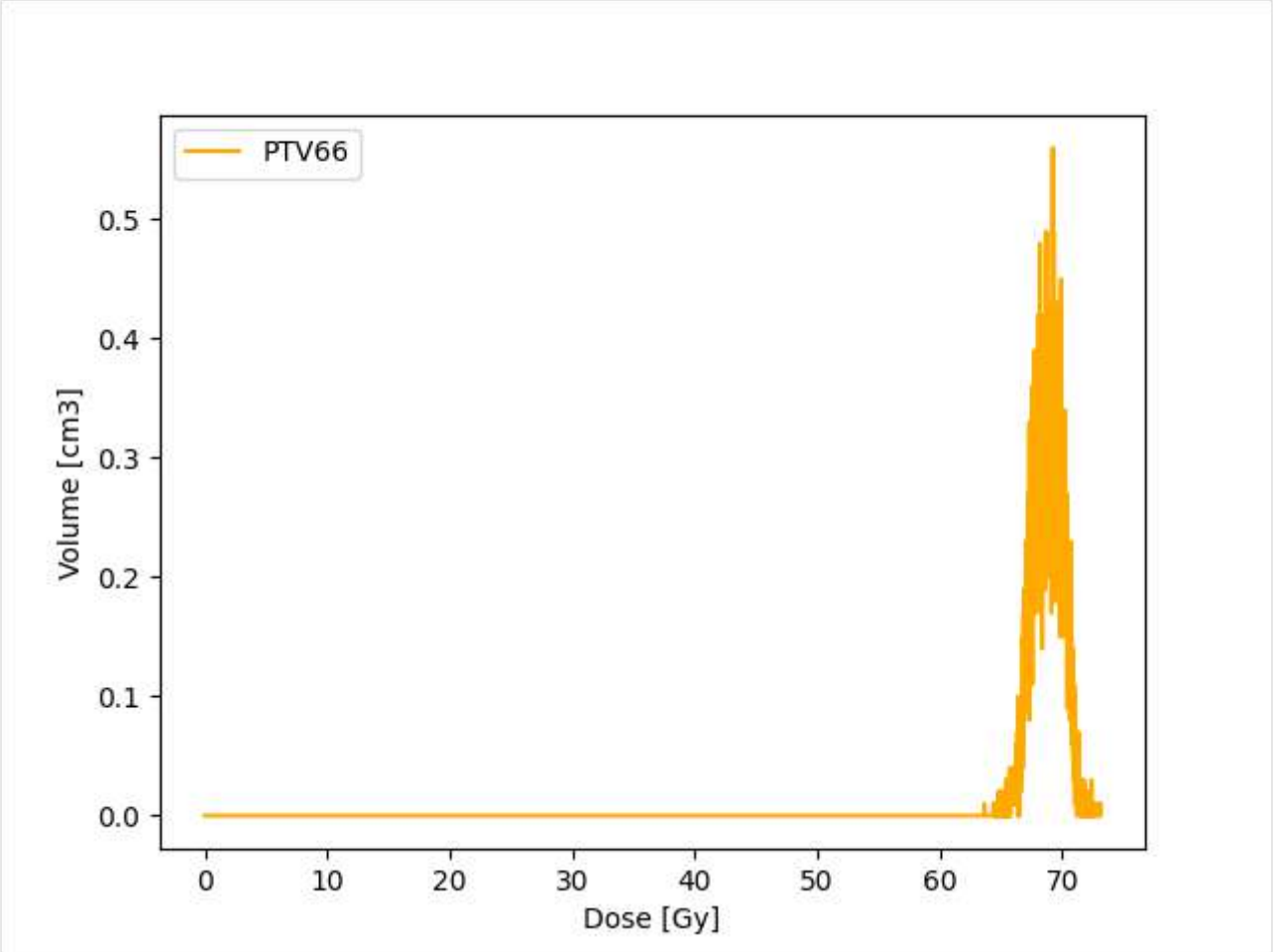

Figure I.22 – differential dose volume histogram

DHV for tumour:

For the PTV, DVHs should show a uniformly high dose throughout the volume. The shape approximates to a step function and a steep slope shows that a large percentage of the volume has a similar dose. A typical evaluation criterion for the target volume is that at least 95 per cent of the target volume should receive a dose equal or higher than the prescription dose.

DHV for OARs:

DVHs for organs-at-risk which are intended to be protected should preferably have a concave appearance: it may be acceptable either to deliver a relatively high dose to a small volume or a small dose to a large volume

6.2 Usual dosimetric indexes

In 1993, the Radiation Therapy Oncology Group (RTOG) proposed guidelines for routine evaluation of stereotactic radiotherapy (SRT) plans based on several parameters:

a) Quality of coverage:

Quality of coverage is an indication of the minimum dose in the target. When the minimum dose is closer to the prescribed dose, then this index will be close to unity. RTOG Quality of Coverage (Q_{RTOG}):

$$Q_{RTOG} = \frac{I_{min}}{RI} \tag{I.35}$$

I_{min}: Minimal isodose surrounding the target RI: Reference isodose [40]

b) Dose Homogeneity::

Dose homogeneity characterizes the uniformity of the absorbed-dose distribution within the target volume.

A perfectly homogeneous dose to the PTV would be characterized by a spike (a delta function) in the differential DVH or a vertical drop of the cumulative DVH line for the PTV at that absorbed dose [41]. Homogeneity index:

$$HI_{RTOG} = \frac{I_{max}}{RI} \tag{I.36}$$

I_{max}: is the maximum dose in the target RI: is the prescription dose [40] A more descriptive formula: Homogeneity index can be defined as the ratio of dose homogeneity in PTV. $D_{2\%}$, $D_{98\%}$, and $D_{50\%}$ are the doses received by 2%, 98% and 50% volume of the PTV dose (HI = 1 was an ideal homogeneity)

$$HI = \frac{D_{2\%} - D_{98\%}}{D_{50\%}} \tag{I.37}$$

c) Dose conformity:

Dose conformity characterizes the degree to which the high-dose region conforms to the target volume, usually the PTV [41].

It is defined as the ratio of the volume receiving the prescribed dose ($V_{PTV}^{D_{100\%}}$)) and volume of PTV (CI = 1 was an ideal conformity) [42].

$$CI = \frac{V_{PTV}^{D_{100\%}}}{PTV} \tag{I.38}$$

d)Geometric conformity index::

The geometric conformity index was designed by the Saint-Anne, Lariboisiere , Tenon (SALT) group in their effort to quantify global treatment quality. For this index geometric conformity is optimal at minimum values as it is the sum of two indices that each captures an aspect of plan deficiency [43].

$$g = LUF + HTOF \tag{I.39}$$

LUF Presents the lesion under dose volume factor:

$$LUF = \frac{TV_{RI}}{TV} \tag{I.40}$$

TV: target volume (tumor volume)
$TV_{<RI}$: Volume of target not receiving the prescription dose (it receives a dose less than the reference isodose)
HTOF Presents the healthy tissue overdose volume factor:

$$HTOF = \frac{HTV_{\geq PI}}{TV} \tag{I.41}$$

TV : target volume (tumor volume) $HTV_{\geq PI}$: Healthy tissue overdose volume factor Volume of nontarget tissue receiving the prescription dose (it receives a dose equal to or greater than the reference isodose)

6.3 Accuracy and uncertainty in external radiotherapy

•Terminology
Numerous reports and publications are available, defining, updating and revising the notion of precision and uncertainty in external radiotherapy **FigI.23**. The International Atomic Energy Agency (IAEA) has published a report in the Human Health section on precision and uncertainty in radiotherapy. The report defines the terms "uncertainty", "precision" and "accuracy". The definitions are given below.

► ***Accuracy*:** refers to the degree of agreement between the results obtained by repeated application of a measurement under prescribed conditions and the reference value.

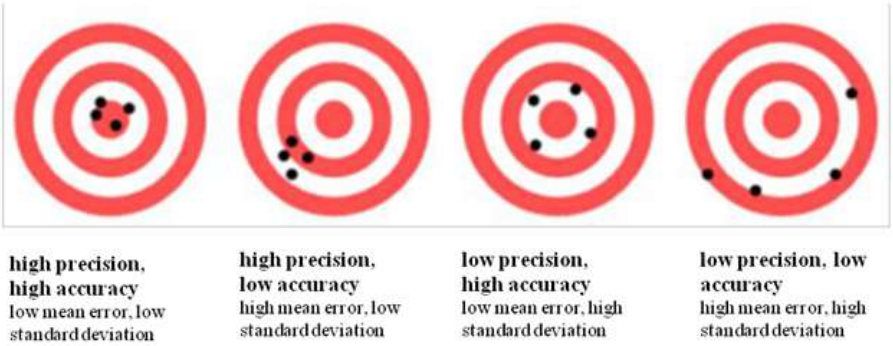

Figure I.23 – Diagram showing precision and accuracy as a function of mean (systematic) error and standard deviation (random error)

► ***Precision*:** refers to the degree of agreement between results obtained by repeated application of a measurement under the same conditions. Accuracy is usually quantified with a standard deviation on the test results. A higher standard deviation value reflects a lower degree of accuracy. Quantitative measures of accuracy are dependent on the conditions in which the measurements are carried out.

► **Tolerance concept**: is generally applied in quality control (QC) contexts. Tolerance can be defined as the range of acceptability beyond which corrective action is required. For example, if a measurement such as the distance between the source and the patient's skin (DSP) is given with a tolerance of 5 mm, any value outside DSP $\pm$ 5 mm cannot be "tolerated", i.e. the situation encountered must be analyzed in depth and corrected if necessary. The action level is the threshold level above which corrective action is required. Beyond the maximum action level, the situation is rejected.

► **Uncertainty**: is defined as a parameter characterizing the dispersion of values obtained by repeated application of a measurement under prescribed conditions. For such a measurement, the results can be described by a statistical distribution, which can be interpreted by specific statistical quantities such as the mean, mode or standard deviation. In addition, uncertainties can be divided into two categories, depending on whether the evaluation method is based on a statistical method (type A uncertainty) or by any other means (type B uncertainty).

► **Random and Systematic error**: Random errors vary arbitrarily in direction and magnitude, while systematic errors tend towards a similar direction and value.

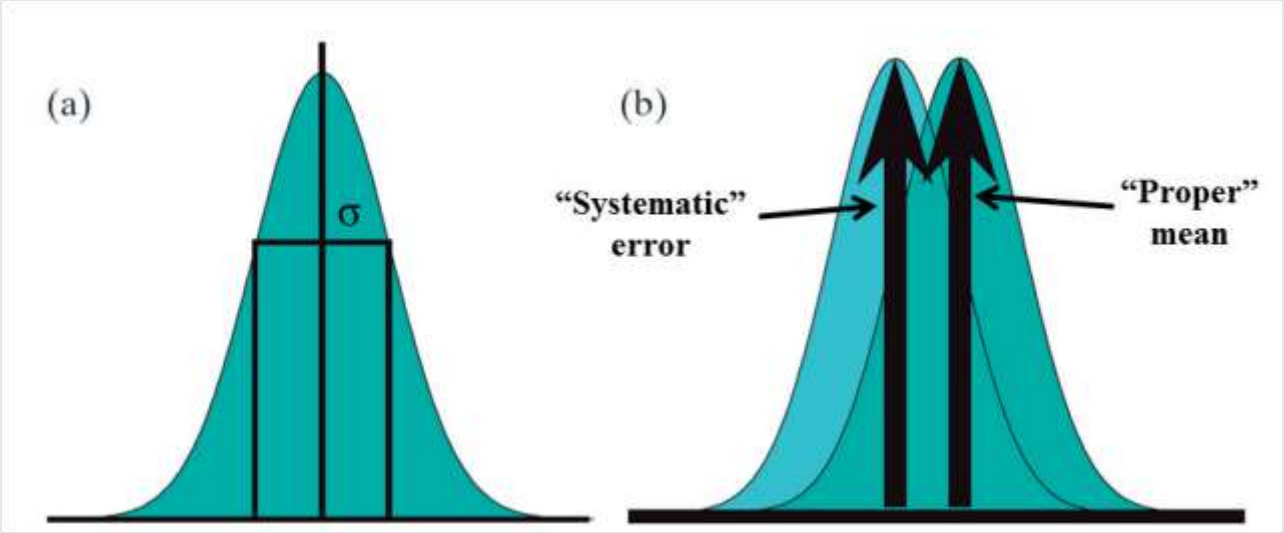

Figure I.24 – (a) Distribution of measurement uncertainty. (Vertical axis shows frequency; horizontal axis shows measured value). (b) Comparison of two uncertainty distributions, one the "proper" mean distribution and the other the "systematic" error distribution.

FigI.24 shows an example of a Gaussian-type statistical distribution and the corresponding standard deviation.

6.4 Safety margin calculation formulas

In chapter III section I, we aimed to calculate and analyze PTV margins from the CTV, and we used margin models to quantify the geometric uncertainties associated with random σ and systematic Σ errors:

• To determine the margin of confguration, ICRU 62 recommends the quadratic combination of random and systematic errors, as shown in the following equation I.44:

$$ICRU\ \ 62 : M = \sqrt{\Sigma^2 + \sigma^2} \tag{I.42}$$

• The margin recipe of Stroom et al assumed a dose of 95% to 99% to the CTV on average, on the basis of design tests carried out as indicated in the equation I.45:

$$Stroom\ et\ al : M = 2\Sigma + 0.7\sigma \tag{I.43}$$

• The margin recipe of Parker et al assumed a minimum dose of 95% and 100% for 95% of

the volume. The probability levels were as shown in equation I.46: Prker et al:

$$Parker\ et\ al : M = \Sigma + \sqrt{\Sigma^2 + \sigma^2} \tag{I.44}$$

• Van Herk et al assumed that the minimal dose at CTV was 95 for 90% of patients. The analytical solution for perfect conformation is shown in the equationI.47:

$$Van\ Herk\ et\ al : M = 2.7\Sigma + 0.7\sigma \tag{I.45}$$

• Using a Monte Carlo test, Van Herk et al assumed a 1% loss of TCP due to geometric errors for the prostate. Their formula is defined as follows:

$$Van\ Herk\ et\ al : M = 2.7\Sigma + 0.7\sigma - 3mm \tag{I.46}$$

Chapter II

Clinical caracteristics for dosimetrique parameters using photon Beams

1 Introduction :

In radiotherapy, the treatment plan of a patient is made from the calculation of the dose distribution by computer (by dose calculation algorithms implemented in the TPS).
Absorbed dose calculation algorithms have been continuously evolving since the 1950s thanks to the development of the field of particle physics and the power of computers. There are currently a large number of algorithms for calculating the absorbed dose implemented in different TPS in radiotherapy.
The purpose of the calculation algorithms used for clinical routine is to model the transport of all particles to simulate the energy deposition in the patient. For this the treatment planning system must:

- Contain a good description of physical processes for primary and secondary particles.
- Make a "true" 3D calculation.
- Take heterogeneities into account.
- Have a calculation time compatible with the clinical routine.
- Provide acceptable accuracy.
- The three main types of dose calculation algorithm are:

∗ **Type 1: Algorithms based on correction methods**

This type of algorithm is based on empirical data obtained in water (water tank) such as

PDDs (depth yields) for different field sizes at a certain source-skin distance (PSD). The introduction of the concepts of tissue-air ratio (RTA), tissue-phantom ratio (RTF or TPR) and tissue-maximum ratio (TMR) [Maqbool et al. 2017] makes this type of algorithm efficient in homogeneous media. Algorithms based on the Clarkson technique [Clarkson 1941] and IRREG [Cunningham 1972] belong to this category. This technique allows a rapid estimation of the absorbed dose for simple geometries in a homogeneous medium such as water. However, given the current advanced techniques and the precision required in terms of the planned absorbed dose, it is difficult to achieve the precision required with this method, especially in the presence of heterogeneities such as bone and lung.

∗ **Type 2: Model-based algorithms**

Model-based algorithms use photon fluence and kernels precomputed by Monte Carlo simulation to model the deposited energy by performing a convolution.

∗ **Type 3: Algorithms based on physical principles**

Algorithms based on physical principles are considered to be the most accurate. Two types of algorithms are identified in this category: Monte-Carlo algorithms and deterministic algorithms. Monte-Carlo algorithms are based on the use of pseudo-random numbers and interaction probabilities (cross sections) to determine the absorbed dose in the medium. The numbers are considered "pseudo" random since the algorithm can repeat the same sequence and the numbers are not perfectly random. These algorithms also offer the possibility of calculating the absorbed dose in water by multiplying it by the ratio of the average mass stopping power between the water and the medium [Siebers et al. 2000].

2 Treatment Planning Principle (TPS)

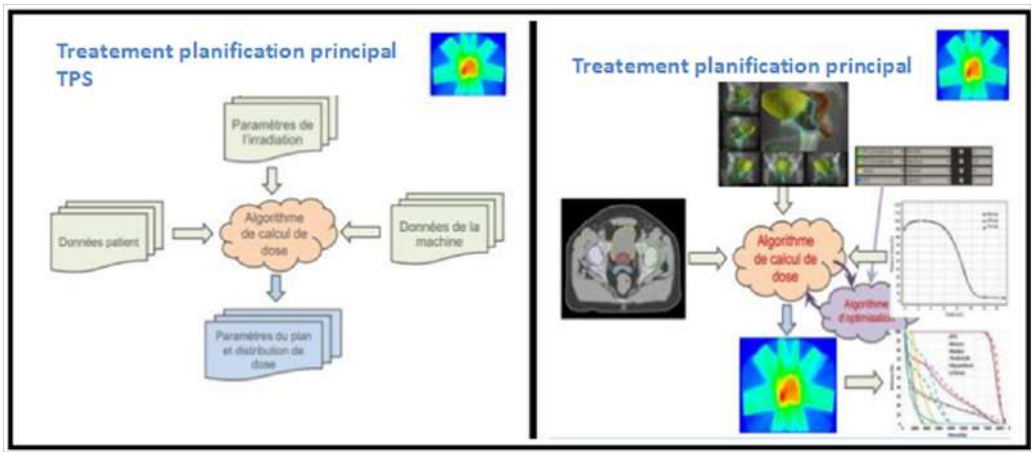

Figure II.1 – Treatment Planning Principle (TPS)

A treatment planning system, commonly abbreviated TPS for English: treatment planning system, is a software allowing to prepare a treatment plan by irradiation in radiotherapy.
In external radiotherapy, it makes it possible to define treatment ballistics thanks to the prior acquisition of tomodensitometric images of a patient and then to simulate the dose deposited in the various tissues of the latter.

The **Fig II.1** explains the principle of treatment planning (TPS) :
♣ The starting data that must be given to the TPS
• Patient data: Positioning and acquisition of patient CT images
• Machine data: PDF, FOC air, FOC water, RTA,
• Irradiation parameters
♣ The result of the algorithm treatment
• Plan parameters and dose distribution.

3 Physical principle of energy deposition:

3.1 Radiation reaching the patient:

a) Primary photons.
b) The photons scattered in the head of the accelerator.

c) The electrons created in the head of the accelerator by the scattered photons.

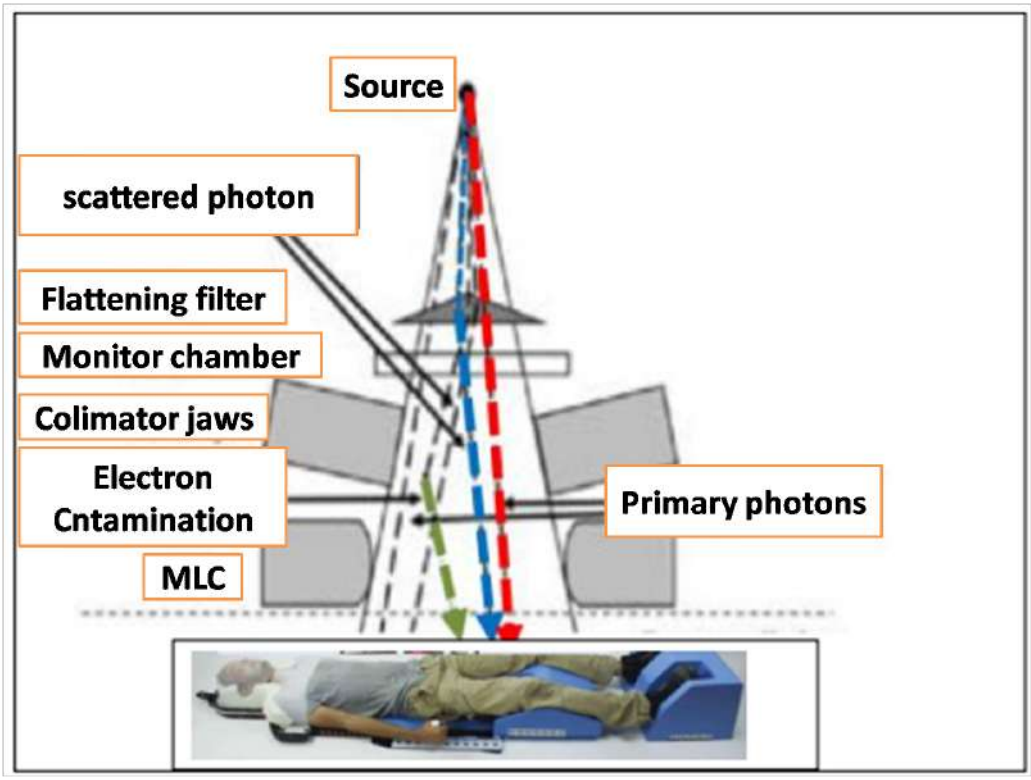

Figure II.2 – Radiation that reaches the patient during a therapeutic act in external radiotherapy.

3.2 Types of absorbed doses delivered to the patient:

The total dose delivered to the patient is the sum of:

a) The dose from primary photons.

b) The dose from photons scattered in the head of the accelerator.

c) The dose from primary photon scatter in the patient.

d) The dose coming from the electrons of contaminations.

To be able to accurately calculate the dose delivered to the patient, the TPS must model the 4 types of doses mentioned above.

4 Absorbed dose calculation algorithm: Convolution/Superposition

The Convolution/Superposition algorithms use the fluence of the photons as well as dose kernel points precalculated by Monte-Carlo calculations to model the energy deposited and the calculation of the absorbed dose is carried out by convolution of the "TERMA" with "the punctual kernel"

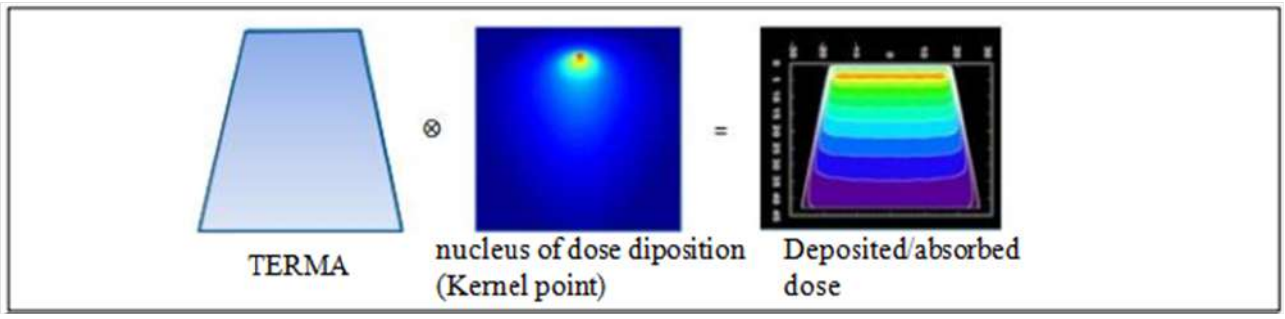

Figure II.3 – Representation of the absorbed dose calculation form a point of Kernel and TERMA

The 2 necessary quantities to apply this method are the "TERMA" and the "kernel":

4.1 The kernel: Definition

A kernel represents the average distribution of the elementary energy deposit, i.e. the fraction of energy per unit volume deposited by the secondary particles (electrons set in motion by the primary and/or scattered photons) in the vicinity from one point.

Types of kernels used

There are two types of Kernels used:

a)The kernel point (PK): 0D

The kernel point models the absorbed dose distribution that results from the punctual interaction of a photon as shown in the figure. It is the fraction of energy distribution around a point interaction site in 3D.

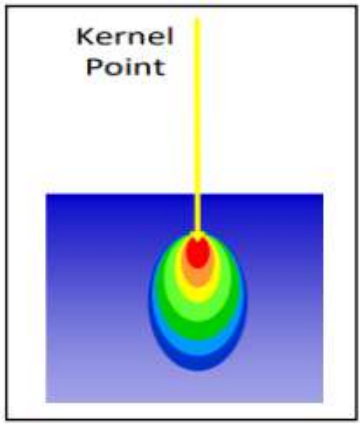

Figure II.4 – Representation of a point kernel

b) The pencil beam kernel (PBK): 1D

The pencil kernel describes the energy deposited in a medium from the interaction at a point of a monodirectional elementary beam as shown in the figure.

The pencil kernel is therefore the result of the integration of a kernel point along a thin beam. The point kernel models lateral scatter and inhomogeneities better than the pencil kernel and thus gives better accuracy.

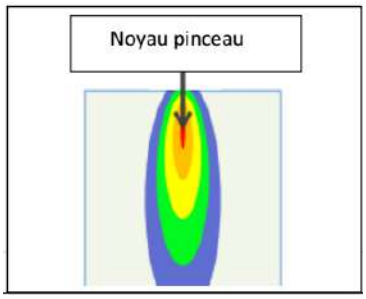

Figure II.5 – Representation of the pencil beam kernel

4.2 TERMA: Total Energy Released per unit Mass

a) Particle Fluence:

It corresponds to the number of particles N crossing the sphere of transverse surface da.

$$\Phi = \frac{dN}{da}\{\frac{particles}{m^2}\} \tag{II.1}$$

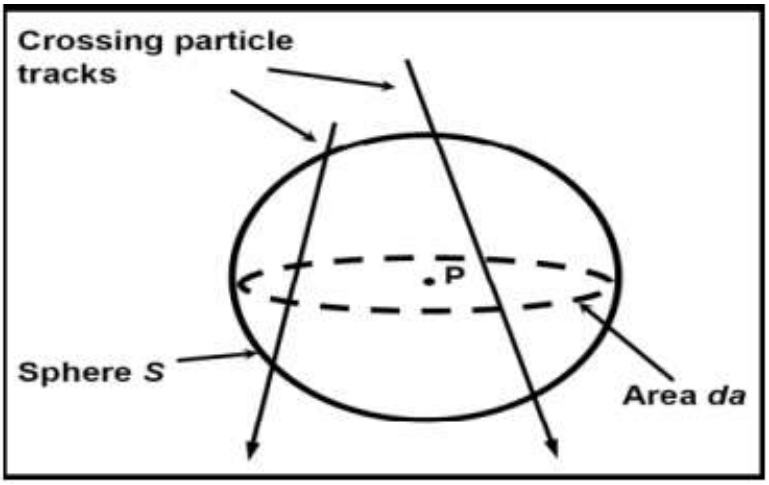

Figure II.6 – Particle fluence

a) Energy Fluence

The energy fluence corresponds to the energy crossing a sphere of transverse surface da.

$$\Psi = \frac{d(N * E)}{dt} \tag{II.2}$$

For a monoenergetic source:$\Psi = \frac{d(N * E)}{dt} = \frac{E * d(N)}{dt} = E * \Phi$

TERMA is the total energy per unit mass released by the radiation field in the medium.

$$T(r) = \frac{\mu}{\rho}(E, r).E.\Phi_E(r) \tag{II.3}$$

$$\Phi_E(r) = \Phi_E(r_0)(\frac{r_0}{r})^2.e^{\frac{\mu}{\rho}(E,r).\rho(r-r_0)} \tag{II.4}$$

4.3 Convolution/Superposition de kernels:

Convolution/Kernels Superposition consists in calculating the dose D(x, y, z) at the point P(x, y, z) from the sum of the energy deposits due to all the interactions of the primary photons at different points P'(x', y', z') of the medium. The operation of this method is based on:

a) Modeling of the energy fluence coming from the accelerator.

b) Absorption of primary photons: Calculation of TERMA

TERMA (T') = (Attenuation coefficient) x (photon energy fluence)

$$T(x', y', z') = \frac{\mu}{\rho} \times \Psi(x', y'; z') \tag{II.5}$$

c) Taking into account the transport of this energy by the secondary electrons and photons.

• The convolution of the TERMA with the kernels of dose and superposition

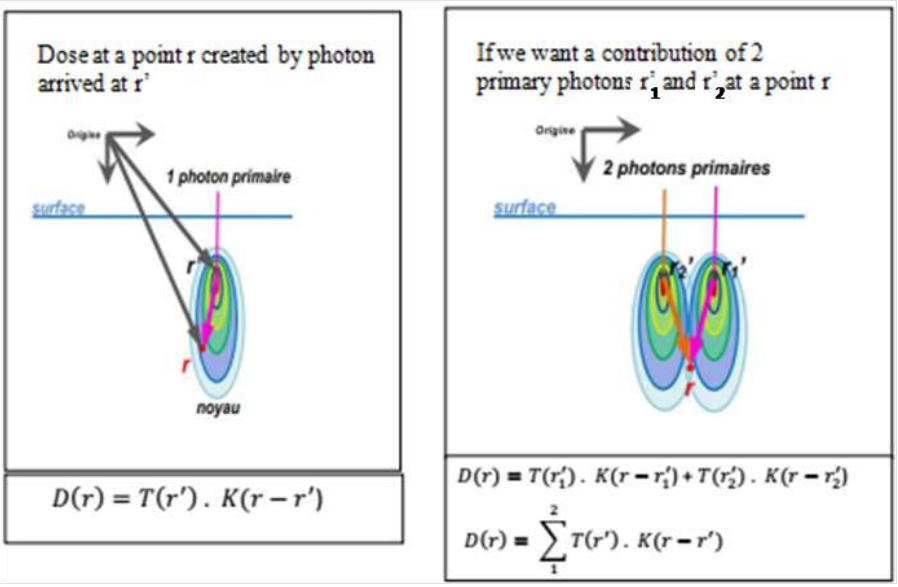

Figure II.7 – Dose at a point r created by a single and double primary photons

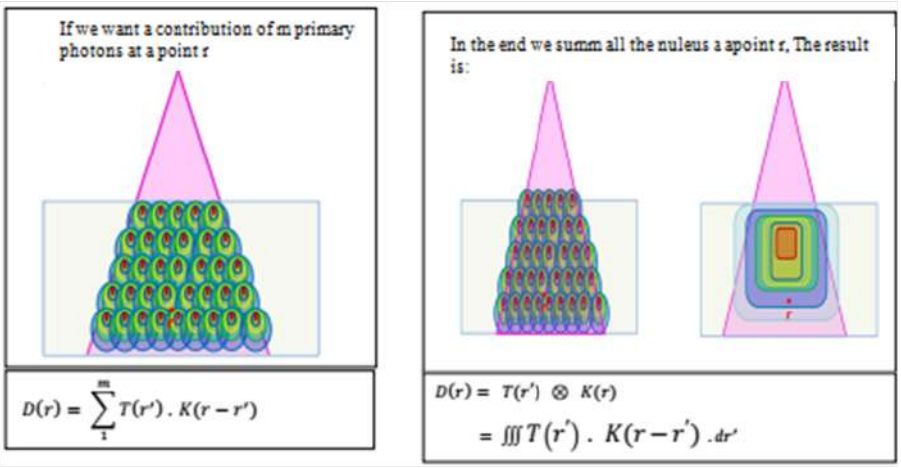

Figure II.8 – Dose at a point r created by a single and double primary photons

5 Absorbed dose calculation algorithm: AAA (Analytical Anisotropic Algorithm)

The AAA is a valid convolution/overlay algorithm in the Eclipse TPS for clinical applications. This algorithm was developed by the company VARIAN and is based on the work of Ulmer et al [Sievinen et al. 2005; Ulmer and Harder 1995, 1996; Ulmer et al. 2005]. It uses pencil kernels (1D pencil kernels) precalculated by Monte-Carlo to determine the absorbed dose. Clinical beam fluence is represented by multiple source models to enable accurate modeling of the total beam

5.1 The AAA source model in Eclipse:

a) The primary source: it is defined by the user in circular or elliptical form on the plane of the source and it models the braking radiations which are created in the target but which do not interact in the head of the accelerator. The fundamental parameters used to model the source of the primary photons are the energy spectrum of the photons, the mean radial energy and the intensity profile.
b) The extra-focal secondary source: flat Gaussian source located below the flatning filter. It models the photons that come from the interactions in the flatning filter and the primary and secondary jaws. This source is not taken into account for calculations of absorbed dose with beams without an flatning filter.
c) Contamination electrons: these represent the electrons coming from the head of the accelerator which serve to reproduce the absorbed dose in the build-up region. The contamination electrons are modeled with a depth-dependent curve that describes the absorbed dose of the contamination electrons at different depths. An energy spectrum for the contamination electrons is defined.
d) Photons scattered from the wedge filter (if present)

5.2 principle operation of AAA algorithm

For a 3D absorbed dose calculation, the patient's body is divided into a voxel matrix based on the user-defined calculation grid. Each voxel is then assimilated to an average electronic density ρ calculated from the HUs (Hounsfilds Units) of the CT images according to a calibration curve.

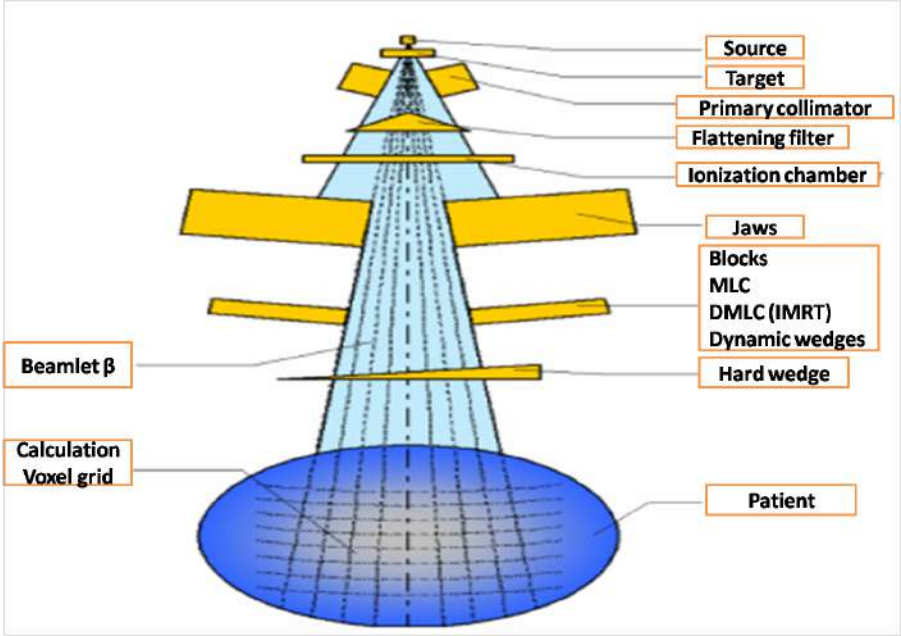

Figure II.9 – Representation of the components of the linear accelerator head and the division of the total field into mini-beams [Sievinen et al. 2005]

♣ The 3D absorbed dose distribution is calculated by separate convolutions of each source mentioned above.

♣ **The total field is divided into several mini beams** ("Beamlets") β in order to achieve convolutions (See figure 9). The final absorbed dose is obtained by superimposing the contributions of each mini-beam

• The attenuation of the mini-beams is modeled with an energy $I_\beta(z,\rho)$ deposition function. The scattered photons are taken into account with the kernel defining the absorbed dose of the lateral scattered $K_\beta(x,y,z,\rho)$. The fluence of photons Φ is considered uniform inside a mini-beam.

• The absorbed energy distribution of a mini-beam of photons at a point is calculated by convolution according to:

$$E_{\beta,ph}(X,Y,Z) = \Phi_\beta I_\beta(z,\rho) \int\int K_\beta()u-x,\upsilon-y,z,\rho)dud\upsilon \qquad \text{(II.6)}$$

• The fluence of contamination electrons and their contribution to the final absorbed dose is determined by convolution of the photon fluence with a contamination electron kernel.

♣ The total absorbed energy at a point E(X, Y, Z) will be determined by superimposing

the energy contributions of the primary photons (ph1), secondary (ph2) and contamination electrons (cont):

$$E(X,Y,Z) = \sum_{\beta} E_{\beta,ph1}(X,Y,Z) + E_{\beta,ph2}(X,Y,Z) + E_{\beta,cont}(X,Y,Z) \tag{II.7}$$

♣ Absorbed energy is converted into absorbed dose. An assumption is made that heterogeneities can be modeled as the ratio between the electron density of water and that of the medium. The AAA then gives an absorbed dose related to the water D_w. Electron densities are used to convert energy to absorbed dose instead of mass densities and the final absorbed dose is given as:

$$D(X,Y,Z) = cE(X,Y,Z)\frac{\rho_e(water)}{\rho_e(X,Y,Z)} \tag{II.8}$$

C used to convert J/m^3 and D will be in Gy

Chapter III

Innovative techniques ad optimizations for the treatment of cancer by advanced radiotherapy

1 CTV to PTV margins based on CBCT method for prostate cancer of Patients treated with VMAT technique

1.1 Introduction

An additional margin (PTV) around the CTV is mandatory to ensure the tumor volume irradiation in each treatment session. This margin considers the uncertainties in patient setup, organ motion, and beam delivery. The main goal of this margin is to ensure that the prescribed dose effectively covers the entire CTV, even when these uncertainties are present. likewise, our medical physics group has carried out a CTV-PTV margin study for head and neck, and prostate cancers using an electronic portal imaging device (EPID) to account for translational errors only. However, in this study, we based on cone beam computed tomography (CBCT) device to determine the PTV margin for prostate cancer and account for translational errors along the (X, Y, and Z) axis, and rotational errors around the (X, Y, and Z) axis.

1.2 Backround

Advanced techniques in radiation therapy such as intensity modulated radiation therapy (IMRT and Volumetric modulated arc Therapy (VMAT) accurately shape the radiation dose to the tumor and enhance protection of healthy tissues. These techniques affect Higher gradients of dose distribution which necessitate accurate determination of the target position; otherwise, one can miss the target "entirely" [44–46]. Furthermore, several studies have been previously confirmed that VMAT generate better planning quality than IMRT for prostate cancer [47–50]. For example, Enzhuo M. Quan, et al.[47] have performed a study showing that the VMAT plan quality and the delivery efficiency may be considered in better modality compared to that of IMRT, for Prostate cancer. Moreover, the quality of the patient's treatment plan and the sparing of the adjacent normal organs achieved better results by using VMAT technique compared to conventional irradiation, and reduced the required monitor units compared to that of IMRT [51]. The authors of Ref. [52] have performed for prostate cancer, an evaluation of planning target volume (PTV margins using electronic portal imaging (EPID and IMRT techniques. The obtained result was 10 mm in all directions which is comparable to the previous works [53, 54]. The mean factor that increases the variation of the target volume position in the treatment of the prostate is its motion characteristics proportional to the surrounding bony anatomy. According to the online imaging protocol (once a week or more frequently), the treatment margins can be decreased when the on-line setup correction based on the implanted radio-opaque markers and megavoltage radiography. However, many authors have been previously shown the capability of gold nanoparticles to enhance the effect of physical dose radiation on tumor cells [55–66]. H.Khosravi et al. demonstrated that administration of gold nanoparticles (GNPs based on keV photon energies were in good agreements with previous studies, and for MeV photon energies the dose factor was enhanced to its maximum value for 2 and 6 MeV photon beams at the depths of 2.6 and 5.6 cm, respectively [67]. In addition, Khosravi et al. evaluated the implementation of the GNPs to identify its impact on dose distribution for the treatment of the prostate under the internal Ir-192 and external 18MV radiotherapy. However, the presence of GNPs increased the mean dose by 15% and 8% compared to the relevant results without GNPs under the internal and external radiation therapies, respectively.
These results are reduced by 1% using MC simulation under the same conditions [68].All treatment delivery needs high precision of volumes delineations for increasing treatments quality.
More and more attention isconducted to determine errors of patients positioning as well as the determination of the PTV margin and the impact of its dosimetric errors. Based on the CT scanner, GTV and/or CTV delineations aredefined for each patient. Determination of target

volumes for photon radiotherapy have been previously published by International Commission on Radiation Units and Measurements (ICRU) in 1993 [69]. During the patient positioning, uncertainties in the target volume involved related to the treatment beams, however, an additional margin should be added to CTV to ensure an adequate tumor irradiation. This expansion of CTV is the Planning target volume (PTV) that is a compromising between the risks underdosage to target volume and the risk of toxicity to the irradiation healthy tissue. Hence, Patient positioning related to the treatment beams and tumor localization within the patient are the main sources of the uncertainties in the target volume,consequently internal and set-up margin probabilistically added to consider both systematic and random errors. Thus, Image-guided radiation therapy (IGRT) is the preferred method for curative treatment of tumor localization, because it considers derivation in 3-Dimentions, translation and rotation as it allows smaller treatmentmargins and escalate dose to the target volume[70].
The reproducibility of the patient position in his immobilization system is a fundamental requirement to ensure an optimal treatment of cancers. The daily use of imaging before each radiotherapy session permits the detection and almost total correction of the set-up error. This is realized by moving the processing table along the three axes X, Y and Z(lateral, longitudinal and anterior-posterior) equal to the measured error.Rotational errors correction was also considered. For this, the aim of our work was conducted to 20patients with Prostate Cancer to investigate PTV margin determination in the IGRT using cone-beam computedtomography (CBCT) or kilovoltage (kV/kV) radio-opaque fiducialmarkers (FM) imaging.

1.3 Material and Method

We conducted our study on a sample of 20 consecutive patients who had been irradiated for Prostate cancer in our department. All patients were immobilized with arms folded over the chest, pillow under the head and a wedge under the knees.
CT simulation was performed in 3-mm slices with a resolution of 0.97 mm along the X and Y axesusing SiemensSomatom Sensation Open CT (Siemens, Erlangen, Germany).Target volumes and OARs were delineated using ELEKTA SOMAVISION Focal workstations v.10.0.28 (ELEKTA, Palo Alto,CA, USA).
Three points had been tattooed on the patient's skin to allow their positioning under the treatment device. Before each Computed Tomography (CT) acquisition, radio-opaque beads were placed on these three points to make them appear in the image.
All planning techniqueswere customized for each patient to obtain high dose conformity distribution. A uniform margin of 10 mm wide from CT to PTV in all directions,except in the

dorsal side 5mm was used, including the prostate, seminal vesicles, and in the patients at high risk, also regional lymph nodes. The dose prescription was 76 Gy in 38 fractions.
VMAT technique using two full arcs for each patient was delivered with 6MV by a linear accelerator (Elekta Oncology Systems,Crawley, UK).The dose prescribed to cover 98% of the PTV. CBCT was derived for each patient prior to treatment fraction for a sample of 20 patients suffers from Prostate and Cancer 125 kVp and 1.6mAs per projection were the selected parameter. Each treatment session for all patients was delivered with half full bladder and empty rectum. Automatic rigid volumetric image registration of the CBCT to the planning CT was performed on XVI (Elekta Oncology Systems, Crawley, UK)to correct patient's set-up errors in the treatment. However, registration of correction set-up errors was performed in three translations T(x, y, z) and three rotations R($\theta_X, \theta_Y, \theta_Z$). Here X, Y, and Z were lateral, longitudinal and anterior-posterior directions respectively, in treatment machine coordinate.
The calculation of set-up error was performed by calculating the distance between the field margin and selected bony structures for pelvis of the digitally reconstructed radiographs (DRRs). The images were displayed, compared and measured by the multi-access computer program, Version 8,00J0, Impact medical system. In most treatment machines, the set-up error correction in translational directions is acquired manually; these corrections may produce rotational errors that can only be eliminated by robot treatment couch. However, the robot six-degree couches certainly not available in all radiotherapy departments.
In this study, the rotational correction was done manually on treatment couch, to consider any misalignment for the purpose of PTV calculation.
Van Herk et al. [71] assumed minimum dose to CTV to be 95% for 90% of patients. The equation for PTV margin calculation is given by :

$$M_{PTV} = 2.5 \sum + 0.7\sigma \tag{III.1}$$

Random errors are mainly composed of the positioning error of the patient and anatomical variations occurring between two irradiation sessions or during a session. The impact of random errors can be simulated by blurring the dose distribution (by convolution of the dose distribution with distribution laws of the position of the organ).

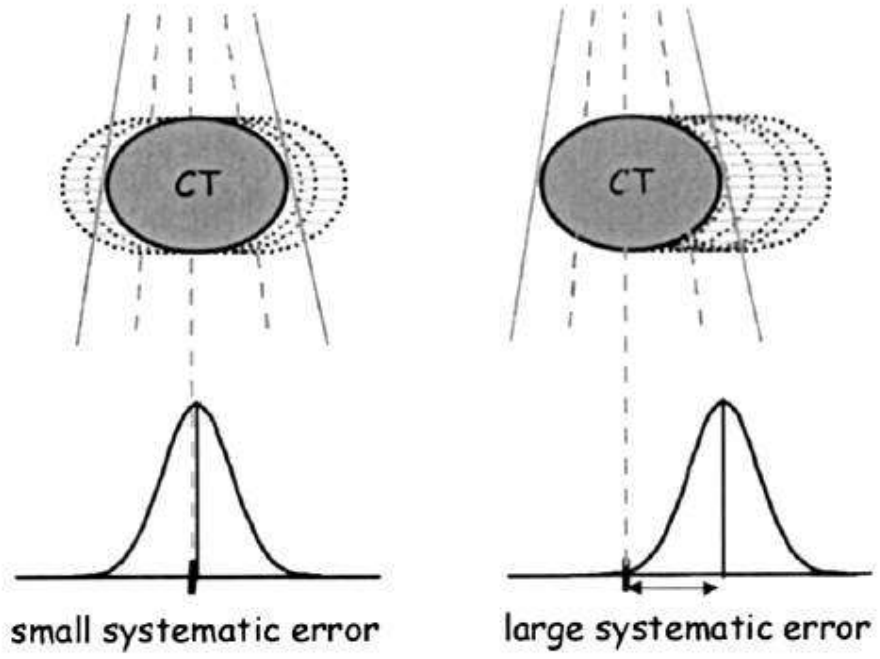

Figure III.1 – Schematic illustration of systematic and random errors [72]

1.4 Results

This study was performed on a sample of 20 patients with prostatic cancer treated with VMAT technique. Daly CBCT imaging was mad for each individual patient, to measure the intrafraction set-up errors deviation in translational T(X, Y, Z) and rotational R(X, Y, Y) axis. However, bladder and rectum filling were prepared prior each treatment session to control as much as possible the variability of the prostate.

According to our measurements, the deviation along the lateral axisranged from -15 to +15mm, along the anterior-posterior axis from -13 to +15 mm, and along the superior-inferior axis from-11 to +11 mm **Fig III.2**.

The rotational deviation around lateral axis ranged from-5 to 5 deg, around the longitudinal axis from 2 to 5 deg, and around the anterior-posterior axis from -2 to 4 deg **Fig III. 3**

The total results for systematic error calculation along the lateral axis, longitudinal and anterior posterior were 2.32, 2.42 and 3.54 respectively. Moreover, Random error was 1.82, 2.19 and 1.76 along lateral axis, anterior-posterior and superior inferior respectively Table 1. In addition, the rotational systematic error was calculated for all the studied patients, and the results were as follow: 1.49, 2.04 and 2.14 around lateral, longitudinal and anterion-posterior axis respec-

tively.Random error 1.78, 1.75 and 1.63 deg anround lateral, longitudinal and anterior-posterior axis, respectively (Table2).
From the obtained systematic and random errors, the size of safety margin from CTV was derivedin deferent directions, in order to compensate the error of patient positioning along and around each of X, Y and Z axis.
By using Van Herk formula, we calculated CTV to PTV margin for translational T(X, Y, Z) axis 7.55, 8.08 and 10.79 mmrespectively as shown in Table 1.

1.5 Discussion

As known on prostate cancer difficulties that make its treatment unreliable, are the intra-fractional organ movement and errors created in the subsequent repositioning of the patient. Our exacting task in this study was to determine an adequate safety margin considering translational and rotation set-up errors around and along X, Y and Z axis. However, monitoring the prostate position variability was the main task to perform CTV-PTV safety margin. Then, the addition margin from CTV to PTV while, keeping the precision of target volume irradiation and Organ at risk protection is dependent on the precision of the patient repositions in the initial position. Several studies based on IGRT modality such a CBCT that has become of crucial importance. According to our results performed in this work on patients repositioning, it may be considered that our data is comparable to that published by Brut Kragelj [74], on safety margin calculation for prostate cancer.
Van Herk and colleagues found that 7 mm margin was enough to be added from clinical target volume (CTV), without considering for intra-fraction motion of the prostate [72, 73]. Approximately 1cm of PTV margin was reported by various authors of the studies on the prostate irradiation, except in the dorsal side which was accepted to be smaller than 1cm [75, 76]. Zelefsky, reported also, if the safety margin is less than 1cm, the CTV coverage can be affected. For patient that was treated in prone position with 1cm in the anterior lateral and craniocaudal directions and of 0.6 cm at the dorsal side, the coverage of CTV at the dorsal side is 85 % before and 96% after the corrections for setup error and prostate displacement [77].
In our study, to consider for target volume coverage, we evaluate the translational and rotational set-up error. However, rotational set-errors most often contribute to affect the target coverage, though it is insignificant as reported by Zhang et al [78]. Results of translational set-up errors for all measurements of our patients are in the form of symmetric Gaussian distribution, and more than 95% of the patients in the interval of -7mm to 7mm except for the lateral left side that was between -9mm and 10mm. Anterior-posterior measurements varied from -7mm to

11mm and this means the calculated 10.79mm additional safety margin should be reduced to almost 7mm in the dorsal side Fig 2. The calculate CTV to PTV margin along translational axis,were 7.55, 8.08 and 10.79 mm for the lateral, longitudinal and anterior-posterior respectively as shown in Table 1. Our total mean Intra-fraction prostate movement measurements for all patients were 2.32; 2.42 and 3.54.

However, these values can change with treatment time as resulted from the literature (was 1-2mm) for around 90 seconds [79]. Prolonged Radiotherapy treatment duration can increase intra-fraction prostate movement up to 3-6 mm [80]. Consequently, the safety margin will also increase. Furthermore, rotational uncertainties can potentially cause target messing during irradiation especially for the region away from treatment center. A study published by Laursen et al, suggested increasing the margin with the distance from the isocenter in order to take rotational errors into account [81, 82]. In this study, we evaluated also rotational errors, that was almost symmetric in the interval between $-5°$ and $+5°$ deg but most of the deviations was between -2 and $+2°$ as show in **Fig III.3**.

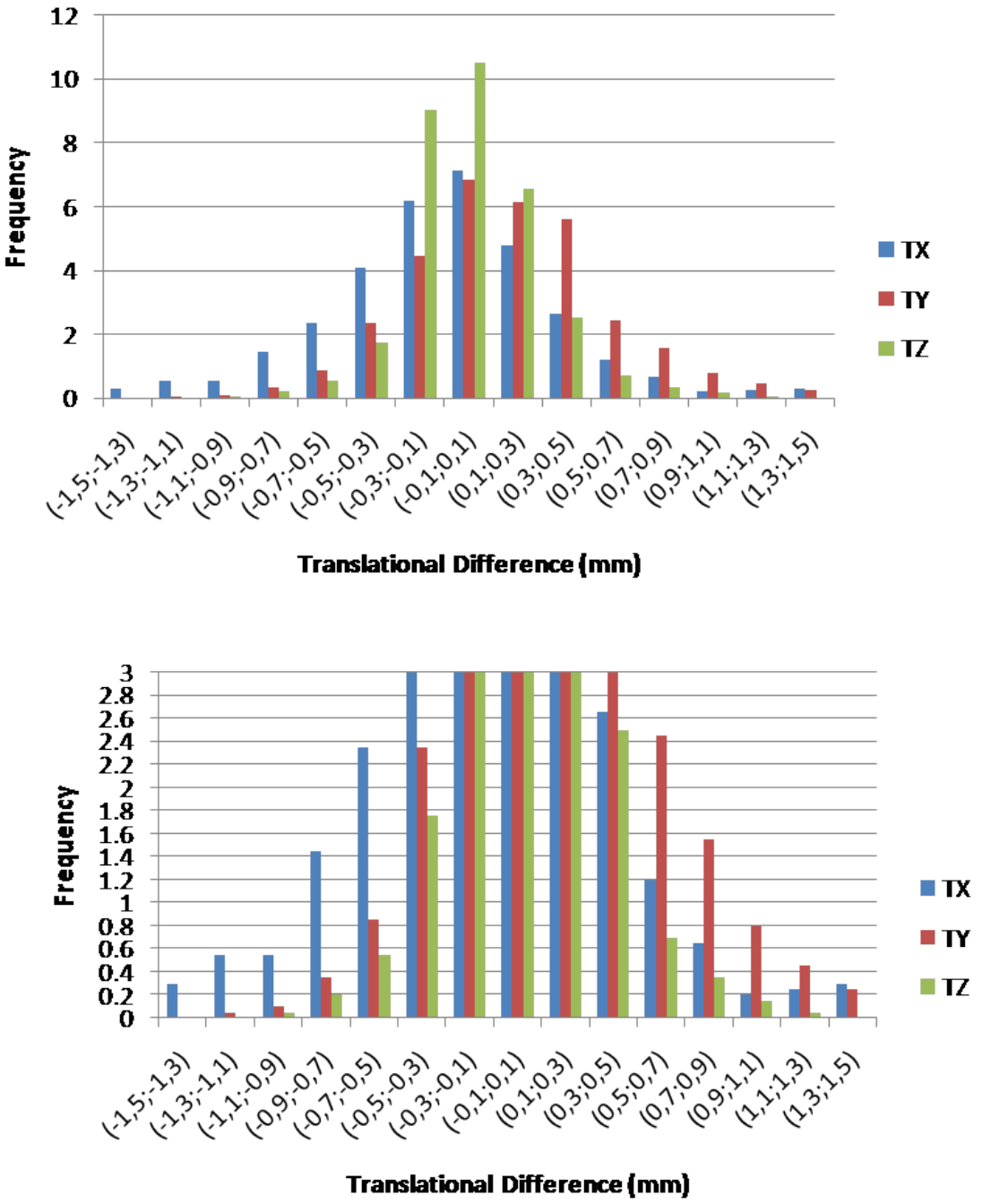

Figure III.2 – Distribution of translational set-up errors in X, Y, Z axes

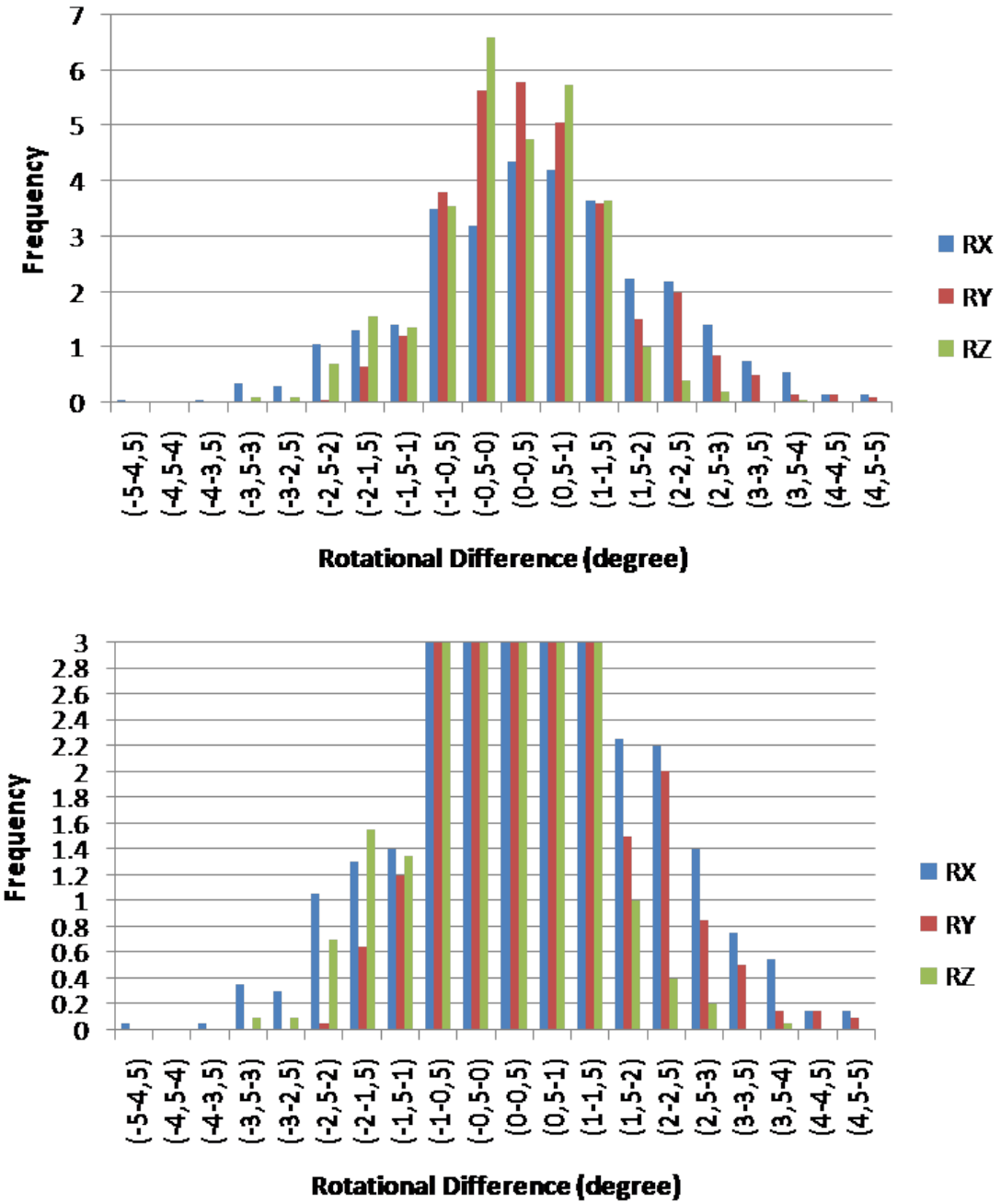

Figure III.3 – Rotional set-up errors around X, Y, Z axes

1.6 Conclusion:

The main objective of this study concentrated on evaluating the set-up error; taking into account the translational and rotational variability of patients treated for prostate cancer by VMAT technique. Applying Van Herk formula in PTV calculation provides comparable results with the previous study.

The use of CBCT method before each treatment, allowed us to obtain a safety margin smaller than 1 cm in all directions, except in the anterior side that should be 1cm and perhaps more; to ensure an adequate treatment of the target volume while, sparing organs at risques, and almost 2° of deviation around X, Y and Z axis.

2 A planning study to optimise a simultaneously integrated boost treatment of larynx cancer with seven intensity-modulated radiation therapy (IMRT) beams

2.1 Introduction :

Intensity-modulated radiation therapy (IMRT) is an important and beneficial treatment option for head and neck cancers treatment. IMRT is an innovative radiotherapy technique that delivers precise radiation doses adapted to the tumor, while minimizing exposure of surrounding healthy tissue.Since, IMRT technique relies on inverse planning optimization,it is important to precisely contour the volumes of interest including: organ at risks (OARs), clinical target volume (CTV), and planning target volume (PTV) which is preferably calculated for each ownradiotherapy department. In this study we evaluated three different techniques for the localization of head and neck treatment using IMRT.The initial technique (IMRT-0) involved delivering radiation through 7 beams, with the first field set at 0Â° and subsequent fields incremented by 51Â°. The second technique (IMRT-26) shared similarities with IMRT-0, differing only in the initial angle of radiation delivery. In contrast, the third approach (IMRT-CT) was executed in a dual-phase manner: the first half of the fractions using the IMRT-0 technique and the second half using the IMRT-26 technique. The combination of the two techniques IMRT-0 and IMRT-26 increases the number of field entries and consequently, the beamlet number which improves the conformation to the target volume and achieved better protection to OARs. This will be discussed in the next section by the evaluation of leaf sequencing and its effect on dose distribution.

2.2 Backround :

Head and neck (HN) cancer treatment is one of the most difficult treatments to plan, due to target volume shape, high dose prescription, complex patient anatomy, as well as to several organs at risk (OARs) surrounding the target volume. Thus, planning has to balance between the dose coverage of planning target volumes (PTVs) and the dose constraints to OARs.
To overcome planning difficulties, highly sophisticated techniques, such as fixed-gantry intensity-modulated radiation therapy (IMRT), rotating-gantry intensity-modulated arc therapy or volumetric-modulated arc therapy, have been developed improving significantly the resulting dose distribution in HN cancer treatment[83–86].
The use of IMRT beams, together with inverse planning, allows increasing the dose to the

PTVs while minimising the irradiation to OARs and normal tissue. Several studies have been performed for HN cancer treatment and proved that a partial sparing of parotid glands results in preservation of salivary flow, greatly improving the quality of life for patients [87, 88]. As an example, Marta et al.[89] found that IMRT could reduce the incidence of grade 2-4 xerostomia in patients with HN cancers without compromising loco-regional control and overall survival, when compared with two dimensional or three dimensional conformal radiation therapy.
In IMRT plans of HN cancer, five to nine beams are sufficient to reach clinically acceptable doses within target volumes, with a good protection of parotid glands.[90, 91] Wu et al.[92] report that the quality of plans improves with the number of beams, but reaches a saturation level, which for those plans was found to be nine. According to Popple et al.[93] who investigated the effect of IMRT beam number on OAR sparing in complex HN plans from 5 to 27, the optimal trade-off seems to be seven to nine equispaced beams, although beam geometry optimisation may reduce the number of beams required to provide adequate target coverage.
As for advanced laryngeal cancer, few studies have focused on IMRT treatment, but it is thought that, as for other HN cancer sites, IMRT can be advantageous over conventional radiotherapy techniques, which often need a troublesome low-neck junction to cover the lower extent of the caudal PTV [94]. A recent paper [95] compared IMRT plans for the treatment of Hypopharynx / larynx cancer, delivered in the two irradiation modes with and without flattening filter; in both cases, nine equispaced beams were used.
In this study, we aimed at optimising treatment with seven equispaced IMRT beams, a number which could be a compromise between ensuring a good clinical quality and keeping an accep table delivery time. Optimisation was pursued by varying the beam entrance angles or by splitting the treatment into two phases, each using different beam entrance angles. Thus we investigated three different IMRT planning techniques, used for each patient by the same equipment, in order to compare their performance and their effect on OARs sparing and target volume coverage. The first technique (IMRT-0) comprised seven equally spaced beams, which started from 0Â° and ended at 312 deg. The same beam numbers are used in the second technique (IMRT-26) but shifted to an angle of 26 deg (this shift could be slightly different depending on patients anatomy) with respect to the first technique. The third technique (IMRT-CT) is obtained by the combination of the first and second techniques in the same plan. This permits the increase of beam entries to PTVs, and thus an improvement of dose distribution. Spearing of OARs (parotid glands, spinal cord, mandible, brainstem) and healthy tissue (PTVs subtracted from the body) was statistically significant. The objective is to find which technique is the most advantageous with respect to plan quality (homogeneity/conformity of PTV dose), minimisation of OAR doses and delivery time.

Tableau III.1 – Dosimetric parameters for Lateral and Longitudinal techniques in the pelvic treatment

Patient	Tumor location	Stage
1	Larynx	T4N0M0
2	Larynx	T1N0M0
3	Larynx	T1N0M0
4	Larynx	T4N0M0
5	Larynx	T4N0M0
6	Larynx	T3N0M0
7	Larynx	T3N1M0
8	Larynx	T4N2M0
9	Larynx	T4N0M0
10	Larynx	T3N0M0

2.3 Methods

A retrospective planning study was conducted on a sample of 10 consecutive patients who had been treated for larynx cancer in our Department. Most patients presented an advanced cancer stage as detailed in **Table III. 1**
All patients were immobilised in supine position, with HN thermoplastic mask attached at five fixation points to a carbon-fibre plate support.
CT simulation was performed in 3-mm slices using Siemens Somatom Sensation Open CT (Siemens, Erlangen, Germany).

Target volumes and OARs were delineated using Varian SOMAVISION Focal workstations V.10.0.28 (Varian, Palo Alto, CA, USA). PTVs delineation for two different dose levels (PTV boost and PTV elective) was made on transverse CT datasets. The primary gross tumour volume (GTV) and clinical target volume (CTV) were contoured by radiation oncologists. The GTV was defined as the gross extent of the tumor. The boost CTV included the GTV and potential direct routes of microscopic spread; the elective CTV included the elective nodes according to internationally accepted guidelines. PTV was defined as CTV with a uniform margin of 5 mm, thus taking into account organ motion and set-up errors.

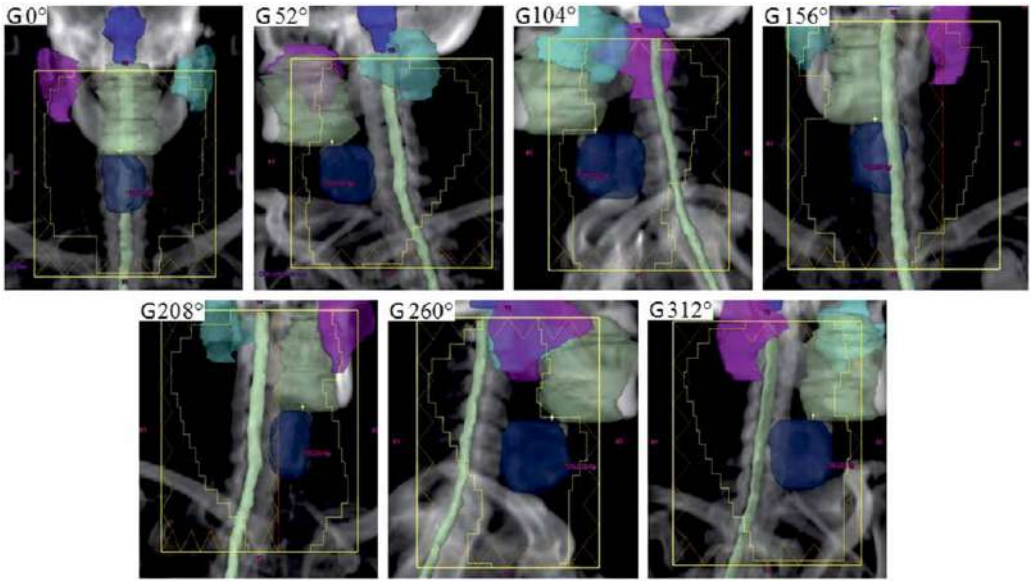

Figure III.4 – Beam's eye view at the seven gantry angles of the IMRT-0 planning technique (0° , 52° , 104°, 156° , 208°, 260°, 312°). Note: The planning target volume-boost is in light green colour, spinal cord in light grey, brainstem in solid blue, left parotid in blue-sky, right parotid in purple and mandible in white.

OARs included parotid glands, spinal cord, mandible, brainstem. An additional volume, the "healthy tissue", defined as the body covered by the CT scan minus the PTVs, was introduced to help to minimise the dose outside PTVs and OARs during the inverse planning and to have a metrics for low-dose distribution in the patient. Dose optimisation and calculation were performed in a Varian Eclipse treatment planning system by using the AAA Algorithm (V.10.0.28) and 6 MV beams from a Varian Clinac 2300 DHX (Varian) linear accelerator equipped with an 80-leaf dynamic MLC, with 1-cm leaf width projected at the isocenter. Two dif- ferent dose levels of 2.12 Gy/fraction to the PTV-boost and 1.65 Gy/fraction to the PTV-elective were prescribed for a total dose of 69.96 Gy and 54.45 Gy, respectively, delivered in 33 fractions with a simultaneously integrated boost (SIB) IMRT technique. Three sets of plans were generated and compared for this study by applying to each patient three IMRT techniques, differing in geometrical beam configuration. All techniques used coplanar equally spaced beams as the 3D geometry of PTVs does not allow to choose preferential entrance angles straightly. Moreover, as shown by Stein et al[96], optimising beam orientations is most valuable for a small number of beams (≤ 5) and the gain diminishes rapidly for higher numbers of beams.
In the first technique (IMRT-0), beam geometry consisted of 129 seven equally spaced fields (gantry angles: 0° , 52° , 104°, 156° , 208°, 260°, 312°) **Fig III.4**. In the second technique

(IMRT-26), beam angles are shifted by 26 deg with respect to the first technique (gantry angles: 26° , 78° , 130°, 182° , 234°, 286°, 338°) **Fig III.5**. The rationale for this angle shift is to exploit the observation of OARs partially enclosed by the target volume (parotids, in our case), whose the beams coming from their direction allow greater control on dose distributions [96].
The third technique (IMRT-CT) consists in delivering the first 17 fractions using the IMRT-0 technique and the last 16 fractions using the IMRT-26 technique. **Fig III. 4 and Fig III. 5** shows the beam's eye view at the seven gantry angles of the IMRT-0 and IMRT-26 techniques, respectively, for a sample patient, with the contoured PTVs and OARs highlighted.
As a planning objective for PTV coverage, at least the 95% of the prescribed dose was requested to cover 98% of the target volume (near-minimum dose D98% > 95%) for both boost and elective PTVs. In addition, 107% of the prescribed dose was set as an upper limit on the near-maximum dose D2%, that is the dose to the 'hottest' 2% volume of each PTV (D2% < 107%).

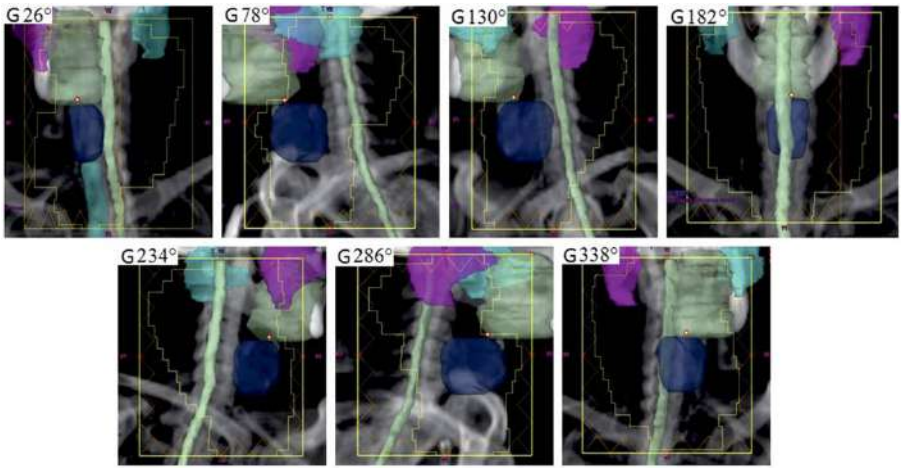

Figure III.5 – Beam's eye view at the seven gantry angles of the IMRT-26 planning technique (26° , 78° , 130°, 182° , 234°, 286°, 338°). Note: The planning target volume-boost is in light green, spinal cord in light grey, brainstem in solid blue, left parotid in blue-sky, right parotid in purple and mandible in white. Abbreviation: IMRT, intensity-modulated radiation therapy.

As for OARs and healthy tissue, the main planning objective was to minimise the dose as much as possible while keeping the maximum homogeneity and conformity of the dose to the PTVs. The mean dose of each parotid should be <26 Gy as suggested in Eisbruch et al.[87] When both parotids are exposed to higher doses, noxious effects can affect patient quality of life. [97–99] For the other OARs, the maximum (point) dose Dmax was constrained to be <45 Gy for the spinal cord, 54 Gy for the brainstem, 70 Gy for the mandible.
After the completion of treatment planning, plan quality was assessed by analysing the dose-

volume histograms (DVH) of PTVs and OARs, and comparing results with the planning objectives and constraints.

The homogeneity index (HI) was used to evaluate the homogeneity of the dose in each PTV, as defined by the formula:

$$HI = \frac{D2\% - D98\%}{D1} \tag{III.2}$$

where D1 is the prescribed dose to PTV.[100–102] The ideal value of HI is 0 as it decreases by increasing the dose homogeneity inside the volume of interest.

Moreover, the conformity index (CI) was calculated to estimate the degree of the conformity of the dose to the PTV volume, according to the Radiation Therapy Oncology Group (USA) definition:

$$CI = \frac{V_{RI}}{V_{TV}} \tag{III.3}$$

where VRI is the volume of 95% of the prescribed dose and VTV the total volume of the PTV. With this definition, CI = 1 corresponds to the ideal conformity. If CI is larger than 1, healthy tissues are irradiated. If CI is less than 1, the target volume is only partially irradiated.

For plan efficiency evaluation, the number of monitor units was considered.

Statistical differences among the plans obtained for the three techniques were analysed using the t-test for matched pairs. A statistical significance level of 0.05 was used ($p < 0.05$).

2.4 Results

All treatment techniques produced clinically acceptable plans for all the patients. As an example, **Figure III. 6** shows the dose distributions obtained with the three planning techniques, in the three orthogonal planes through the isocenter, for one patient of the sample, while **Fig III. 7 nd Fig III.8** show the corresponding DVHs for PTVs and OARs, respectively.
Mean and standard deviation values of the main results obtained in the patient sample from DVH analysis are given in **Tables III.2** and **III.3** for PTVs. Each table also shows the results of the t-test performed to assess the statistical significance of the differences observed for each pair of techniques. The results are expressed in terms of p, that is the probability that the differences are random in nature and not due to the techniques.

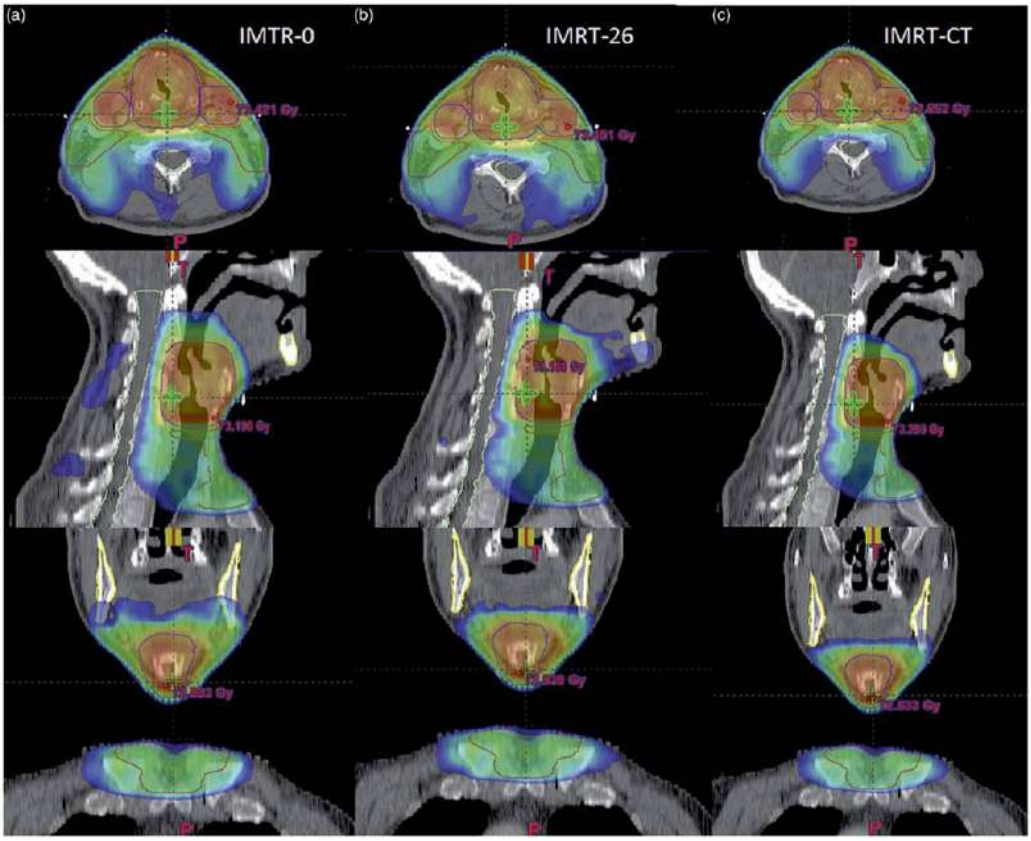

Figure III.6 – Comparison of the dose distributions obtained with the three techniques (a, b, c) in axial, sagittal and coronal planes at the beams isocenter for a patient from the studied sample. Only doses higher than 36 Gy are shown in order to evidence the dose fall-off for each technique.

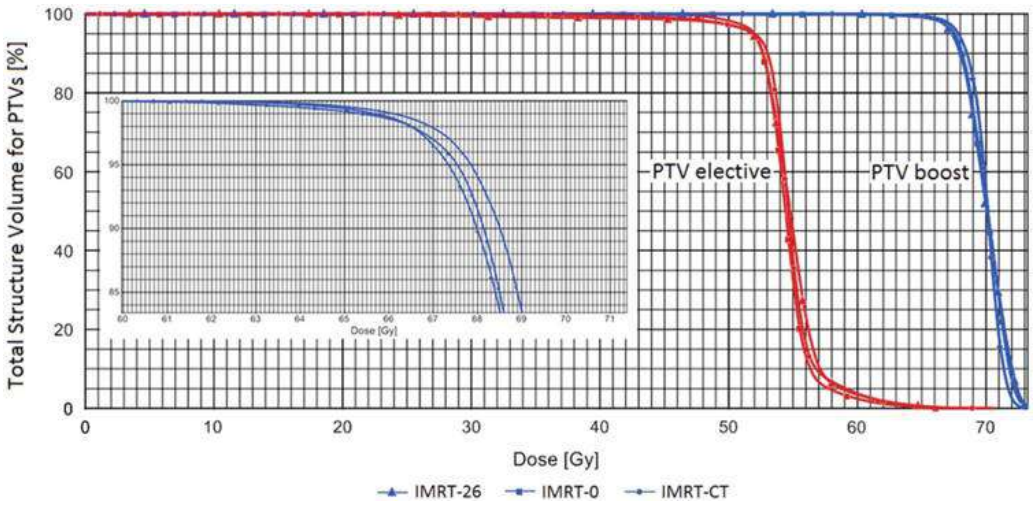

Figure III.7 – Comparison of planning target volumes (PTVs) dose volume histogram's of the sample patient shown in **Fig III.6**.

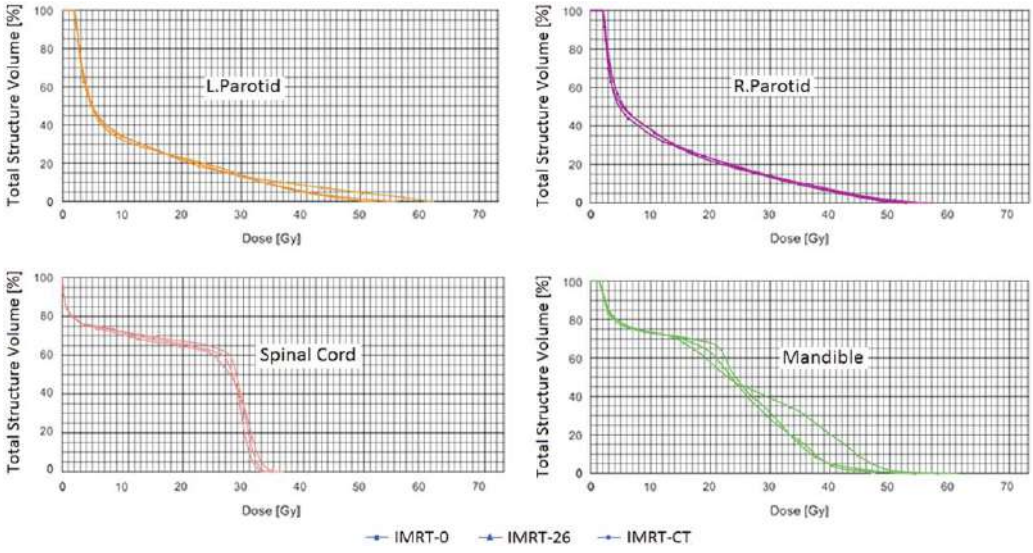

Figure III.8 – Comparison of organ at risks dose-volume histogram's of the sample patient shown in **Fig III.6**.

2.5 PTVs dosimetric evaluations

Table III.2 shows that on the average D98% of PTV-boost complies with the objective of being $\geq 95\%$ of the prescription dose (i.e., 66.46 Gy) for all the techniques. While no significant

III.2 A planning study to optimise a simultaneously integrated boost treatment of larynx cancer with seven intensity-modulated radiation therapy (IMRT) beams

Tableau III.2 – Dosimetric parameters for Lateral and Longitudinal techniques in the pelvic treatment

Parameter	Objectives	IMRT-0	IMRT-26	IMRT-CT	P1	P2	P3
D98% (Gy)	D98% ≥ 66.46	67.67 ± 0.98	67.51 ± 1.01	68.05 ± 0.92	0.036	0.06	0.44
D2% (Gy)	D2% ≤ 74.86	73.74 ± 0.9	74.19 ± 0.66	74.03± 0.67	0.242	0.242	0.01242
HI	-	0.087 ± 0046	0.097 ± 0.015	0.085 ± 0.019	0.50	0.03	0.01
CI	-	1.10 ± 0.106	1.02 ±0.13	1.03 ± 0.04	0.02	0.80	0.26

difference is observed for the first two techniques, a small statistically sig-nificant increase is observed for IMRT-CT with respect to IMRT-0 (68.05 versus 67.67 Gy, p = 0.0366). Also the average of the near-maximum dose D2% complies with the objective of being ≤ 107% of the prescription dose (i.e., 74.86 Gy) for all the techniques, without any significant difference.
The best (lowest) HI for PTV-boost corresponds to IMRT-CT, with HI = 0.085 ± 0.019, but results in significantly different only from that of IMRT-26 technique (p = 0.03236).

As for CI, the best (lowest) results were achieved in IMRT-26 and IMRT-CT with (1.02 ± 0.13) and (1.03 ± 0.04), respectively; however, only the difference between IMRT-0 and IMRT-CT is statistically significant with p = 0.025. For the PTV-elective, Table 3 shows also that, in this case, all the average values of parameters D98% and D2% comply with the planning objectives and that their differences across the techni-ques have no statistical significance. The HI observed for the IMRT-CT technique (0.095 ± 0.014) is significantly better than for IMRT-0 and IMRT-26. The same trend is found for the CI, which is significantly better than the results of the other two techniques (CI = 1.11 ± 0.05).
Thus it can be concluded that, as far as PTVs are concerned, differences among the three techniques are significant only for the homogeneity and conformity of the dose, with the IMRT-CT providing best results.
This trend is evidenced for one sample patient in **Figure III.6**, which clearly shows that IMRT-CT achieves a better dose fall-off outside PTVs than the other two techniques. **Figures III.7** and **Fig III.8** provide the DVHs of PTVs and OARs, respectively, comparing the three plans for this patient. **Figure III.7** shows clearly that both PTVs elective and boost achieved the best dose coverage (D98%) with IMRT-CT compared with IMRT-0 and IMRT-26, and the lowest

Tableau III.3 – Dosimetric results for the planning target volume-elective

Parameter	Objectives	IMRT-0	IMRT-26	IMRT-CT	P1	P2	P3
D98% (Gy)	D98% ≥ 51.3	52.12 ± 0.39	52.16 ± 0.69	52.31 ± 0.6	0.07508	0.242	0.50926
D2% (Gy)	D2% ≤ 57.78	58.51 ± 0.56	58.47 ± 0.51	58.03 ± 0.76	0.05876	0.16758	0.80258
HI	-	0.118 ±0.009	0.205 ± 0.273	0.095498 ± 0.014	0.00512	0.02202	0.88076
CI% (Gy)	-	1.15 ± 0.08	1.14 ± 0.05	1.11 ± 0.05	0.01078	0.00804	0.939584

maximum dose, which yields a better dose homogeneity in the target volumes. **Figure III.8** shows that IMRT-CT also provides the best sparing of OARs.

Table 4 gives for the PTVs of the same patient the relevant DVH parameters and quality indeces, HI and CI. It can be seen that PTVs coverage is clinically acceptable and almost the same for all the techniques. A slight improvement in dose homogeneity and conformity is obtained with IMRT-CT, which could explain the least value of the mean dose observed for the 'healthy tissue'.

2.6 OAR dosimetric evaluations

• **Spinal cord**:

All techniques respect the dose constraint for the spinal cord, that is Dmax < 45 Gy as shown in **Fig III.8**. By using IMRT-CT, Dmax is reduced by 5.8% compared with IMRT-0 and 4.2% to IMRT-26 (statistically significant differences, with p-values of 0.0124 and 0.0164, respectively.

• **Parotids**

All plans achieved clinically acceptable results, with respect to the constrained dose value of Dmean ≤ 26 Gy. By using IMRT-CT, Dmean is reduced on average by 4.8 and 8.6% in the left and right parotid, respectively, compared with IMRT-0, and by 5.6 and 6.1% when compared with IMRT-26. All these differences are statistically significant ($p < 0.01$).

• **Mandible**

All techniques keep the maximum dose fairly under the con- straint of 70 Gy. Also, in this case, IMRT-CT achieved the best results for mandible Dmax, with statistically significant differences with the other techniques ($p < 0.01$).

• **Brainstem**

Tableau III.4 – Dosimetric results for the planning target volume-elective

-	Parameters	IMRT-0	IMRT-26	IMRT-CT
PTV Boost	D98% (Gy)	66.46	66.5	66.94
-	D2% (Gy)	0.06	0.063	0.05
-	CI	0.09	0.09	0.07
-	4.623	4.694	4.59	IMRT-CT
PTV elective	D98% (Gy)	52	51.8	52.3
-	D2% (Gy)	60.54	61.8	60.1
-	HI	0.09	0.1	0.08
-	CI	0.16	0.18	0.14

In this case, the constraint value of Dmax < 55 Gy is easily respected for all the techniques because of the fair distance of the brainstem from the PTVs. Thus the mean Dmax results as low as 16.37, 17.76 and 17.94 Gy for IMRT-CT, IMRT-0 and IMRT-26, respectively. Difference between IMRT-CT and IMRT-0 is statistically significant ($p = 0.0124$).

• **Healthy tissue**

Table 5 shows that IMRT-CT achieves the lowest value of the mean dose to the tissues outside the PTVs, with differences statistically significant ($p = 0.009$ and 0.037 when compared with IMRT-0 and IMRT-26, respectively).

2.7 Discussion

The present work investigated three IMRT techniques (IMRT- CT, IMRT-0 and IMRT-26), differing for beam configuration, with the objective of improving plan quality for the treatment of advanced laryngeal cancer.

All techniques obtained an excellent PTV coverage (as expressed by the near-minimum dose D98%) with clinically insignificant differences among them. However, the best plan quality, in terms of dose homogeneity and conformity, was achieved with the technique IMRT-CT, that combines the other two techniques by delivering them sequentially in two treatment phases. This, in turn, translated into the best sparing of OARs and the healthy tissue.

The suggested technique takes advantage of using 14 entrance beams in total, increasing the number of freedom degrees in optimisation, while delivering only seven per fraction in order

to reduce the delivery time. Beam configuration can be changed after the first half of the treatment, or on alternate days, as it is more comfortable. In this way, the resulting treatment will achieve both good plan quality and OAR sparing.

Comparison with the results obtained by other authors is difficult due to different dose prescription or different metrics used to report the results. As an example, Dobler et al. used V95% (i.e., the volume enclosed by the 95% isodose) to express the PTV coverage, while we constrained D98% to be larger than 95%. As they obtained V95% = 93.7 ± 1.2% for the SIB PTV in the IMRT treatment, our IMRT-CT result of D98% = 68.05 ± 0.92 Gy (i.e., 97.3 ± 1.4% of the prescription dose) indicates a better coverage of the volume. On the contrary, no comparison is allowed for the HI and CI due to the different definitions.

Also for OARs such as spinal cord and brainstem, the com- parison is not direct as they expressed Dmax = D1ccm while we considered the maximum point dose. Anyway, we can reasonably assume that maximum point dose can be larger than D1ccm. In this way, our IMRT-CT Dmax = 39.73 ±1.93 Gy obtained for the spinal cord and Dmax = 16.37 ± 12.04 Gy obtained for the brainstem should be consistent with their corresponding values D1ccm = 31.7 ± 2.1 Gy and D1ccm = 34.6 ± 4.7 Gy.

As for the parotids, in our study, the mean dose was considered, while in Dobler et al. D50%, that is, the median dose. After looking at a typical parotid DVH obtained in our study, as shown in Figure 5, we can infer that D50% should be less than Dmean. Thus, our IMRT-CT results of Dmean = 17.68 ± 4.62 Gy for the left parotid and Dmean = 18.93 ± 4.34 Gy for the right parotid seem better than the corresponding D50% = 29.0 ± 4.8 Gy and D50% = 30.5 ± 4.8 Gy. Limitations of our study include no specification of the anatomical subsite of the tumors (supraglottis, glottis or subglottis), which can possibly affect the extension of PTVs [94]. In addition, OARs such as oral mucosa, thyroid gland, carotid arteries, submandibular glands and constrictor muscles were not contoured for dose evaluation, though most of them are usually not constrained in planning [94].

2.8 Conclusion

The IMRT-CT technique, combining two different seven-beam setups, delivered in two treatment phases, improves dose distribution for the treatment of larynx cancer, with respect to plan quality (dose homogeneity and conformity in PTVs) and to the reduction of dose in OARs and peripheral tissues. This latter result could be of clinical interest as it could potentially reduce the toxicity associated with this HN treatment and improve quality of life especially for patients with a good prognosis.

3 Performance of different Strength Aperture Shape Controller in Optimization with VMAT technique for Head and Neck, Pelvic and Breast Cancer using Halcyon Machine.

3.1 Introduction :

The Multi-Leaf Collimator (MLC) is a fundamental and indispensable component in modern radiotherapy treatment techniques. It plays a crucial role in shaping the radiation beams and precisely delivering the prescribed dose to the tumor while minimizing exposure to surrounding healthy tissues. It consists of multiple individual leaves that move independently. By adjusting the positions of the leaves, the MLC shapes the radiation beam to match the irregular contours of the tumor, conforming closely to the target volume. This beam shaping is essential in high and sophisticated techniques such as IMRT, VMAT, SBRT, and SRS. Halcyon Machine uses MLC similarly to other advanced radiotherapy systems to shape the tumor volume. The present study evaluated six options for optimization using VMAT technique, each individual option has different leaf shaping in treating such localization. Head and Nech, Breast, and Prostate cancer are planned with six options (OFF, VERY LOW, LOW, MEDIUM, HIEGHT, and VERY HIGHT) for each individual localization to certify what is the convenient beam shaper option for each form of the tumor volume. The next section III. 4 we will focuson the treatment of big volume (Pelvic bone metastases) using the OFF option.

3.2 Backround :

Improvement in machines technology for radiotherapy treatment is one of the mean factors that contribute on delivering high dose to target volume,while providing maximum protection to organs at risks. The shape of the beam plays a very important role in improving the accuracy, efficiency and quality of radiation treatments. Over three decades Multileaf Collimators (MLCs) have been used and considered one of the cornerstones of radiotherapy [103–111].Initially, beam shapers eliminated heavy shielding blocks, and then used for intensity modulated radiotherapy (IMRT) and volumetrically modulated arc therapy (VMAT)[112].Initially, beam shapers permitted doing without heavy shielding blocks, using Intensity Modulated Radiation Therapy (IMRT) and Volumetric Modulated Arc Therapy (VMAT) [10]. Moreover, different MLC designs have been described over the years,each version aiming to further improve the outcome

and quality ofradiationtherapy [106, 110, 113–115]. For IMRT and VMAT treatments, the dosedelivered to the target volume is sensitive to leaf positioning and leaftransmission. Characteristics of a well designed MLC therefore arelow leaf transmission, small tongue and groove effect, small penumbra,accurate leaf positioning, and faster speed [107, 110, 115, 116].

Recently more attention focused on LINAC improvement in gantry speed, leaf speed and dose rate that may strengthen the time efficiency of VMAT delivery. Halcyon linear accelerator with O-ring gantry designs has the ability to rotate at higher speeds compared to the current C-arm LINACs. This Machine is mainly designed for intensity modulated radiation therapy and volumetric modulated arc therapy (IMRT/VMAT) because of its specific characteristics such as fast delivery via 4 RPM with a dose rate of 800 MU/s, FFF (Flatting filter Free) only beam, MLC characteristics, and automated daily IGRT workflow. The new model of the Varian(Varian Medical Systems, Palo Alto, CA,USA) Halcyon linear medical accelerator was introduced in May 2017,at the European Society for Radiotherapy and Oncology (ESTRO 36) Meeting, by mid-2017whereinstalled in North America and France, while in Britain in September 2018 [117, 118]. HalcyonTM has a dual-layer MLC system in contrast to other single-layer Varian MLC systems (such as the MillenniumTM120-leaf MLC and High Definition 120-leaf MLC). This design offers fast beam modulation and substantially reduces leakage between MLC leaves. HalcyonTM has no beam shaping jaws, with the MLC being the only beam shaping component. Therefore, MLC positioningand optimization are essential to ensure accurate dose delivery.The HalcyonTM commissioning process is straightforward and streamlined to allow for a short period of time from installation to treatment. While the HalcyonTM beam output has been described,[117] the unique stacked and staggered dual-layer MLC has not been independently characterized. Detailed characterization of the MLC system can provide a deeper understanding of the system's limitations, and thus inform the quality assurance protocols needed to ensureaccurate radiation deliveries.A reference beam model integrated with the Eclipse treatment planning system was used for the preconfiguration of the Halcyon linac. Beam model parameters related to small fields and MLC dosimetry, can then benefit from good agreements between planning and delivery.

In mid-July 2018 The Halcyon 2.0 became clinically available in the market with the new upgraded features over the previous version (1.0). Our institution installed Halcyon 2.0 in July 2020.The upgraded features from Halcyon 1.0 to 2.0 are as follows: (a) kilovoltage (kV) imaging capability (Table 1), (b) maximum treatmentlength of 36 cm using multiple isocenters, (c) 0.5 cm MLC effective resolution, and (d) dynamic beam flattening sequences that flatten the treatment field beam profiles for three dimensional (3D) conformal planning. Most other parts remain the same as 1.0 for hardware,beam data/modeling, MLC characteristics (dimension,

Dosimetric gap,transmission, and interleaf leakage), integrated electronic portal imaging device (EPID) with portal dosimetry and treatment workflow [119, 120]. Several studies were shown good agreements between measurements and calculated or reference values on Halcyon 1.0 [121, 122]. In our center we have halcyon 2.0 combined with Eclipse TM treatment planning software (v16.1.0) using a 6X flattening filter free (FFF) energy and 600 MU/min dose rate, six option of Aperture Shape Controller can be used before starting optimization and thus, beamlet number that are higher in off option and decrease respectively when we select very low, low, moderate, high, and very high, these optimization options may affect plans quality and treatment time.To the best of our knowledge, no precise data are available for the optimal option technique for different treatment sites. Therefore,the purpose of this study was to identify the impact of different Strength Aperture shape controller,and its effect on planning quality by evaluating homogeneity index, conformity index, target coverage, dose max and the treatment time delivery (HI, CI, D98%, D2%, DMAX, MUs and gamma index passing rate). Three different localizations (Head and Neck, Pelvic (Prostate, Cervix and Endometrium) and Breast Cancer) have been selected for this study because of different shape and most frequent site, and for each individual plan, we realized six different options of optimizations.

3.3 Materials and methods

A retrospective study was conducted to nine consecutive patients representing with three different and most frequent cancer sites, including advanced tumors of the nasopharynx, oropharynx and hypopharynx forHead and Neck, low risk for the Pelvic and breast cancer. All patients were treated with Halcyon 2.0 using VMAT technique. Treatment plans are generated within Eclipse TM treatment planning software (v16.1.0) using a 6X flattening filter free (FFF) energy and 600 MU/min dose rate to minimize differences between treatment units and directly compare MLCs.

- **Patient's prescriptions**:

CT simulation for all patients was performed in 2-mm slices using Siemens Somatom Sensation Open CT (Siemens, Erlangen, Germany). Target volumes and OARs were delineated using Varian SOMAVISION Focal workstations v.16.1.0 (Varian, Palo Alto, CA, USA). The primary clinical target volume was delineated according to the clinical protocol in use. Necklymph nodes and OAR were delineated according to published guidelines [123, 124].
PTVs delineation for two different dose levels (PTVboost and PTV elective) was made on transverse CT datasets. The primary gross tumor volume (GTV) and clinical target volume (CTV) were contoured by radiation oncologists. The GTV was defined as the gross extent of the

tumor. The boost CTV included the GTV and potential direct routes of microscopic spread; the elective CTV included the elective nodes according to internationally accepted guidelines. PTV was defined as CTV with a uniform margin of 6 mm, thus taking into account organ motion and set-up errors.

In the treatment of Head and Neck, two different dose levels of 2.12Gy/fraction to the PTV-boost and 1.65Gy/fraction to the PTV elective were prescribed for a totaldose of 69.96Gy and 54.45Gy, respectively, delivered in 33fractions with a simultaneously integrated boost (SIB) VMAT technique. The selected patient for Pelvic Cancer was treated in supine position and placed on room laser system according to markers on body and used customized immobilized device.The planning CT scan was done with semi-full bladder and empty rectum, and this filling status was kept to be the same in the daily treatment as well. According to van Herk and our clinical protocol, the CTV-PTV uniform margin recipe of 6 mm was used.Theprescription dose for Cervix and Endometriumwas 50Gy in 25 treatment fractions and 46Gy with 2Gy/fr for Prostate Cancer.The prescribed dose to the breast cancer was 50Gy in 25 fractions for all the studied patients.

• **Planning Technique**

The used VMAT technique for all plans on the fast O-ring linacestablished of two full arcs with one isocenter and the same collimator angles, that can be (45 deg, 315 deg or 23 deg, 293 deg) in opposite arcs direction. In the treatment of breast cancer two to four half arcs are used for optimization depending on the volume and the side (left, right) of the patient. However, when multiple lymph nodes are found to be positive in the staging of breast cancer two isocenter might be used if the target volume extended into the supraclavicular axillary region and occupied a volume bigger than $28cm^2 \times 28cm^2$.

For each patient, six different optimization plans were performed with variant Strength Aperture Shape Controller(P-off, P-very low, P-low, P-moderate, P-high and P-very high), in the same conditions to check their effect on plan quality, treatment timeand gamma index passing rate for three different localization.

• **Planning objectives**

As a planning objective for PTVs coverage, at least the 95% ofthe prescribed dose was requested to cover 98% of the target volume (near-minimum dose D98% > 95%), this criteria was for both boost andelective PTVs in the treatment of head and neck. In addition, 107% of the prescribed dose was set asan upper limit on the near-maximum dose D2%, that is the dose tothe 'hottest' 2% volume of each PTV (D2% < 107%).As for OARs and healthy tissue, the main planning objectivewas to minimize the dose as much as possible while keeping the maximum homogeneity and conformity of the dose to the PTVs. In the end of treatment planning, plans quality were assessed by analyzing the dose volume histograms (DVH) of PTVs and OARs, and comparing results with the planning objectives and constraints for each optimization option technique.

The homogeneity index (HI) was used to evaluate the homogeneity of the dose in each PTV, as defined by the formula:

$$CI = \frac{V_{RI}}{V_{TV}} \tag{III.4}$$

Where, VRI is the volume of 95% of the prescribed dose and VTV the total volume of the PTV. With this definition, CI =1 corresponds to the ideal conformity. If CI is larger than 1, healthy tissues are irradiated. If CI is less than 1, the target volume is only partiallyirradiated.For plan efficiency treatment time evaluation, the number of monitor units in each using technique was considered.

3.4 Results

The results of three different clinical cases (Pelvic, Breast and Head and Neck) were analyzed by changing the strength aperture shape controller (off, very low, low, high and very high) and thus, optimizations and calculations. A total of 18 VMAT plans were generated to compare different optimization methods. Dosimetric and clinical parameters were calculated and evaluated using DVHs and dose statistics from Eclipse TM treatment planning software (v16.1.0).due to the impact of the used algorithm (AAA), some similarity and differences were noted when different optimization methods were used. To highlight the differences when comparing the results for each individual patient, figures, and tables were used.

The Dosimetric results for all the studied patients in Pelvic and Breast cancer case, seems to be different. However, the alteration between the used treatment techniques observed to be very small. Pelvic treatment show a slight improvement in PTV coverage in the used VERY LOW technique compared to others, by identifying the volume covered by 98% of the prescription dose (D98%), and the percentage of the dose that cover 98% of the Volume (V98%). The value of D98% for all treatment techniques were very closed, between 96.5% and 97% and the higher value acquired by the VERY LOW technique. these variations were asynchronized with V98% that was between 95% and 96% for all techniques except in VERY HIGH that was under 95% **Fig III.9-a**. the Dosimetric parameters that describe PTV coverage (D98% and V98%) chows no difference between all techniques in Breast treatment, almost 93% for D98% and 89% for V98% with 1% lower for the OFF technique $FigIII.10-a$. the effect of using different optimization techniques in Head and Neck treatment is more important compared to other localizations, the best results of PTV coverage is obtained in High and VERY HIGH techniques with almost 5% to 6% higher for D2% and small improvement also found in V2%, except for the OFF technique that was 2% more than HIGH technique **Fig III.11-a**. The same remarque is noted in the analysis of the point dose max (DMAX) and the near maximum dose D2% for different localizations and techniques. No significant differences in DMAX and D2% for Breast treatment. DMAX was between 110% and 110.5% for all techniques, and between 106% and 106.5% for D2% always with 0.5% lower in VERY LOW technique **Fig III.10-b**.For Pelvic treatment, the maxim and near maximum dose variation of 2% between all techniques is clearly shown in **Fig III.9-b**, 106.5% for DMAX and 103.75% for D2% always with lower value in VERY LOW technique. In Head and Neck treatment only 106% maximum dose is achieved as the best value for HIGH technique with the gain of almost 3% compared to the worst value that obtained in VERY LOW technique, in contrary Pelvic case that was the best result. Conformity index isalways considered one of the fabulous parameters to easily compare

the performance of multiple plans,and mostly used in combination with homogeneity index to check both the uniformity of dose distribution withing the target volume and the conforms of reference isodose to target volume.

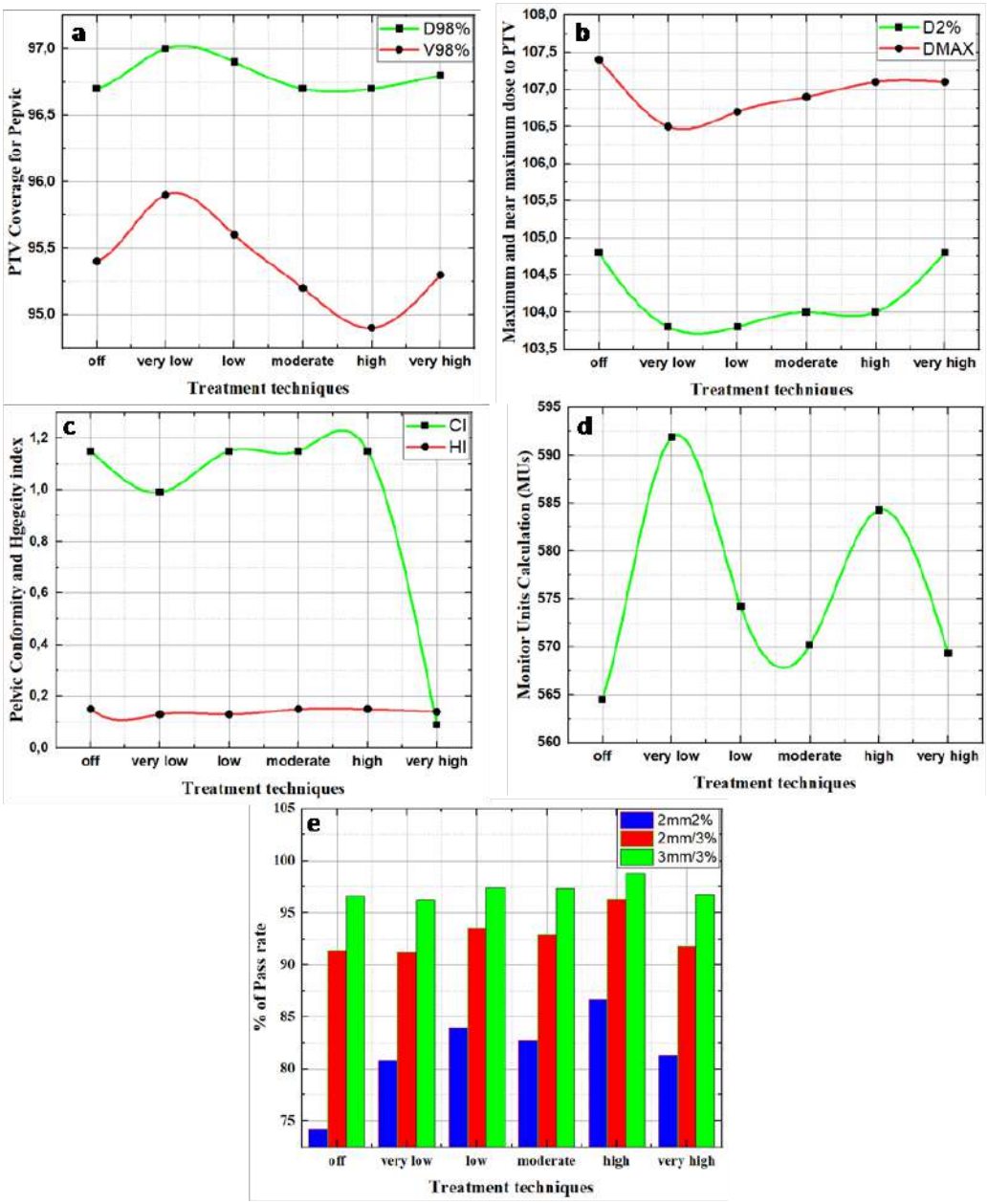

Figure III.9 – Pelvic treatment using different strength aperture shape controller a) OFF technique b) VERY LOW technique c) LOW technique d) MODERATE technique e) HIGH technique f) VERY HIGH technique

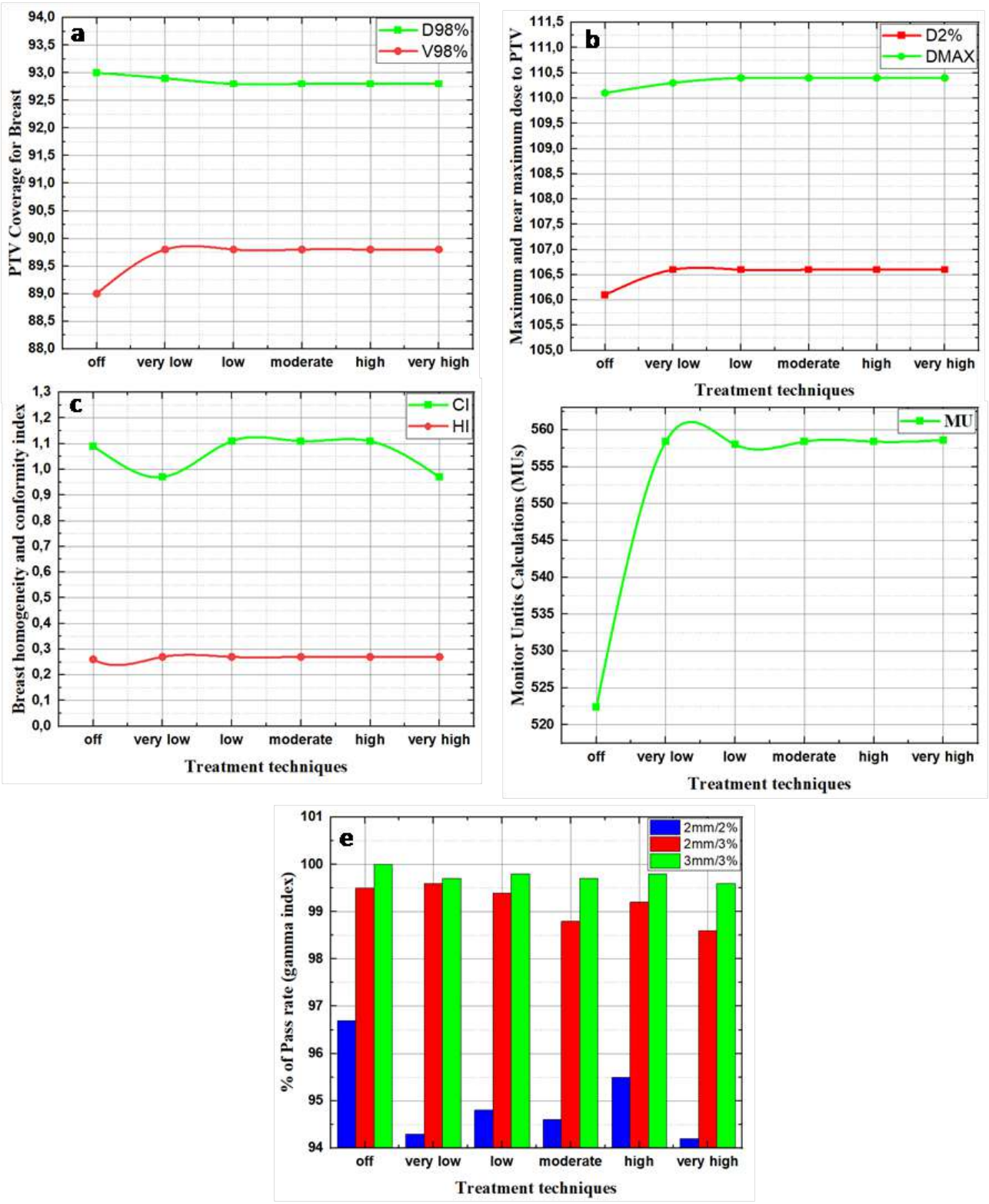

Figure III.10 – Breast treatment using different strengthaperture shape controller a) OFF technique b) VERY LOW technique c) LOW technique d) MODERATE technique e) HIGH technique f) VERY HIGH technique

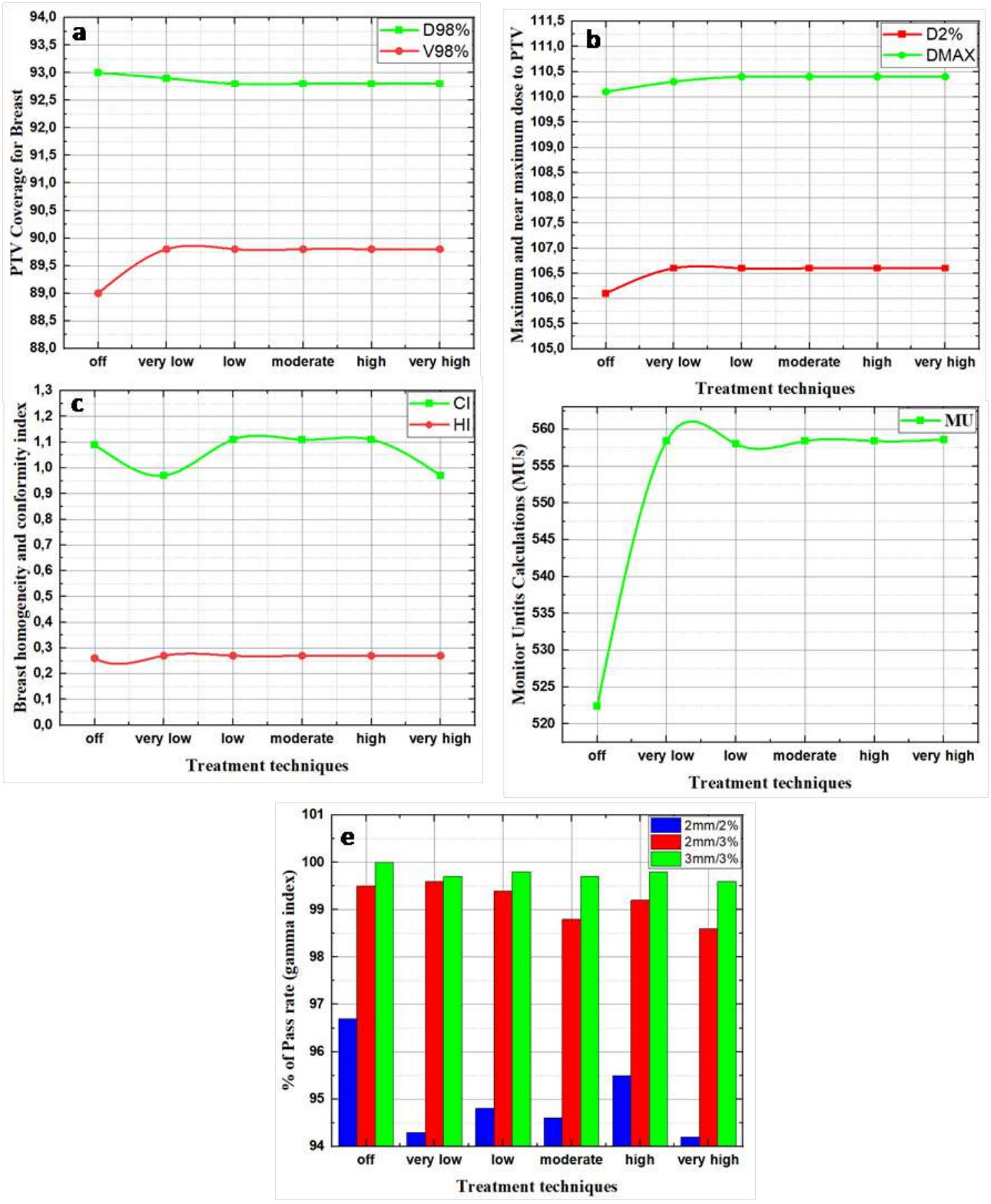

Figure III.11 – Head and Neck treatment using different strength aperture shape controller a) OFF technique b) VERY LOW technique c) LOW technique d) MODERATE technique e) HIGH technique f) VERY HIGH technique

Homogeneity index recognized no gain between techniques for all localizations, except for head and neck in the application of HIGH and VERY HIGH, the HI=0.2 against 0.25 to 0.3 for others, in other hands the best conformity index attained in the VERY LOW and VERY HIGH techniques for Pelvic and Breast with CI ranges from 0.97-0.99 **Fig III.9-c**, **Fig III.10-c** and 0.97 forHead and Neck **Fig III.11-c**. Monitor units calculation achieved the best results when using off technique for Pelvic and Breast treatment with 565 MUs and 523 MUs respectively **Fig III.9, III.10-d**, for head and neck the off technique was the worst with 585 MUs and the best result obtained with high and very technique with 480 MUs.Quality control chowsno significant differences between all techniques in all cases when 3mm distance to agreement and 3% dose difference is used.

3.5 Discussions

In this study, a Halcyon fast-rotating O-ring linac with fastmoving leaves was used to treat three different localizations with VMAT technique. Six differents aperture shape controller were used to optimize plans for each patient. In view in the fact that the Halcyon V2mounted with EclipseTM treatment planning software (v16.1.0) has newly been used, this investigation represents an initiative to compare the performance of each optimization technique in the studied localizations.

The prime objective of this study is to select the best aperture shape controllerprior starting optimization for each localization.Our results of Pelvic treatment recognize some variations when aperture shape controller changed and used for optimization. As seen from the plans quality review (Table 2), CI for all the studied patients achieved a good results and ranges between 0,99 to 1,15 and almost similar HI is obtained, always with advantage of the VEY LOW and VERY HIGH optimization technique. This results was comparable to that of KIM et all, for gynecological cancer treatments [128].Better coverage andhot spot reduction is obtained by VERY LOW technique, in other hands more treatment time was needed to perform this accomplishment. Pretreatment patient specific QA was performed with portal dosimetry with electronic portal imaging device (EPID),3mm/3%, 2mm/3% and 2mm/2% were evaluated.Our pretreatment QA results were ranges from 96,2% to 98,8% for 3mm/3% criteria and from 91,2% to 96,3% for 2mm/3% passing rate. This results were consistent with the recent report by De Roover et al [129] that achieved between 92,5% and 96,5% for 2mm/3% using Halcyon 1. The evaluation of 2mm/2% is identified to clarify the strength between techniques in small area as shown in Fig 1-e, since the VERY LOW and VERY HIGH techniques showed some advantage compared to others in terms of PTV coverage and dose conformity, the difference

between them was not significant and achieved just 0,6% better usingthe VERY HIGH technique. Variation between all techniques in Breast treatment was not meaningful in the used dosimetric parameters in this study, but in term of Conformity index the VERY LOW and VERY HIGH techniques was clearly better with 12,6% compared to the LOW, MODERATE and HIGH techniques and 11% compared to the OFF technique Table 2.

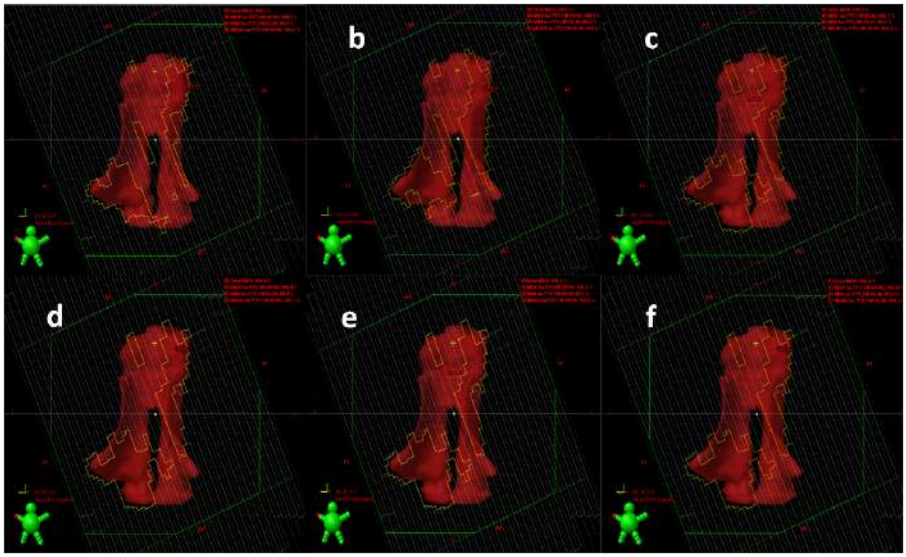

Figure III.12 – Variation of beamlet sizes for different strength aperture shape controller from the same angle gantry rotation a) OFF technique b) VERY LOW technique c) LOW technique d) MODERATE technique e) HIGH technique f) VERY HIGH technique

Our results for treating complicated shape of target volume as head and neck achieved a remarkable advantage when the size of beamlet increased by using the HIGH and VERY HIGH technique **Fig III.12**. More than 100 MUs reduction is obtained compared to the OFF technique, where the small size of beamlet is applied to irradiate target volume. However, our results in dose conformity for HIGH and VERY HIGH were comparable to that obtained by S. Michiels et al, for PTV elective coverage and improved the maximum dose [129]. The VERY LOW technique recorded the best conformity index for all localizations, Smaller beamlet sizes in the applied VMAT Plans offer the potential to upgrade dose conformity and homogeneity. While there are still some computational limitations for applying smaller beamlet size to clinical planning practice, such limitations are expected to diminish with increased computational speed.

3.6 Conclusion

The effect on changing strength aperture shape controller for optimization on VMAT dose calculation can be significant. The results disclosed that using HIGH and VERY HIGH technique for Head and Neck can improve the dose coverage, dose max and significantly reduced the treatment time compared to LOW technique. VERY LOW technique showed some advantage for treatment of Pelvic and Breast cancer to balance between treatment time and target volume coverage.

4 Solution for processing pelvic bone metastases with HalcyonTM 2.0 on lateral and longitudinal isocenters treatment plans using the VMAT technique: A comparative study.

4.1 Introduction :

Treating pelvic bone metastases using the Halcyon machine can pose challenges during theplanningphase, particularly for larger volumes due to the machine's field size limitations. This study aimed to assess the benefits of the suggested technique in addressing these Halcyon machine limitations and attaining favorable clinical outcomes.In the previous section III. 3 we identified six options of optimization to evaluate the benefit of each option in terms of delivered dose and treatment time. However, all the studied localizations were covered with the field size during the treatment. In the present work, we investigated the treatment approach involving volumes larger than the machine's field size using the OFF optimization option.

4.2 Backound :

Several technologies have been developed to provide faster treatment and optimal doses. The latest cancer radiotherapy treatment device, offered by Varian, is its modern, faster, and more ergonomic Halcyon TM accelerator. It is mainly designed to revolutionize radiotherapy by delivering faster treatment time and reducing treatment errors compared to conventional linear accelerators.Its evolved treatment quality and maintained CBCT imaging in approximately 15 seconds, Accelerated RapidArc delivery at 2RPM, 4RPM gantry speed saves time between fields, and fast MLC motion allows for treatment to be delivered at close to maximum dose rate (800MU/mim) [130]. In recent years, three versions of the Halcyon machine (Varian Medical Systems, Palo Alto, CA, USA) are developed and introduced a treatment delivery platformthat is designed to have an efficient, high-throughput, and simplified workflow. Itis a closedsystemwith a 100 cm diameter bore opening and a single 6 MV flattening filter-free (FFF) photon beam [131–141].

Daily image guidance is required on the Halcyon TM as there is neither a light field nor anoptical distance indicator (ODI). For each treatment plan,a kilo-voltage cone beam computed tomography (KV-CBCT) or MV (orthogonal pair or CBCT) imaging fieldmust be added before treatment approval for actual delivery on the machine. The MV imaging dose is calculated

in the Eclipse (Varian Medical System, CA) treatment planning system prior to optimization which is added tothe prescribed dose [142].
Moreover, HalcyonTM has a dual layer MLC system in contrast to other single layer Varian MLC systems (such as the MillenniumTM 120 leaf MLC and High Definition 120 leaf MLC). This design provides fast beam modulation and significantly reduces leakage between the MLC leaves. Further, HalcyonTM has no beam shaping jaws, with the MLC being the only beam shaping component. Therefore, MLC positioning and optimization are essential to ensure accurate dose delivery. Additionally, the Halcyon commissioning process is straightforward and streamlined to allow for a short period of time from installation to treatment. While the HalcyonTM beam output has been described in the literature, the unique stacked and staggered dual layer MLC has not been independently characterized, see Ref. [143] for more details. Detailed characterization of the MLC system can provide a deeper understanding of the system's limitations, and thus inform the quality assurance protocols needed to ensure accurate radiation deliveries. Notice the way that a reference beam model integrated with the Eclipse treatment planning system was used for the pre-configuration of the Halcyon LINAC. Notice also that the Beam model parameters related to small fields and MLC dosimetry can benefit from good agreements between planning and delivery.
Halcyonmachine was upgraded from version one to three; each improvement was aiming to accomplish the previous limitations. Only one isocenter per plan is allowed with a maximum field size of $28 \times 28 cm^2$ for Halcyon 1.0, though in Halcyon 2.0 this geometry can be extended 8 cm longitudinally through two isocenter per plan, while in Halcyon 3.0 also two isocenter per plan can be used but with a maximum additional distance of 10 cm; hence the length (longitudinal direction) will up to 38 cm.
Metastatic bone disease (MBD) is the most common malignant tumor of the bones. About 70% of all malignant bone tumors are of metastatic origin [144]. The pelvis is the second most frequent site of the metastatic bone lesion after the spine.Metastatic tumors of the pelvis can result in pain and substantial reduction in function and weight bearing capacity.The pelvis is characterized by:(a) the large size of the cavity,(b) the elastic nature of the organs; and (c) the muscles around it, for this reason,tumors in this region generally reach a significant volumebefore causingsymptoms. Bone metastasis mostly originated from the carcinoma of the breast, renal, lung, thyroid, and prostate. In addition, bone metastasis is the third highly frequent site, following lung and liver. Moreover, the detailed incidence of bone metastasis is not completely understood [145]. Furthermore, up to 70% of skeletal metastases are caused by prostate and breast cancer (BC) and are characterized by severe pain, impaired mobility, pathologic fractures, spinal cord compression, bone marrow aplasia, and hypercalcemia [146]. The relative

incidence of bone metastasis by type of tumor, in patients with advanced metastatic disease, is 65-75% in BC; 65-75% in the prostate; 60% in the thyroid; 30-40% in the lung; 40% in bladder; 20-25% in renal cell carcinoma and 14-45% in melanoma. The median survival from diagnosis of bone metastasis is 6 months in melanoma; 6-7 months in the lung; 6-9 months in the bladder; 12 months in renal cells carcinoma; 12-53 months in the prostate; 19-25 months in BC and 48 months in thyroid [147].

Radiation therapy is most often used for pain relief for the palliative treatment of bone metastases and is reported in many doses per fractionof randomized studies [48, 148]. Many authors reported clinical characteristics and radiotherapeutic strategies in hepatocellular (HCC) carcinoma patients with bone metastasis, as well as stereotactic body radiotherapy for spine metastasis [149–152] . Contrary to vertebral metastases, a handful of studies have evaluated HCC patients with pelvic bone metastasis.

Recently Uehara et al. described the use of Halcyon machine for the total body irradiation (TBI)[153]. Moreover, many authors have described the treatment of bigger volume as the TBI and the total marrow irradiation (TMI) using C-ARM linear accelerator and Tomo therapy [154–162, 164, 165]. However, this requires more time in the treatment, about 1.5 h or more depending on the group experience [166]. The optimal solution of this problem could be the Halcyon or Tomo therapy machine [136, 145, 152–156]. In addition,the use of these techniques, performed by Hui et al, allowed to obtain a dose reduction to OARs by 34-70% between TMI and TBI plans [154].In this study we will focus only on the treatment of Pelvic bone metastases to solve the problem of irradiating the largest part of the bone.

Our center has installed Halcyon2.0in December 2020 combined with EclipseTM treatment planning software (v16.1.0) using a 6X FFF energy and 600 MU/min dose rate.In this study, we reported our clinical experienceof treating patients with volumes bigger than the authorized field size(Pelvic bone metastases).However, this presents a challenge for planners and more time to achieve clinically acceptable results.

4.3 Materials and methods

Patient's Selection and perceptions: Since we installed only Halcyon 2.0 in our center to treat all patients with different localizations, some difficulties as recommended and allowed field size of 36cm using two isocenter, single energy of 6 MV flattening filter free(FFF), and closed bore system that limit the table movement laterallyare the main factors that restrict planners in treating larger volumes. A CT image dataset of 8 patients diagnosed with Pelvic bone metastases, who received radiotherapy in our department, were selected. The pelvis is

first of all a bony framework limited dorsally by the sacrum and below the coccyx, laterally and ventrally by the two coxal bones which meet in front at the level of the pubic symphysis.Due to lumbar lordosis, the axis of the pelvis, in the anatomical position of reference, is oblique dorsally and caudally at an angle of approximately °with respect to the horizontal.
CT simulation for all patients was performed in 2 mm slices with head-first supine using Siemens Somatom Sensation Open CT (Siemens, Erlangen, Germany). Target volumes and OARs were delineated using Varian SOMAVISION Focal workstations v.16.1.0 (Varian, Palo Alto, CA, USA). The primary clinical target volume was delineated according to the clinical protocol in use. The bony pelvic and OARs were delineated according to published guidelines [167, 168]. The clinical target volume (CTV) was contoured by radiation oncologists afterward; a uniform margin of 5mm was added to define Planning Target Volume (PTV). The prescription dose was 30Gy in 10 fractions.
Planning Technique All patients were treated with Halcyon 2.0 using VMAT technique. Treatment plans were generated within Eclipse treatment planning software (v16.1.0) using a 6X flattening filter free (FFF) energy and 600 MU/min dose rate. For all patients, two different planning techniques were applied. The first technique performed by two longitudinal isocenters technique (loIT) at a maximum distance of 8 cm from each other, it is the allowed distance by Halcyon version 2.0; however, the choice of the convenient distance between isocenter sdepends on the treatment region length, **Fig III.13** to irradiate the whole volume of the PTV. In spite of this, some limitations still present, more precisely if the treated PTV larger than 28cm, a part of the volume laterally is not irradiated from all gantry angles direction. Mostly, the shape of the irradiated volume is larger than the treatment field size from the anterior and posterior direction. From the oblique to thelateral directions, depending on the "beam's eye view",the width of the PTV decreases while, the depth increases and the whole volume will be included in the irradiated field size. The missing regions will be in the irradiated field only from the lateral directions when the gantry rotates far from the anterior and posterior angles. Consequently, these resultsa complex plan with the production more MUs, hot spot, and time consuming for the user to achieve the desired objectives. Likewise, to overcome this constraint the second technique based on two lateral isocenters technique (laIT) **III.14**. Using this technique makes it possible to irradiate the total volume from all gantry angle directions. Thus, no messing region during irradiation, no leaf sequencing complexity that may increase errors in the delivery, no hot spot, and more dose homogeneity is obtained. The distance between the two isocenters was kept to be less than 8cm for both techniques; two full opposite arcs per isocenter are created for all plans.

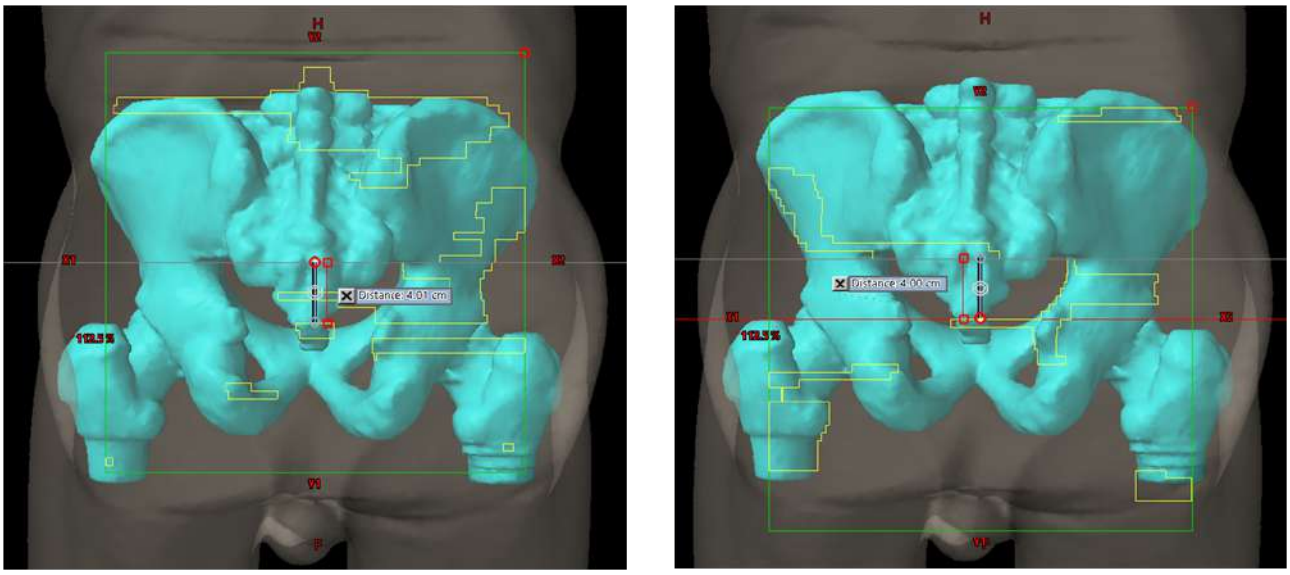

Figure III.13 – pelvic treatment using two longitudinal (loIT) with distance under 8cm between isocenters

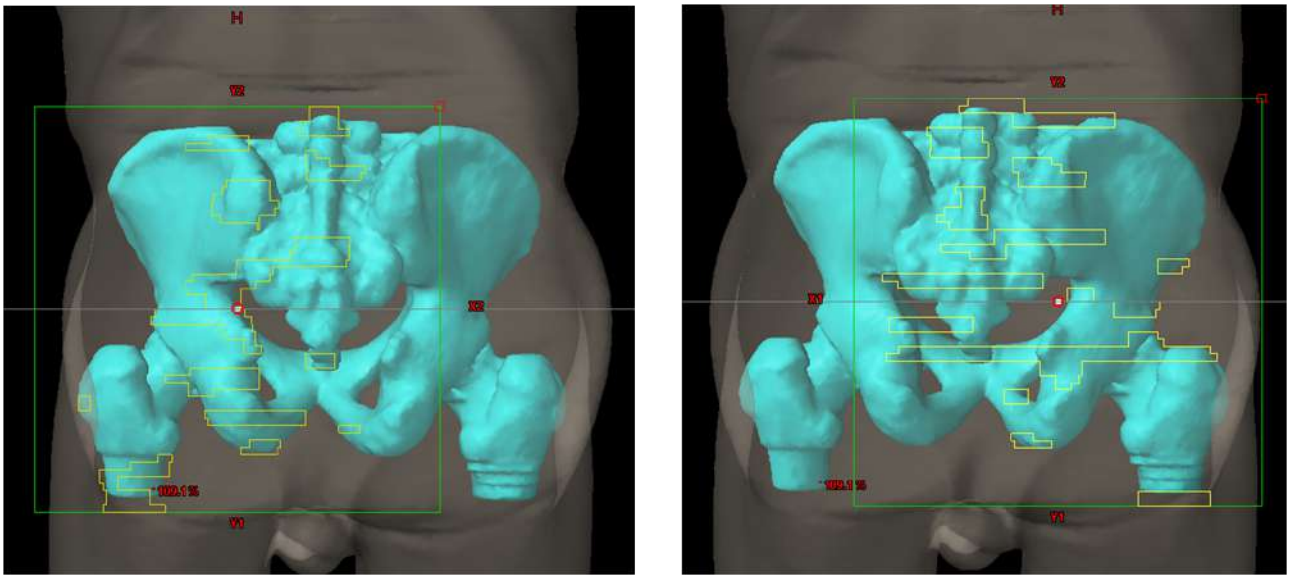

Figure III.14 – pelvic treatment using two lateral isocetenters (laIT) with distance under 8cm between isocenters

After the plan's calculation, the lateral technique is not allowed in the treatment machine; for this reason, we split each plan on two separate plans with one isocenter; Right Lateral and

Left Lateral (RL, LL) **Fig III.14**. More precision in the positioning using CBCT imaging is mandatory in this technique, since the delivery is performed by two separate plans with an overlap region.

Planning Objectives

As a planning objective for PTVs coverage, at least 95% ofthe prescribed dose was requested to cover 95% of the targetvolume (near-minimum dose D95% > 95%), this criterion wasfor both techniques in Pelvic treatment. In addition, 107% of the prescribed dose was set asan upper limit on the near-maximum dose D2%, that is the dose tothe 'hottest' 2% volume (D2% < 107%).As for healthy tissue, the main planning objectivewas to minimize the dose as much as possible while keeping the maximum homogeneity and conformity of the dose to the PTVs. By using indices, as Homogeneity index (HI), conformity index (CI), Healthy tissues conformity index (HTCI)and confirmation number (CN) that takes into account both; PTV coverage and healthy tissue protection;we evaluated the quality of the plans to compare the performance of each used technique.

The homogeneity index (HI) was used to evaluate the homogeneity of the dose in each PTV, as defined by the formula:

$$HI = \frac{D2\% - D98\%}{Dp} \tag{III.5}$$

Where DP: isthe prescribed dose to PTV, [169, 170] the ideal value of HIis 0 as it decreases by increasing the dose homogeneity inside thevolume of interest.Moreover, the conformity index (CI) was calculated to estimate the degree of the conformity of the dose to the PTV volume,according to the Radiation Therapy Oncology Group (USA)definition:

$$CI = \frac{V_{RI}}{V_{TV}} \tag{III.6}$$

Where, VRIis the volume of 95% of the prescribed dose and VTV the total volume of the PTV. With this definition, CI =1 corresponds to the ideal conformity. If CI is larger than 1, healthy tissues are irradiated. If CI is less than 1, the target volume is only partiallyirradiated.to simultaneously take into account irradiation of the target volume and irradiation of healthy tissue; van't Riet et al. proposed an index called conformation number that is defined as [171]:

$$CN = \frac{TV_{RI}}{TV} \times \frac{TV_{RI}}{V_{RI}} \tag{III.7}$$

Where: CN is the confirmation number, TVRIis the target volumecovered by the reference isodose, TV is thetarget volume, andVRIis the volume of the reference isodose. The first fraction

Tableau III.5 – Dosimetric parameters for Lateral and Longitudinal techniques in the pelvic treatment

-	CI	HI	D2%	D95%	DMAX	CN	MHs
Lat	1.09	0.36	105.4	96.2	109.4	0.82	1036
Long	1.1	0.45	105.78	94.6	112.3	0.76	1057

of this equation proposed by SALT-Lomax [171, 172] and defines the quality ofcoverage of the target; the second fraction proposed by Lomax [172] and defines the volume of healthy tissue receiving a dose greater than or equalto the prescribed reference isodose.For plan efficiency and treatment time, the number of monitor units in each using technique was considered.

4.4 Results

The mean results of the used dosimetric parameters of our study for the upper and lower part of pelvicbone metastases for both, laIT and loIT are outlined in table 1. No difference between the two techniques in terms of dose conformity is achieved, though a better homogeneity index (HI) is obtained in the laIT. The HI valueswere 0.36 and 0.45 for loIT and laIT. PTV coverage was clearly better in laIT with 96.2% against 94.6% as well as the maximum dose was 109.4% for laIT against 112.3% for loIT. CN evaluation also showed an improvement of 7.3% for laIT compared to that of loIT. However, MUs also was taken into account to compare the treatment time differences between the two techniques, and only 21 MUs of difference were obtained with the advantage of laIT.

Fig III.15 , 16, and 17 show, with respect to PTV coverage and dose homogeneity, the advantage of using laIT for large volume treatment.Table 1 demonstrated the benefit of the previously mentioned technique by examining dosimetric parameters. The same CI is obtained for both techniques and the HI was better with 20% for laIT compared to loIT, as well as the PTV coverage was 2% favored to laIT and 3% in terms of maximum dose. We also used CN which takes into account both; PTV coverage and healthy tissue irradiation, which can give an expectation of organs at risk protection.

The ideal value of this index is 1 when 100% of the PTV is covered by reference isodose and 0% of reference isodose irradiates healthy tissue. Our results on the calculated CN for the studied patients were 0.82 for latIT and 0.76 for loIT **Table III.5**.

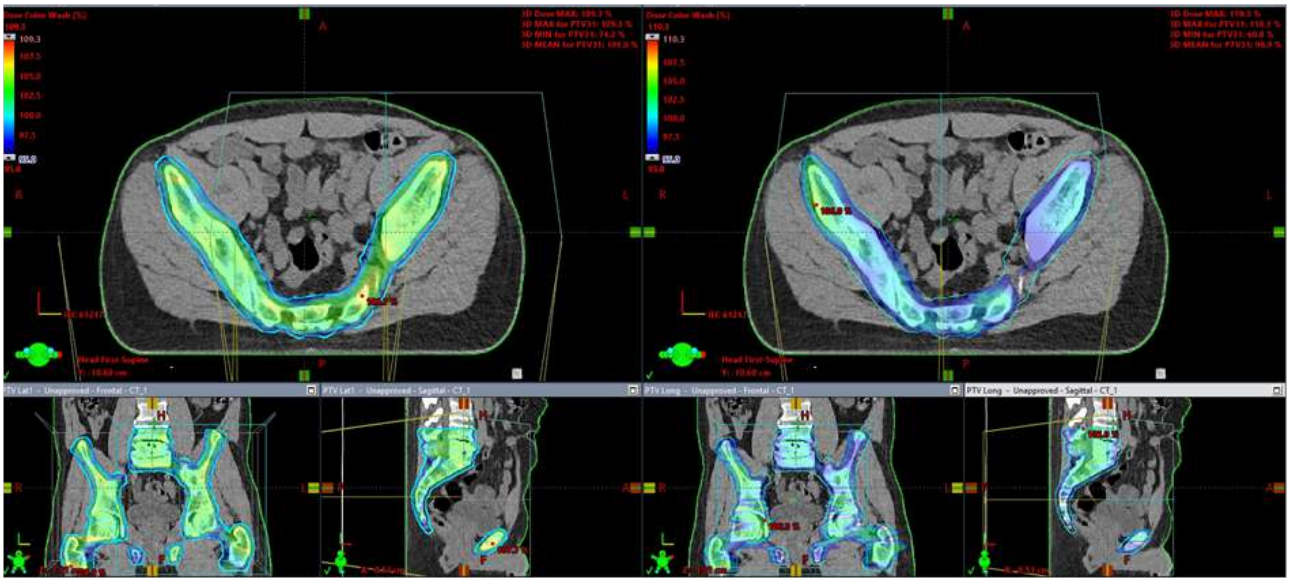

Figure III.15 – Comparison of dose distribution in axial, coronal, and sagittal slices for a patient treated with loIT (left) and loIT (right).

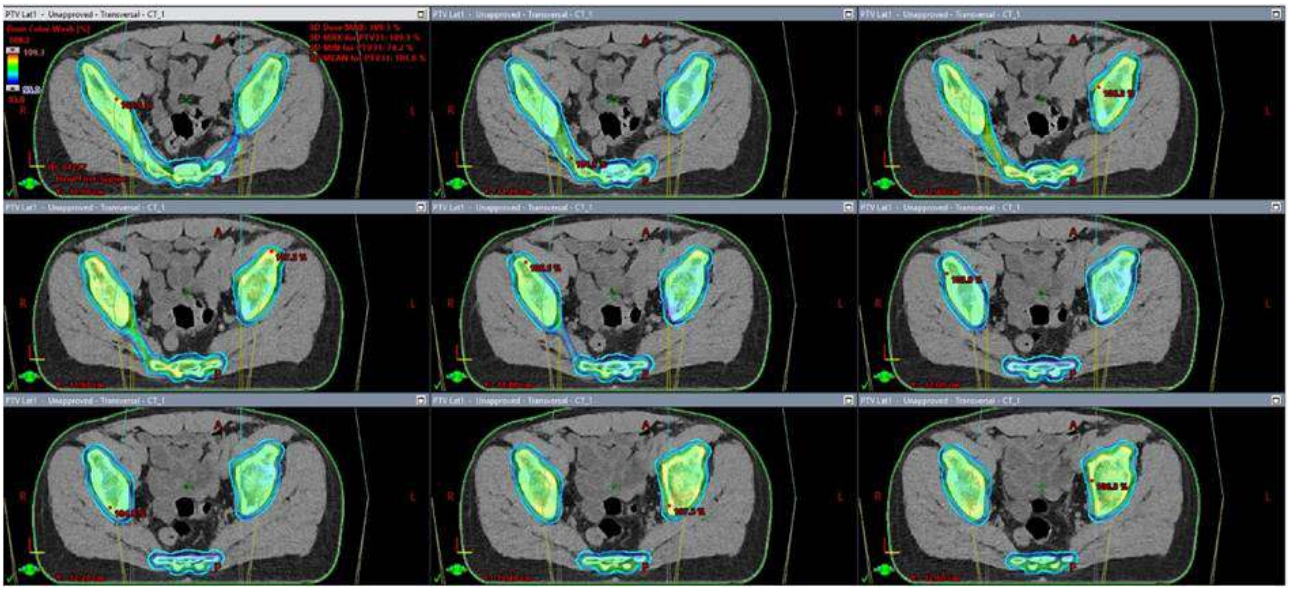

Figure III.16 – dose distribution comparison in multi-axial slices, for a patient treated by laIT

III.4 Solution for processing pelvic bone metastases with HalcyonTM 2.0 on lateral and longitudinal isocenters treatment plans using the VMAT technique: A comparative study.

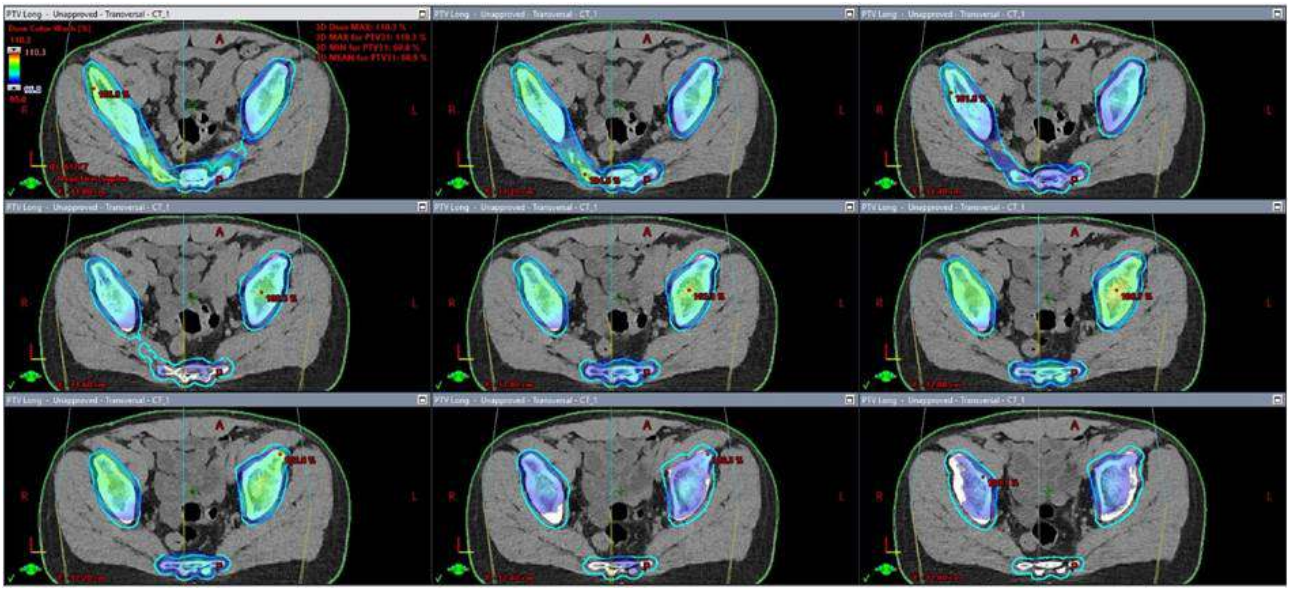

Figure III.17 – dose distribution comparison in multi-axial slices, for a patient treated by loIT

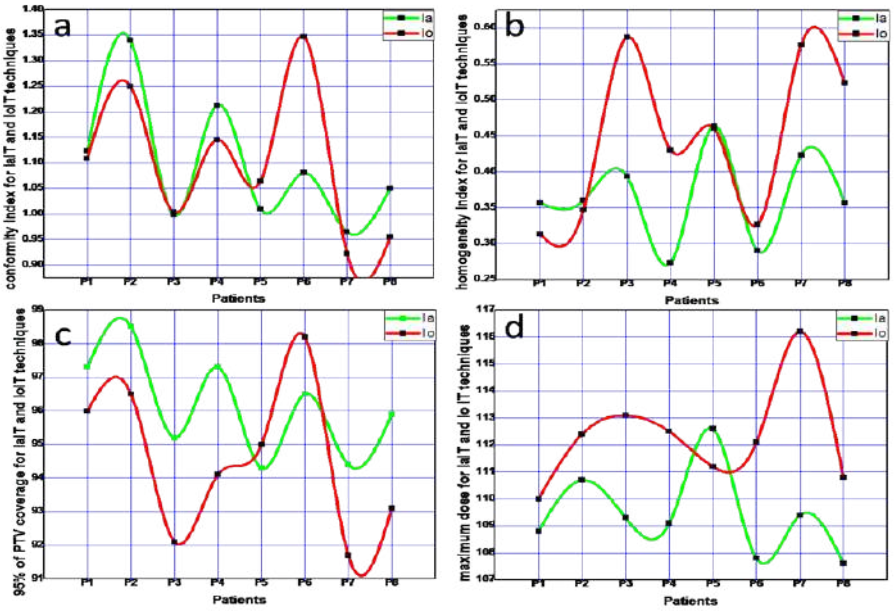

Figure III.18 – Dosimetric parameter curves for each individual patient treated with both, laIT and loIT techniques

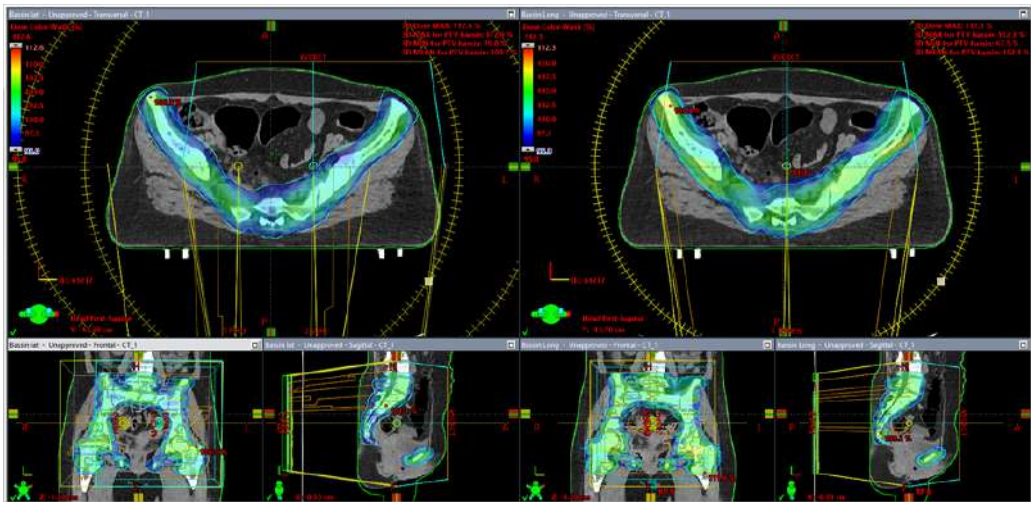

Figure III.19 – dose distribution comparison, for a patient treated with laIT (right side) and loIT (left side)

In pelvic treatment, when the size of the PTV is small and covered by the treatment

field size; acceptable clinical objectives can be reached by using loIT, and the results are not significantly different from that of laIT as shown in Fig 4for patient 5 (P5), whereall dosimetric parameters are almost the same for both techniques with an advantage to loIT except for CI.On theother hand, for P6 and P7 where the PTV is big, laIT was clearly better in all the studied dosimetric parameters.

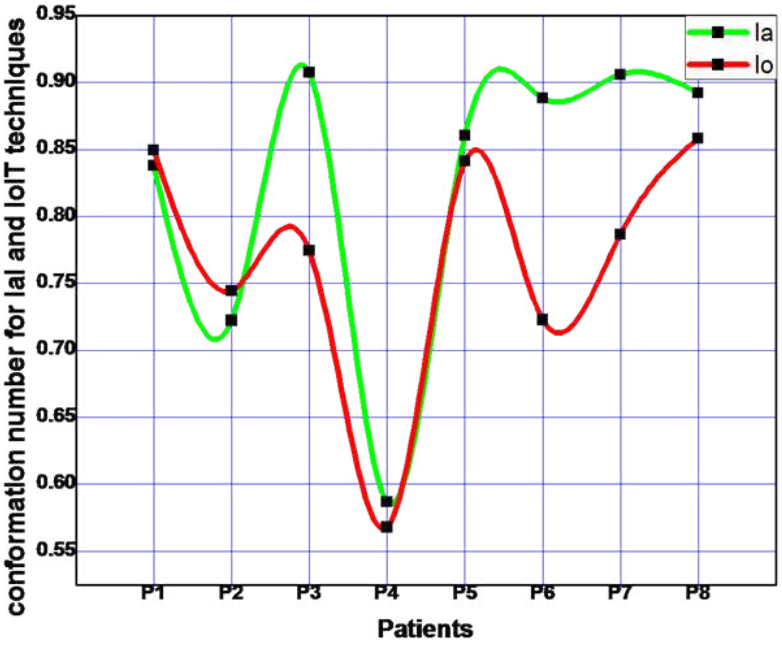

Figure III.20 – conformation number for each individual patient treated by loIT and laIT

Dose distribution differences for a patient with a small pelvic size treated by laIT and loITare shown in **Fig III.19**. Conformation numbers for all patients are calculated and plotted in Fig 6(CN laIT and loIT) to display the gain and quality of each technique.

4.5 Discussion

The pelvic skeleton supports the balance of the trunk and has complex bone anatomy. Many organs such as the intestines, urinary bladder, and internal sex organs are located within or near the pelvis which is mostly larger and longer than the field size of the Halcyon machine.

With these considerations, radiotherapy(RT) planning for pelvic bone metastases presents some difficulties to irradiate the whole volume and healthy tissue sparing. Shahid et al used more than two isocenters in the treatment of total body irradiation but only longitudinal shift was allowed between the first and subsequent isocenters [173]. However, this study investigated longitudinal and lateral isocenter techniques to treat only pelvic bone metastases and compare their performance by identifying dose coverage, Homogeneity, and conformity as well as healthy tissue sparing. A strong recommendation based on high quality evidence exists that single dose, low fractionated RT is appropriate for use in adults with pain from bone metastases if indicated and available. All patients with bone metastases must be considered for external beam radiation therapy (EBRT) or radioisotope therapy [174]. Practically, the EBRT of localized pain is used with various doses per fraction. Therefore, the efficacy of a unique fraction of 8Gy is equal to that of 20Gy in 5 fractions as well as 30Gy in 10 fractions for pain relief [175, 176].This study is administered to 8 patients with pelvic bone metastases with 30 Gy in 10 fractions through two techniques loIT and laIT **Fig.III.13** and **Fig.III.14**. these two techniques are reviewed based on Dosimetric parameters to investigate the advantage of each technique and go beyond the limit of the machine to treatlarge volumes. For Halcyon.2, two isocenters with an additional length of 8 cm mostly are sufficient to cover the PTV longitudinally. Unfortunately, lateral isocenters are not allowed in Halcyon machines. However, this presents a problem in treating patients with the large pelvis.

Therefore, loIT remains restricted if the treated volume is larger than 28 cm because a part of the volume will not be in the radiation field from all directions. Hence, a complicated plan will be acquired with the need for more optimization time to respond to user demands, also MUs calculation for loIT was bigger with 21 MUs compared to laIT **Table III.5**.More heterogeneities will be obtained for such plans and messing dose coverage to target volume as shown in **Fig III.15**(right side) and **Fig III.17**. To conquer these difficulties, laIT is based on two isocenters but in lateral directions. Though this isocenters arrangement is not allowed in the treatment machine.It was necessary to split each laIT plan before loading it to the treatment machine into two plans with one isocenter per plan. In addition, this technique needs accurate positioning since the two plans will overlap during the, which may produce a hot spot or missing dose in the edge of the plans, also the number of CBCTs is twice that of loIt. However, according to our experience, the overlapping problem can be solved by contouring structures on the edge of each imaging setup field. Consequently, using laIT requires more time in the treatment machine. For patient treatment, the studied Dosimetric parameters achieved better coverage; the mean value of D95% was 96% for loIT against 94% for loIT **table 5**, also a dose distribution for a studied patient in **Fig III.16** showed better coverage in all slices for

laIT compared to loIT **Fig III.17** where some slices are not covered with the reference isodose. **Fig III.18** demonstrated the benefit of laIT in terms of dose coverage for each patient and no gain is obtained for Patient 5. However, this disadvantage can be explained by the small size of the treated volume and this was clearly noticed in all the studied dosimetric parameters **Fig III.18**.In addition, 95% of dose distribution for this patient with a small size of the treated volume **Fig III.19**, shows no differences between the two techniques. At last, the advantage of laIT increases with the size of the treated volume. Organs at risk are not considered in this study because the delivered dose is only 30 Gy which is tolerable for Rectum, Bladder, and small bowel. Nevertheless, the conformation number is calculated in both techniques for each patient to take into account healthy tissue sparing; and the superiority favored laIT **Fig III.20**. This study was performed to surmount the difficulties of treating big volumes with the permitted technique in the treatment machine which is time consuming to achieve the desired objectives whenever the size of the PTV is larger than 28cm. Although, both techniques are still limited if the PTV longer than 36 cm. in this situation, a part of the PTV will not be covered by the treatment field. However, a further study will focus on treating volumes larger than 28cm and longer than 36cm.

4.6 Conclusion

This study presents the results of our clinical experience in treating patients with volumes larger than the allowed field size while seeking to achieve clinically acceptable results. Due to the limitations of the Halcyon machines, it was mandatory for us, as planners, to find solutions to these kinds of constraints.

Thus, the use of the lateral isocenter technique for the treatment of pelvic bone metastases allowed us to achieve clinically satisfied results. We were able to go beyond the limits of the Halcyon, making it possible for us to approach other locations with large fields such i.e. pelvis and lumbar simultaneously or craniospinal cases.

General conclusion

The main goal of radiation therapy over the years is to effectively separate the tumor control probability (TCP) and normal tissue complication probability (NTCP) curves from each other with the respect of clinical objectives. Nonetheless, with the use of advanced and sophisticated techniques available today, it is relatively feasible to widen the gap between these two curves. The degree of treatment complication is primarily determined by factors such as the tumor's localization, shape, and volume.

In this thesis we calculated the required additional margin from the clinical target volume (CTV) for prostate cancer; This organ is known for its mobility within the patient, significant volume, and the high number of treatment fractions, which can reach up to 78. In this study, CBCT pre-treatment imaging was performed for each treatment session to precisely monitor the whole errors including internal and external deviations. In each treatment fraction, we considered translation and rotation errors to accurately calculate the necessary additional margin. It was determined that a margin of less than 1 cm in all directions was sufficient to deliver the prescribed dose to the tumor volume while significantly reducing the risk of toxicity.

The treatment of the head and neck region often poses a challenge for users during the planning process. However, the success of the optimization technique relies on the user's expertise and skills to attain the desired clinical objectives. Similarly, in this thesis, we introduce planning techniques for the treatment of larynx cancer utilizing the Intensity Modulated Radiation Therapy (IMRT) approach. We assessed three distinct techniques: IMRT-0, which employed seven beams starting at 0° and incremented by 26° for subsequent beams; IMRT-26, which followed a similar approach but with a starting angle of 26°; and IMRT-CT, which combined the two aforementioned techniques. This technique enhances the dose distribution for larynx cancer treatment, focusing on plan quality by improving dose homogeneity and conformity within the Planning Target Volumes (PTVs), while concurrently reducing the radiation dose

to Organs at Risk (OARs) and surrounding peripheral tissues.

During optimization, the configuration and quantity of beamlets can greatly influence the planning outcomes, particularly in complex anatomical regions. We examined six optimization options across three different treatment localizations (Pelvis, Breast, and Head and Neck) to identify the most suitable optimization approach for each specific treatment region, aiming to achieve the optimal results. The findings revealed that employing the HIGH and VERY HIGH techniques for head and neck treatments led to improved dose coverage, maximum dose control, and a substantial reduction in treatment time when compared to the LOW technique. Conversely, the VERY LOW technique demonstrated certain advantages in the treatment of pelvic and breast cancers by striking a balance between treatment duration and target volume coverage.

Finally, we shared our clinical experience with the Halcyon machine for treating large volumes, which are typically considered a limitation for this type of machine. The pelvic bone is one of the largest structures in the human body, which is why we chose this region for treatment using the Halcyon machine. It's worth noting that the field size of the machine is often smaller than the area being treated in this case. Our proposed technique involves the use of two isocenters placed laterally to irradiate the entire volume, aiming to achieve the best clinical results.

Bibliography

[1] Registre des cancers du Grand Casablanca pour la pÃ©riode, Fondation Fondation Lalla Salma prÃ©vention et traitement des cancers, Edition 2016.

[2] Arnfield M, Siebers J, Kim J, Wu Q, Keall P, Mohan R. A method for determining multileaf collimator transmission and scatter for dynamic intensity modulated radiotherapy. Med Phys. 2000;27:2231-2241

[3] Zygmanski P, Rosca F, Kadam D, Lrenz F, Nalichowski A, Chin L.Determination of depth and field size dependence of multileaf collimator transmission in intensity-modulated radiation therapy beams. JAppl Clin Med Phys. 2007;8:2693.

[4] Lorenz F, Nalichowski A, Rosca F, Kung J, Wenz F, ZygmanskiP.Spatial dependence of MLC transmission in IMRT delivery. Phys MedBiol. 2007;52:5985-5999.

[5] Thompson C, Weston S, Cosgrove V, Thwaites D. A dosimetric characterization of a novel linear accelerator collimator. Med Phys.2014;41:031713.

[6] Galvin J, Smith A, Lally B. Characterization of a multileafcollimatorsystem. Int J Radiat Oncol Biol Phys. 1993;25:181-192.

[7] Maleki N, Kijewski P. Analysis of the field defining properties of amultileaf collimator. Med Phys. 1984;11:390.

[8] Helyer S, Heisig S. Multileaf collimation versus conventional shieldingblocks - a time and motion study of beam shaping in radiotherapy.Radiother Oncol. 1995;37:61-64.

[9] Huq M, Das I, Steinberg T, Galvin J. A dosimetric comparison of various multileaf collimators. Phys Med Biol. 2002;47:N159-N170.

[10] Jin J, Yin F, Ryu S, Ajlouni M, Kim J. Dosimetric study using differentleaf-width MLCs for treatment planning of dynamic conformal arcsand intensity-modulated radiosurgery. Med Phys. 2005;32:405-411.

[11] Losasso T. IMRT delivery performance with a varianmultileaf collimator. Int J Radiat Oncol Biol Phys. 2008;71:S85S88.

[12] Thompson C, Weston S, Cosgrove V, Thwaites D. A dosimetric characterization of a novel linear accelerator collimator. Med Phys.2014;41:031713.

[13] Huq M, Das I, Steinberg T, Galvin J. A dosimetric comparison of various multileaf collimators. Phys Med Biol. 2002;47:N159-N170.

[14] Webb S. A new concept of multileaf collimator (the shuttling MLC) an interpreter for high-efficiency IMRT. Phys Med Biol. 2000;45:3343-3358

[15] Tacke M, Nill S, Haring P, Oelfke U. 6 MV dosimetric characterization of the 160 MLC, the new Siemens multileafcollimator. MedPhys. 2008;35:1634-1642.

[16] Cai B, Li H, Yang D, et al. Performance of a multi leaf collimatorsystem for MR-guided radiation therapy. Med Phys. 2017;44:6504-6514.

[17] S. Webb. The physics of conformal radiotherapy: advances in technology. Institute of Physics Publishing, 1997.

[18] Cho B. Intensity modulated radiation therapy: a review with a physics perspective. Radiat Oncol J. 2018;36:1-10.

[19] Fitzmaurice, 2017; Jemal et al., 2017

[20] Rajamanickam Baskar 1, Kuo Ann Lee, Richard Yeo, Kheng-Wei Yeoh. Cancer and radiation therapy: current advances and future directions, Int J Med Sci 2012; 9(3):193-9.

[21] J .L. Peng, L. Chihray, C. Yu, et al. Dosimetric consequences of rotational setup errors with direct simulation in a treatment planning system for fractionated stereotactic radiotherapy. Journal of Applied Clinical Medical Physics, 12(3), 2011.

[22] Andrew Dhawan, Mohammad Kohandel, Richard Hill, and Sivabal Sivaloganathan. Tumour control probability in cancer stem cells hypothesis. PLoS ONE, 2014

[23] Luc J. Bos, Joris Van Der Geer, Marcel Van Herk, Ben J. Mijnheer, Joos V. Lebesque, and Eugane M.F. Damen. The sensitivity of dose distributions for organ motion and set-up uncertainties in prostate IMRT. Radiotherapy and Oncology, 2005.

[24] Andrew Dhawan, Mohammad Kohandel, Richard Hill, and Sivabal Sivaloganathan. Tumour control probability in cancer stem cells hypothesis. PLoS ONE, 2014.

[25] M Baumann and C Petersen. TCP and NTCP : A basic introduction. Rays, 2005.

[26] Brad Warkentin, Pavel Stavrev, Nadia Stavreva, Colin Field, and B. Gino Fallone. A TCP-NTCP estimation module using DVHs and known radiobiological models and parameter sets. Journal of Applied Clinical Medical Physics, 2004.

[27] B. J. Mijnheer, J. J. Battermann, and A. Wambersie. What degree of accuracy is required and can be achieved in photon and neutron therapy, mar 1987.

[28] Neil G Burnet, Simon J Thomas, Kate E Burton, and Sarah J Jefferies. Defining the tumour and target volumes for radiotherapy. Cancer imaging : the official publication of the International Cancer Imaging Society, 4 :153-161, 2004.

[29] Basic Concepts in Radiation Dosimetry

[30] E. B. Podgorsak, Radiation Oncology Physics: A Handbook for Teachers and Students, International Atomic Energy Agency (Vienna, 2005)

[31] (from IAEA Syllabus on radiation therapy

[32] ICRU. Prescribing, Recording and Reporting Photon Beam Therapy (Supplement to ICRU Report 50). Report 62. Bethesda, MD: International Commission on Radiation Units and Measurements, 1999.

[33] Handbook of Radiotherapy Physics, Theory and Practice Edited ByP Mayles, A Nahum, J.C Rosenwald, 2007

[34] Handbook of Optimization in Medicine, ALGORITHMS FOR SEQUENCING MULTI-LEAF COLLIMATORS By SRIJIT KAMATH

[35] ICRU REPORT 50 Prescribing, Recording, and Reporting Photon Beam therapy

[36] Journal of the ICRU Vol 10 N o1 (2010) Report 83 Oxford University Press

[37] A technique for the quantitative evaluation of dose distributions Daniel A.Low, William B.Harms, Sasa Mutic, and James A.Purdy Mallinckrodt Institute of Radiology, Division of Radiation Oncology, 510 South King shigh way Blvd., St. Louis, Missouri 63110 Received 9 June 1997; accepted for publication 2 March 1998.

[38] Perez, Carlos, and Luther Brady, "Principle sand Practice of Radiation Oncology," 5th Ed. Philadelphia: Lippincott William sand Wilkins, 2008. Print

[39] Hand book of Radiotherapy Physics, Theory and Practice Edited By PMayles, ANahum, J.C Rosenwald, 2007

[40] Shaw E, Kline R, Gillin M, Souhami L, Hirschfeld A, Dinapoli R, et al. Radiation therapy oncology group: Radiosurgery quality assurance guidelines. Int J Radiat Oncol Biol Phys. 1993;27:1231-9

[41] Journal of the ICRU Vol 10 No 1 (2010) Report 83 Oxford University Press

[42] Feuvret L, Noel G, Mazeron J, Bey P. Conformity index: a review. Int J Radiat Oncol Biol Phys 2006;64(2):333-42.

[43] radiotherapy in managing brain metastases, Evaluation of the quality of a radiosurgery plan Evan M. Thomas, Richard A. Popple, and John B. Fiveash

[44] Wu VW , Law MY, Star-Lack J, Cheung FW, Ling CC. Technologies of image guidance the development of advanced linear accelerator system for radiotherapy. Front Radiat Ther Oncol. 2011; 43:132-64.

[45] Kim J, Meyer JL, Dawson LA. Image guidance and the new practice of radiotherapy: what to know and use from a decade of investigation. Front Radiat Ther Oncol. 2011; 43:196-216.

[46] Verbakel WF, Cuijpers JP, Hoffmans D, Bieker M, Slotman BJ, Senan S. Volumetric intensity modulated arc therapy vs. conventional IMRT in head and neck cancer: a comparative planning and dosimetric study. Int J Radiat Oncol Biol Phys. 2009;74:252-9

[47] Quan EM, Li X, Li Y, Wang X, Kudchadker RJ, Johnson JL, Kuban DA, Lee AK, Zhang X. A comprehensive comparison of IMRT and VMAT plan quality for prostate cancer treatment. International Journal of Radiation Oncology Biology Physics. 2012 Jul 15;83(4):1169-78.

[48] Palma D, Vollans E, James K, Nakano S, Moiseenko V, Shaffer R, et al. Volumetric modulated arc therapy for delivery of prostate radiotherapy: comparison with intensity modulated radiotherapy and three dimensional conformal radiotherapy. International Journal of Radiation Oncology Biology Physics. 2008 Nov 15;72(4):996-1001.

[49] Bedford JL. Treatment planning for volumetric modulated arc therapy.Med Phys. 2009;36:5128e5138.

[50] Wolff D, Stieler F, Welzel G, Lorenz F, Abo-Madyan Y, Mai S, et al. Volumetric modulated arc therapy (VMAT) vs. serial tomotherapy, step and shoot IMRT and 3D conformal RT for treatment of prostate cancer. Radiotherapy and oncology. 2009 Nov 1;93(2):226-33.

[51] Palma D, Vollans E, James K, Nakano S, Moiseenko V, Shaffer R, et al. Volumetric modulated arc therapy for delivery of prostate radiotherapy: comparison with intensity-modulated radiotherapy and three-dimensional conformal radiotherapy. International Journal of Radiation Oncology Biology Physics. 2008 Nov 15;72(4):996-1001.

[52] Youssoufi MA, Bougtib M, Douama S, Erraisse MA, Abboud FZ, Hassouni K, et al. Evaluation of PTV margins in IMRT for head and neck cancer and prostate cancer. Journal of Radiotherapy in Practice. 2021 Mar;20(1):114-9.

[53] Wortel RC, Incrocci L, Pos FJ, Lebesque JV, Witte MG, van der Heide UA, et al. Acute toxicity after image guided intensity modulated radiation therapy compared to 3D conformal radiation therapy in prostate cancer patients. International Journal of Radiation Oncology Biology Physics. 2015 Mar 15;91(4):737-44.

[54] Graf R, Wust P, Budach V, Boehmer D. Potentials of on-line repositioning based on implanted fiducial markers and electronic portal imaging in prostate cancer radiotherapy. Radiat Oncol. 2009; 4: 13-21.

[55] Hainfeld JF, Slatkin DN, Smilowitz HM. The use of gold nanoparticles to enhance radiotherapy in mice. Physics in Medicine and Biology. 2004 Sep 3;49(18):N309.

[56] Rahman WN, Bishara N, Ackerly T, He CF, Jackson P, Wong C, et al. Enhancement of radiation effects by gold nanoparticles for superficial radiation therapy. Nanomedicine: Nanotechnology, Biology and Medicine. 2009 Jun 1;5(2):136-42.

[57] Roa W, Zhang X, Guo L, Shaw A, Hu X, Xiong Y, et al. Gold nanoparticle sensitize radiotherapy of prostate cancer cells by regulation of the cell cycle. Nanotechnology. 2009 Aug 26;20(37):375101.

[58] Chithrani DB, Jelveh S, Jalali F, van Prooijen M, Allen C, Bristow RG, et al. Gold nanoparticles as radiation sensitizers in cancer therapy. Radiat Res 2010;173(6):719-28.

[59] Hainfeld JF, Dilmanian FA, Zhong Z, Slatkin DN, Kalef-Ezra JA, Smilowitz HM. Gold nanoparticles enhance the radiation therapy of a murine squamous cell carcinoma. Phys Med Biol. 2010;55(11):3045-59.

[60] Liu CJ, Wang CH, Chen ST, Chen HH, Leng WH, Chien CC, et al. Enhancement of cell radiation sensitivity by pegylated gold nanoparticles. Phys Med Biol. 2010;55(4):931-45.

[61] Hirn S, Semmler-Behnke M, Schleh C, Wenk A, Lipka J, SchÃ¤ffler M, et al. Particle size-dependent and surface charge-dependent biodistribution of gold nanoparticles after intravenous administration. European journal of pharmaceutics and biopharmaceutics. 2011 Apr 1;77(3):407-16.

[62] Polf JC, Bronk LF, Driessen WHP, Arap W, Pasqualini R, Gillin M. Enhanced relative biological effectiveness of proton radiotherapy in tumor cells with internalized gold nanoparticles. Appl Phys Lett. 2011:193702-3.

[63] Geng F, Song K, Xing JZ, Yuan CZ, Yan S, Yang QF, et al. Thioglucose bound gold nanoparticles enhance radio-cytotoxic targeting of ovarian cancer. Nanotechnology. 2011;22(28).

[64] Yasui H, Takeuchi R, Nagane M, Meike S, Nakamura Y, Yamamori T, et al. Radiosensitization of tumor cells through endoplasmic reticulum stress induced by PEGylated nanogel containing gold nanoparticles. Cancer Lett. 2014;347(1):151-8.

[65] Khoshgard K, Hashemi B, Arbabi A, Rasaee MJ, Soleimani M. Radiosensitization effect of folate-conjugated gold nanoparticles on HeLa cancer cells under orthovoltage superficial radiotherapy techniques. Phys Med Biol. 2014;59(9):2249-63.

[66] Geng F, Xing JZ, Chen J, Yang R, Hao Y, Song K, et al. Pegylated glucose gold nanoparticles for improved in vivo biodistribution and enhanced radiotherapy on cervical cancer. J Biomed Nanotechnol. 2014;10(7):1205-16.

[67] Khosravi H, Mahdavi Gorabi A, Rahmani F, Ebadi A. Te Impact of Nano-Sized Gold Particles on the Target Dose Enhancement Based on Photon Beams Using by Monte Carlo Method. Nanomed Res J. 2016; 1(2):84-89

[68] Khosravi H, Hashemi B, Mahdavi SR, Hejazi P. Effect of gold nanoparticles on prostate dose distribution under Ir-192 internal and 18 MV external radiotherapy procedures using gel dosimetry and monte carlo method. J Biomed Phys Eng. 2015 Mar 4;5(1): 3-14.

[69] ICRU. Prescribing, recording, and reporting photon beam therapy. Report 50. Bethesda, MD: International Commission on Radiation Units and Measurements; 1993.

[70] Dearnaley DP, Sydes MR, Graham JD, Aird EG, Bottomley D, Cowan RA, et al. Escalated-dose versus standard-dose conformal radiotherapy in prostate cancer: first results from the MRC RT01 randomised controlled trial. The lancet oncology. 2007 Jun 1;8(6):475-87.

[71] Van Herk M, Remeijer P, Rasch C, Lebesque J V. The probability of correct target dose: dose population histograms for deriving treatment margings in radiotherapy. Int J Radiat Oncol Biol Phys. 2000; 47: 1121-1135.

[72] Stroom JC, De Boer HC, Huizenga H, Visser AG. Inclusion of geometrical uncertainties in radiotherapy treatment planning by means of coverage probability. International Journal of Radiation Oncology Biology Physics. 1999 Mar 1;43(4):905-19.

[73] Crehange G, Mirjolet C, Gauthier M, Martin E, Truc G, Peignaux-Casasnovas K, et al. Clinical impact of margin reduction on late toxicity and short-term biochemical control for patients treated with daily on-line image guided IMRT for prostate cancer. Radiotherapy and oncology: journal of the European Society for Therapeutic Radiology and Oncology. 2012, 103:244-6.

[74] Skarsgard D, Cadman P, El-Gayed A, Pearcey R, Tai P, Pervez N, et al. Planning target volume margins for prostate radiotherapy using daily electronic portal imaging and implanted fiducial markers. Radiat Oncol. 2010, 5:52

[75] Borut Kragelj, MD, PhD, Department of Radiation Oncology, Institute of Oncology, ZaloÅ¡ka 2, SI-1000 Ljubljana, Slovenia; Setup error and its effect on safety margin in conformal radiotherapy of the prostate

[76] Zelefsky MJ, Valicenti RK, Goodman K, Perez CA. Prostate cancer. Perez CA, Brady LW, Halperin EC, Schmidt Ullrich RK, editors. Principles and practice of radiation oncology. 4th edition. Philadephia: Lippincot, Williams and Wilkins; 2004. p. 1692-762

[77] Zelefsky MJ, Crean D, Mageras GS, Lyass O, Happersett L, Ling CC, et al. Quantification and predictors of prostate position variability in 50 patients with multiple CT scans during conformal radiotherapy. Radiother Oncol 1999; 50: 225-34.

[78] Van Herk M, Remeijer P, Rasch C, Lebesque JV. The probability of correct target dosage: dose-population histograms for deriving treatment margins in radiotherapy. International Journal of Radiation Oncology Biology Physics. 2000 Jul 1;47(4):1121-35.

[79] Zhang X, Shan GP, Liu JP, Wang BB. Margin evaluation of translational and rotational set-up errors in intensity modulated radiotherapy for cervical cancer. Springerplus. 2016 Feb 24;5:153

[80] Adamson J, Wu Q, Yan D. Dosimetric effect of intrafraction motion and residual setup error for hypofractionated prostate intensity modulated radiotherapy with online cone beam computed tomography image guidance. International Journal of Radiation Oncology Biology Physics. 2011 Jun 1;80(2):453-61.

[81] Polat B, Guenther I, Wilbert J, Goebel J, Sweeney RA, Flentje M, et al. Intra-fractional uncertainties in image-guided intensity-modulated radiotherapy (IMRT) of prostate cancer. Strahlentherapie und Onkologie. Organ der Deutschen Rontgen gesell schaft [et al] 2008, 184:668-73.

[82] Laursen LV, Elstrom UV, Vestergaard A, Muren LP, Petersen JB, Lindegaard JC, et al. Residual rotational set up errors after daily cone beam CT image guided radiotherapy of locally advanced cervical cancer. 2012.

[83] Werner Ba, Marco Schwarz, Markus Alber, Luc J. Bos, Ben J. Mijnheer, Coen Rasch,et al.A comparison of forward and inverse treatment planning for intensity-modulated radiotherapy of head and neck cancer. Radiother Oncol 2003;69:251-8.

[84] Vanetti E, Clivio A, Nicolini G, Fogliata A, Ghosh-Laskar S, Agarwal JP, et al. Volumetric modulated arc radiotherapy for carcinomas of the oro-pharynx, hypo-pharynx and larynx: a treatment planning comparison with fixed field IMRT. Radiother Oncol 2009;

[85] Lu SH, Cheng JC, Kuo SH, Lee JJ, Chen LH, Wu JK, et al. Volumetric modulated arc therapy for nasopharyngeal carcinoma: a dosimetric comparison with TomoTherapy and step-and-shoot IMRT. Radiother Oncol 2012;

[86] Peter White, Kit Chi Chan, Ka Wai Cheng, Ka Yiu Chan, and Ming Chun Chau. Volumetric intensity-modulated arc therapy vs conventional intensity modulated radiation therapy in nasopharyngeal carcinoma: a dosimetric study. Journal of Radiation Research. 2013 May; 54(3): 532-545.

[87] Eisbruch A, Ten Haken RK, Kim HM, Marsh LH and Ship JA. Dose, volume, and function relationships in parotid salivary glands following conformal and intensity-modulated irradiation of head and neck cancer. Int J Radiat Oncol Biol Phys 1999;45:577-87.

[88] Parliament MB, Scrimger RA, Anderson SG, Kurien EC, Thompson HK, Field GC et al.Preservation of oral health-related quality of life and salivary flow rates after inverse-planned intensity modulated radiotherapy (IMRT) for head and neck cancer. Int J Radiat Oncol Biol Phys 2004;58: 663-673.

[89] Marta GN, Silva V, de Andrade Carvalho H, de Arruda FF, Hanna SA, Gadia R, et al. Intensity modulated radiation therapy for head and neck cancer: systematic review and meta analysis. Radiother Oncol 2014; 110:

[90] Van Asselen B1, Dehnad H, Terhaard CH, Lagendijk JJ and Raaijmakers CP.Segmental IMRT for oropharyngeal cancer in a clinical setting. Radiother Oncol 2003;69:259-266.

[91] Samuelsson A, Johansson KA. Intensity modulated radiotherapy treatment planning for dynamic multileaf collimator delivery: Influence of different parameters on dose distributions. Radiother Oncol 2003;66:19-28.

[92] Wu Q1, Manning M, Schmidt-Ullrich R and Mohan R. The potential for sparing of parotids and escalation of biologically effective dose with intensity modulated radiation treatments of head and neck cancers: A treatment design study. Int J Radiat Oncol Biol Phys 2000;46:195-205.

[93] Popple, R. A., Fiveash, J. B. and Brezovich, I. A. (2007), Effect of beam number on organ at risk sparing in dynamic multileaf collimator delivery of intensity modulated radiation therapy. Med. Phys., 34: 3752-3759

[94] Merlotti A, Alterio D, Vigna-Taglianti R, Muraglia A, Luciana Lastrucci L, Manzo R,et al. Technical guidelines for head and neck cancer IMRT on behalf of the Italian association of radiation oncology head and neck working group. Radiation Oncology (2014) 9:264

[95] Dobler B, Obermeier T, Hautmann MG, Khemissi A and Koelbl O. Simultaneous integrated boost therapy of carcinoma of the hypopharynx/larynx with and without flattening filter a treatment planning and dosimetry study. Radiation Oncology (2017) 12:114

[96] Stein J, Mohan R, Wang XH, Bortfeld T, Wu Q, Preiser K, et al. Number and orientations of beams in intensity-modulated radiation treatments. Med Phys. 1997 Feb;24(2):149-60.

[97] Kataria T, Sharma K, Subramani V, Karrthick K. P. and Bisht S S. Homogeneity Index: An objective tool for assessment of conformal radiation treatments. J Med Phys. 2012; 37(4): 207-213.

[98] Wu Q, Mohan R, Morris M, Lavue A, Schmidt-Ullrich R. Simultaneous integrated boost intensity modulated radiotherapy for locally advanced head and neck squamous cell carcinomas: Dosimetric results. Int J RadiatOncolBiol Phys. 2003; 26:573-85.

[99] Yoon M, Park S Y, Shin D, Lee S B, Pyo H R, Kim D Y, and Cho K H. A new homogeneity index based on statistical analysis of the dosevolume histogram.Journal of Applied Clinical Medical Physics.2007; Vol 8, No 2.

[100] Huguenin PU1, Taussky D, Moe K, Meister A, Baumert B, LÃ¼tolf UMet al. Quality of life in patients cured from carcinoma of the head and neck by radiotherapy: the importance of the target volume. Int J Radiat Oncol Biol Phys 1999;45:47-52.

[101] Wijers OB1, Levendag PC, Braaksma MM, Boonzaaijer M, Visch LL, Schmitz PI et al. Patients with head and neck cancer cured by radiation therapy: a survey of the dry mouth syndrome in long-term survivors. Head Neck 2002;24:737-47.

[102] Eisbruch A1, Marsh LH, Martel MK, Ship JA, Ten Haken R, Pu AT et al Comprehensive irradiation of head and neck cancer using conformal multisegmental fields: assessment of target coverage and non involved tissue sparing. Int J Radiat Oncol Biol Phys 1998;41:559-68.

[103] Arnfield M, Siebers J, Kim J, Wu Q, Keall P, Mohan R. A method for determining multileaf collimator transmission and scatter for dynamic intensity modulated radiotherapy. Med Phys. 2000;27:2231-2241

[104] Zygmanski P, Rosca F, Kadam D, Lrenz F, Nalichowski A, Chin L.Determination of depth and field size dependence of multileaf collimator transmission in intensity modulated radiation therapy beams. JAppl Clin Med Phys. 2007;8:2693.

[105] Lorenz F, Nalichowski A, Rosca F, Kung J, Wenz F, ZygmanskiP.Spatial dependence of MLC transmission in IMRT delivery. Phys MedBiol. 2007;52:5985-5999.

[106] Thompson C, Weston S, Cosgrove V, Thwaites D. A dosimetric characterization of a novel linear accelerator collimator. Med Phys.2014;41:031713.

[107] Galvin J, Smith A, Lally B. Characterization of a multileafcollimatorsystem. Int J Radiat Oncol Biol Phys. 1993;25:181-192.

[108] Maleki N, Kijewski P. Analysis of the field defining properties of amultileaf collimator. Med Phys. 1984;11:390.

[109] Helyer S, Heisig S. Multileaf collimation versus conventional shieldingblocks a time and motion study of beam shaping in radiotherapy.Radiother Oncol. 1995;37:61-64.

[110]) Huq M, Das I, Steinberg T, Galvin J. A dosimetric comparison of various multileaf collimators. Phys Med Biol. 2002;47:N159-N170.

[111] Jin J, Yin F, Ryu S, Ajlouni M, Kim J. Dosimetric study using different leaf width MLCs for treatment planning of dynamic conformal arcs and intensity modulated radiosurgery. Med Phys. 2005;32:405-411.

[112] Losasso T. IMRT delivery performance with a varian multileaf collimator. Int J Radiat Oncol Biol Phys. 2008;71:S85S88.

[113] Webb S. A new concept of multileaf collimator (the shuttling MLC) an interpreter for high efficiency IMRT. Phys Med Biol. 2000;45:3343-3358

[114] Tacke M, Nill S, Haring P, Oelfke U. 6 MV dosimetric characterization of the 160 MLC, the new Siemens multileafcollimator. MedPhys. 2008;35:1634-1642.

[115] Cai B, Li H, Yang D, et al. Performance of a multi leaf collimatorsystem for MR-guided radiation therapy. Med Phys. 2017;44:6504-6514.

[116] Fiveash J, Murshed H, Duan J. Effect of multileafcollimator leaf width on physical dose distributions in the treatment of CNS and head and neck neoplasms withintensity modulated radiation therapy. Med Phys. 2002;29:1116-1119.

[117] Cosgrove V, Jahn U, Pfaender M, Bauer S, Budach V, WurmR.Commissioning of a micro multi-leaf collimator and planningsystem for stereotactic radiosurgery. Radiother Oncol. 1999;50:325-336.

[118] V. Bernard, S. Fafi, D. Nguyen, and M. Khodri, Phys. Medica 56, 54 (2018).

[119] D. Withers, G. Kidane, L. Crees, D. Farmakidis, J. Greenwood, E. Isaacs, and Y. Miao, in Eur. Soc. Radiother. Oncol. (ESTRO 37) (2017).

[120] Halcyon System. (Accessed 01/21/2019, at https://www.varian.com/oncology/products/treatment-delivery/halcyon) 19) RDS Treatment Planning Instructions for Use Eclipse 15.1.1. ReportNo.: P1017375-004-D

[121] De Roover R, Crijns W, Poels K, et al. Validation and IMRT/VMATdelivery quality of a preconfigured fast-rotating O-ring linac system.Med Phys. 2019;46:328-339.

[122] Lloyd SAM, Lim TY, Fave X, et al. TG-51 reference dosimetry for theHalcyon TM: a clinical experience. J Appl Clin Med Phys. 2018;19:98-102.

[123] GrÃ©goire V, Ang K, Budach W, Grau C, Hamoir M, Langendijk JA, et al.Delineation of the neck node levels for head and neck tumors: a 2013 update.DAHANCA, EORTC, HKNPCSG, NCIC CTG, NCRI, RTOG, TROG consensusguidelines. Radiother Oncol 2013;110:172-81.

[124] Brouwer CL, Steenbakkers RJHM, Bourhis J, Budach W, Grau C, GrÃ©goire V, et al. CT-based delineation of organs at risk in the head and neck region: DAHANCA, EORTC, GORTEC, HKNPCSG, NCIC CTG, NCRI, NRG Oncology and TROG consensus guidelines. Radiother Oncol 2015;117:83-90.

[125] Kataria T, Sharma K, Subramani V, Karrthick K P, Bisht S S.Homogeneity Index: an objective tool for assessment of conformalradiation treatments. J Med Phys 2012; 37: 207-213.

[126] Yoon M, Park S Y, Shin D et al. A new homogeneity index based onstatistical analysis of the dosevolume histogram. J Appl Clin Med Phys2007; 8: 9-17.

[127] Kim H, Huq MS, Lalonde R, Houser CJ, Beriwal S, Heron DE. Early clinical experience with varian halcyon V2 linear accelerator: Dual-isocenter IMRT planning and delivery with portal dosimetry for gynecological cancer treatments. J Appl Clin Med Phys. 2019 Nov;20(11):111-120. doi: 10.1002/acm2.12747. Epub 2019 Oct 29. PMID: 31660682; PMCID: PMC6839386.

[128] De Roover R, Crijns W, Poels K, et al. Validation and IMRT/VMAT delivery quality of a preconfigured fast rotating O-ring linac system. Med Phys. 2019;46:328-339.

[129] Michiels, Steven, et al. "Volumetric modulated arc therapy of head and neck cancer on a fast rotating O-ring linac: Plan quality and delivery time comparison with a C-arm linac." Radiotherapy and Oncology 128.3 (2018): 479-484.

[130] https://varian.widen.net/view/pdf/tbojclmgk3 Halcyon ProductBrief RAD 10520 A High QualityCare June2018.pdf u=bmxzem

[131] Tsiamas p, seco J, han Z, et al. a modifcation of flatnning filter free linac for IMRT. Med phys. 2011; 38(5): 2342-2352, doi: 10.1118/1.3571419, indexed in pubmed: 21776768.

[132] Georg D, Kragl G, Wetterstedtsaf, et al. photon beam quality variations of a flatnning filter free linear accelerator.Med phys. 2010; 37(1): 49-53, doi: 10.1118/1.3264617,indexed in pubmed: 20175465.

[133] ceberg c, Johnsson s, Lind M, et al. prediction of stoppingpower ratios in flatnning filter free beams. Med phys.2010; 37(3): 1164-1168, doi: 10.1118/1.3314074, indexedin pubmed: 20384253.

[134] Kragl G, Wetterstedtsaf, KnÃ¤usl B, et al. Dosimetric characteristics of 6 and 10MV unflattened photon beams.radiother Oncol. 2009; 93(1): 141-146, doi: 10.1016/j.radonc.2009.06.008, indexed in pubmed: 19592123.

[135] cashmore J. The characterization of unflattened photonbeams from a 6 MV linear accelerator. phys Med Biol. 2008; 53(7): 1933-1946, doi: 10.1088/0031-9155/53/7/009,indexed in pubmed: 18364548.

[136] Titt U, Vassiliev ON, pÃ¶nisch F, et al. Monte carlostudy of backscatter in a flatnning filter free clinical accelerator. Med phys. 2006; 33(9): 3270-3273,doi: 10.1118/1.2229430, indexed in pubmed: 17022221

[137] Zhu Xr, Kang Y, Gillin MT. Measurements of in air output ratios for a linear accelerator with and without the flatnning filter. Med phys. 2006; 33(10): 3723-3733,doi: 10.1118/1.2349695, indexed in pubmed: 17089838.

[138] pÃ¶nisch F, Titt U, Vassiliev ON, et al. properties of unflattened photon beams shaped by a multileaf collimator. Medphys. 2006; 33(6): 1738-1746, doi: 10.1118/1.2201149,indexed in pubmed: 16872081.

[139] Vassiliev ON, Titt U, Kry sF, et al. Dosimetric properties of photon beams from a flatnning filter free clinical accelerator. phys Med Biol. 2006; 51(7): 1907-1917, doi: 10.1088/0031-9155/51/7/019, indexed in pubmed: 16552113.

[140] Titt U, Vassiliev ON, pÃ¶nisch F, et al. a flattening filter free photon treatment concept evaluation withMonte carlo. Med phys. 2006; 33(6): 1595-1602,doi: 10.1118/1.2198327, indexed in pubmed: 16872067.

[141] Feng Z, Yue h, Zhang Y, et al. Monte carlo simulation ofbeam characteristics from small felds based on True Beam flatnning filter free mode. radiat Oncol. 2016;11: 30, doi: 10.1186/s13014-016-0601-2, indexed inpubmed: 26921246

[142] Ding GX, Munro p. radiation exposure to patients fromimage guidance procedures and techniques to reducethe imaging dose. radiother Oncol. 2013; 108(1):91-98, doi: 10.1016/j.radonc.2013.05.034, indexed inpubmed: 23830468

[143] Fiveash J, Murshed H, Duan J. Effect of multileaf collimator leaf width on physical dose distributions in the treatment of CNS and head and neck neoplasms withintensity modulated radiation therapy. Med Phys. 2002;29:1116-1119.

[144] E.U. Hutagalung, Metastatic bone disease, Med. J. Indones. 13 (2) (2004)127-131

[145] Coleman R. Metastatic bone disease: clinical features, pathophysiology and treatment strategies. Cancer Treat Rev 2001;27:165-76

[146] Cecchini M, Wetterwald A, Pluijm G, Thalmann G. Molecular and biological mechanisms of bone metastasis. EAU UpdateSeries 2005;3:214-26.

[147] Selvaggi G, Scagliotti G. Management of bone metastases incancer: a review. Clin Rev Oncol Hematol2005;56:365-78

[148] Dworkin RH, Turk DC, Farrar JT, et al. Core outcome measures for chronic pain clinical trials: IMMPACT recommendations. Pain2005;113:9e19.

[149] McQuay H. Consensus on outcome measures for chronic pain trials. Pain 2005;113:1e2.

[150] He J, Zeng ZC, Tang ZY, Fan J, Zhou J, Zeng MS, Wang JH, Sun J, Chen B, Yang P, Pan BS. Clinical features and prognostic factors in patients with bone metastases from hepatocellular carcinoma receiving external beam radiotherapy. Cancer. 2009; 115:2710-2720.

[151] Chang UK, Kim MS, Han CJ, Lee DH. Clinical result of stereotactic radiosurgery for spinal metastasis from hepatocellular carcinoma: comparison with conventional radiation therapy. J Neurooncol. 2014; 119:141-148.

[152] Choi C, Seong J. Predictive factors of palliative radiotherapy response and survival in patients with spinal metastases from hepatocellular carcinoma. Gut Liver. 2015; 9:94-102.

[153] Choi Y, Kim JW, Lee IJ, Han HJ, Baek J, Seong J. Helical tomotherapy for spine oligometastases from gastrointestinal malignancies. Radiat Oncol J. 2011; 29:219-227

[154] Uehara T, Monzen H, Tamura M, Inada M, Otsuka M, Matsumoto K,Nishimura Y. Feasibility study of volumetric modulated arc therapy withHalcyon linac for total body irradiation. Radiat Oncol. 2021;16(1):1-8.

[155] Hui SK, Kapatoes J, Fowler J, Henderson D, Olivera G, Manon RR, GerbiB, Mackie TR, Welsh JS. Feasibility study of helical tomotherapy for totalbody or total marrow irradiation a. Med Phys. 2005;32(10):3214-24.

[156] Fogliata A, Cozzi L, Clivio A, Ibatici A, Mancosu P, Navarria P, Nicolini G,Santoro A, Vanetti E, Scorsetti M. Preclinical assessment of volumetric modulated arc therapy for total marrow irradiation. Int J Radiat Oncol Biol Phys. 2011;80(2):628-36.

[157] Aydogan B, Yeginer M, Kavak GO, Fan J, Radosevich JA, Gwe Ya K. Total marrow irradiation with rapid Arc volumetric arc therapy. Int J Radiat Oncol Biol Phys. 2011;81:592-9.

[158] Miralbell R, Rouzaud M, Grob E, Nouet P, Bieri S, Majno SB, Botteron P,Montero M, Precoma JC. Can a total body irradiation technique be fastand reproducible? Int J Radiat Oncol Biol Phys. 1994;29(5):1167-73.

[159] Wong JY, Liu A, Schultheiss T, et al. Targeted total marrow irradiation using three dimensional image guided tomographic intensity modulated radiation therapy: an alternative to standard total body irradiation. BiolBlood Marrow Transplant. 2006;12:306-15.

[160] Aydogan B, Mundt AJ, Roeske JC. Linac based intensity modulated totalmarrow irradiation (IM TMI). Technol Cancer Res Treat. 2006;5:513-9.

[161] Wilkie JR, Tiryaki H, Smith BD, Roeske JC, Radu CG, Aydogan B. Feasibilitystudy for linac based intensity modulated total marrow irradiation. MedPhys. 2008;35:5609-18.

[162] Karthik V, Osman S, Singh S, Jassal K, Sarkar B, Ganesh T, Giri UK. Utilizationof OSLD as the quality control indicator for in vivo measurements in totalbody irradiation. J Med Phys. 2017;42(suppl. 1):241.

[163] GrÃ©goire V, Ang K, Budach W, Grau C, Hamoir M, Langend ijk JA, et al.Delineation of the neck node levels for head and neck tumors: a 2013 update.DAHANCA, EORTC, HKNPCSG, NCIC CTG, NCRI, RTOG, TROG consensus guidelines. Radiother Oncol 2013;110:172-81.

[164] Brouwer CL, Steenbakkers RJHM, Bourhis J, Budach W, Grau C, GrÃ©goire V, et al. CT based delineation of organs at risk in the head and neck region: DAHANCA, EORTC, GORTEC, HKNPCSG, NCIC CTG, NCRI, NRG Oncology and TROG consensus guidelines. Radiother Oncol 2015;117:83-90.

[165] Kataria T, Sharma K, Subramani V, Karrthick K P, Bisht S S.Homogeneity Index: an objective tool for assessment of conformal radiation treatments. J Med Phys 2012; 37: 207-213.

[166] Yoon M, Park S Y, Shin D et al. A new homogeneity index based onstatistical analysis of the dosevolume histogram. J Appl Clin Med Phys2007; 8: 9-17.

[167] van'tRiet A, Mak AC, Moerland MA, et al. A conformation number to quantify the degree of conformality in brachytherapy and external beam irradiation: Application to the prostate.Int J Radiat Oncol Biol Phys 1997;37:731-736.

[168] Dejean C, Lefkopoulos D, Foulquier JN, et al. [Automatic definition of prescription isodose for stereotaxic radiation of arteriovenous malformations]. Cancer Radiother2001;5:138-149.

[169] Lomax NJ, Scheib SG. Quantifying the degree of conformityin radiosurgery treatment planning. Int J Radiat Oncol BiolPhys 2003;55:1409-1419.

[170] Shahid, T., Mandal, S., Biswal, S.S. et al. Preclinical validation and treatment of volumetric modulated arc therapy based total bone marrow irradiation in Halcyon ring gantry linear accelerator. Radiat Oncol 17, 145 (2022)

[171] WHO Guidelines for the Pharmacological and Radiotherapeutic Management of Cancer Pain in Adults and Adolescents; World Health Organization: Geneva, Switzerland, 2018; ISBN 978-92-4-155039-0

[172] Lutz, S.; Berk, L.; Chang, E.; Chow, E.; Hahn, C.; Hoskin, P.; Howell, D.; Konski, A.; Kachnic, L.; Lo, S.; et al. Palliative radiotherapy for bone metastases: An ASTRO evidence-based guideline. Int. J. Radiat. Oncol. Biol. Phys. 2011, 79, 965-976.

[173] Shahid, T., Mandal, S., Biswal, S.S. et al. Preclinical validation and treatment of volumetric modulated arc therapy based total bone marrow irradiation in Halcyon ring gantry linear accelerator. Radiat Oncol 17, 145 (2022)

[174] WHO Guidelines for the Pharmacological and Radiotherapeutic Management of Cancer Pain in Adults and Adolescents; World Health Organization: Geneva, Switzerland, 2018; ISBN 978-92-4-155039-0

[175] WHO Guidelines for the Pharmacological and Radiotherapeutic Management of Cancer Pain in Adults and Adolescents; World Health Organization: Geneva, Switzerland, 2018; ISBN 978-92-4-155039-0.

[176] Lutz, S.; Berk, L.; Chang, E.; Chow, E.; Hahn, C.; Hoskin, P.; Howell, D.; Konski, A.; Kachnic, L.; Lo, S.; et al. Palliative radiotherapy for bone metastases: An ASTRO evidence-based guideline. Int. J. Radiat. Oncol. Biol. Phys. 2011, 79, 965-976.